A Study Of Transition Metal Acetylides for Broadband Optical Limiters.

By

Yvonne Jansen van Galen

This thesis submitted for the degree of

Doctor of Philosophy

At

Adelaide University (Department of Physics)

July 2005

This work contains no material which has been accepted for the award of any other degree of diploma in any university or any other tertiary institution and, to the best of my knowledge and belief, contains no material previously published or written by another person, except where due reference has been made in the text.

I give consent to this copy of my thesis, when deposited in the University, being available for loan and photocopying.

Signed:..

Date:.....23/08/07.....

Acknowledgements

This project would not have been possible without the support of many people. Many thanks to my adviser, Peter Veitch, who read my numerous revisions and helped make some sense of the confusion.

Thanks DSTO for providing the funds and to Tim McKay and Jullianne Davy and everyone there for their advice and support in the early years.

Thanks to the guys in the optics group for sympathising with lasers that don't work and providing a break from the daily grind. A very special thanks to Alex Hemming for finally fixing my stubborn laser.

I would also like to thank my parents, and numerous friends who endured this long process with me, always offering support and love. And finally, and most importantly, thanks to my husband for suffering with me throughout and especially during the writing up stage.

Abstract

With the increasing use of lasers it is necessary to develop materials that can provide protection to eyes and other sensitive devices. This thesis reports on an investigation into optical limiting of Transition Metal Acetylides (TMAs) that transmit ambient light levels of light but block high energy (laser) light across the visible part of the spectrum.

A standard optical limiting testbed is used to measure optical limiting at 470, 532 and 630 nm for a wide range of Pt:ethynyl related TMAs. I report the effect on optical limiting of altering the central bridge, heavy metal, terminal group, solubilising group and oligomerisation. Most of these materials showed poor optical limiting, especially in the red. Two dimers of Pt:ethynyl, however, have clamping levels at 532 nm better than that for Pt:ethynyl. I therefore describe a detailed spectroscopic investigation of two series of oligomers and discuss their structure/property relationships. This investigation also includes a precursor of Pt:ethynyl, PEPE, which shows remarkable limiting.

I also report modelling of optical limiting using a 5-level model constructed using the spectroscopic data. I show that the 5-level model can be validated and accurately predicts the limiting for PEPE against both ps and ns pulses. It can also be used to predict ps limiting for Pt:ethynyl and its oligomers. For ns pulses, however, it predicts much less limiting than that observed. I therefore propose a new mechanism that is important for ns limiting by TMAs.

Finally I discuss the broadband limiting of these materials and from analysis of the measurements I describe structures of materials that may show promising broadband optical limiting.

List of Symbols

Throughout this thesis, several symbols are used to signify specific physical quantities. For the readers convenience I have listed them below.

Alpha numeric

C	Concentration (mol/L)
f	Focal length of lens
I_0	Irradiance incident on the sample
l	Path length (usually a 2 mm cuvette)
N_A	Avogadro's number, 6.022×10^{23} molecules/mol
N_0	Number of molecules in ground state
N_T	Number of molecules in T_1
R	Surface reflectivity of a cuvette
S_0	Ground state energy level
S_1	First excited singlet state
T	Transmission (usually percentage)
T_1	Lowest excited triplet state
T^*	Excited triplet state
V	Volume

Greek

α	Linear absorption coefficient
β	Two-photon absorption coefficient
ε	Extinction coefficient
Φ	Diameter
λ	Wavelength
λ_{max}	Wavelength of an absorption/ emission maximum
σ_e	Excited state absorption cross section (cm^2/molecule)
σ_g	Ground state absorption cross section (cm^2/molecule)
τ_{S1}	Lifetime of lowest excite singlett state
τ_{T1}	Lifetime of lowest excite triplet state

List of Abbreviations

CRO	Cathode Ray Oscilloscope
DCE	Dichloroethane
DCM	Dichloromethane
ESA	Excited state absorption
FWHM	Full width half maximum
ISC	Intersystem crossing
IR	Infra Red
MPE	Maximum Permissible Energy
ND	Neutral density
OMA	Optical Multi-channel Analyser
OPO	Optical Parametric Oscillator
PEPE	Phenyl ethynylphenyl ethynyl
PMMA	Poly(methyl methacrylate)
RSA	Reverse Saturable Absorption
SiNc	Silicon(IV) bis(trihexylsilyloxide), 2,3 Naphthalocyanine
THF	Tetrahydrofuran
TMA	Transition Metal Acetylides
TPA	Two-photon Absorption
UV	Ultraviolet

Contents

1 Introduction

1.1. General Discussion

With the increasing use of lasers, there is a heightened potential for accidents causing blindness or damage to sensitive optics. The human retina, for example, can be permanently damaged by laser pulses as low as one microJoule [1]. Protecting the eye and sensitive visible-band optics against laser radiation that falls outside the visible part of the spectrum is relatively simple and can be achieved with the use of filters that block all transmissions at these wavelengths. Protecting against visible laser light (450-650 nm) without degrading visibility under normal viewing conditions is much more challenging [2],[3].

Lasers are capable of producing energy far in excess of the damage threshold of the human eye within nanosecond pulses. The human blink response is one quarter of a second, which is far too slow to protect against pulsed laser beams. The response time of an optical limiter needs to be less than the duration of the laser pulse and able to reduce the transmitted energy to below the maximum permissible energy.

It is expected that sensitive optics can be protected from dangerous laser beams using passive devices (optical limiters) that allow transmission of ambient incoherent light, but "switch on" and block laser radiation. However, optical limiters are still in the initial stages of design and have many drawbacks. For an optical limiter to be practical it needs to work fast enough to prevent the eye from receiving a dose of radiation higher than the ED_{50}. This is the energy for which there is a 50% chance of a small lesion on the back of the retina. It must cover all visible wavelengths, must not degrade, must be in a stable host medium and not hinder the user under normal viewing conditions. Many Organometallic

dyes are able to limit laser radiation to some degree, but most are not strong enough or do not cover a wide enough wavelength range to be practical.

This thesis investigates a class of materials that may be used as optical limiters. They are able to transmit ambient light while blocking high intensity laser radiation to some extent. While some of these materials show strong limiting at certain wavelengths, they often do not cover the entire visible spectrum. This thesis concentrates on measuring the optical limiting of several materials and measuring parameters needed to construct five-level models, which can be used to explain the limiting mechanism. From this information it is hoped that better optical limiting materials can be designed.

1.2. Current Laser Protection Technologies

Current limiting devices are very restricted in their applications and while they give the user some protection against pulsed laser radiation there are significant problems that need to be addressed. These devices fall into three broad categories [4],[5]:

- fixed-line filters,
- tuneable filters,
- optical limiters.

The features of these laser protection devices are summarised below.

1.2.1. Fixed-Line Filters

Traditional fixed-line filters are passive devices that work by selectively absorbing or reflecting unwanted wavelengths. Fixed-line filters are the only devices that can be designed to be effective against both damage and dazzle sources. However, they require

advanced knowledge of the threat wavelengths and are ineffective against wavelengths for which they have not been designed.

The best fixed-line filter technology at present is the tri-stimulus filter. These filters block the visible-near IR spectrum (400nm to 1500nm) with the exception of three narrow pass-bands; one in the 'red', one in the 'green' and the third in the 'blue'. It is only within these narrow bands that the user is at risk from laser radiation.

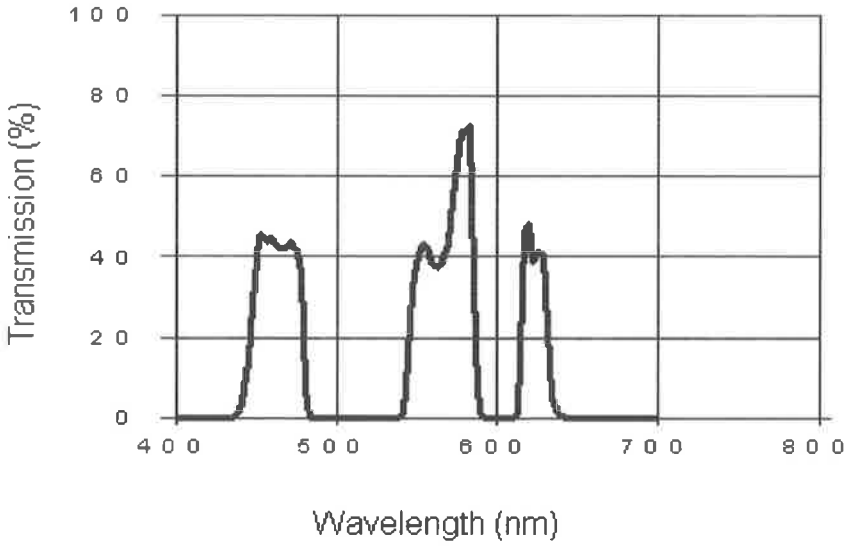

Figure 1-1: Transmission of a tri-stimulus filter produced by Pilkington Optronics for DSTO.

1.2.2. Tuneable Filters

Tuneable filters are active devices that determine the threat wavelength and adjust a filter (liquid crystal, comb, filter wheel, etc) as required to remove the unwanted radiation. These devices are an appropriate countermeasure against frequency-agile laser-dazzle sources but not against laser-damage sources due to their slow response time (in the order of milliseconds).

1.2.3. Optical Limiters

Optical limiters are passive devices whose limiting action is triggered by the intensity (or fluence) of the laser pulse. This limiting action is often achieved by Reverse Saturable Absorption (RSA), where the amount of energy absorbed increases as the laser fluence increases. In most of these materials the RSA is due to excited state absorption from an accessible long-lived singlet or triplet state. Their limiting can often be described by a "five-level" model, as discussed in section 1.3.4.

Several classes of organometallic dyes are able to act as optical limiters. These materials normally have:

- a high degree of unsaturated carbon bonds
- a linear or planar structure
- heavy atoms somewhere along the backbone.

Each of these components contributes to the material's ability to exhibit nonlinear absorption.

1.3. Historical Background of Optical Limiters

Since the invention of the laser in the early 60's, many groups have been investigating the use of organometallic dye molecules for optical limiting. Materials such as porphyrins, phthalocyanines and fullerenes have shown various degrees of optical limiting against visible pulses. Transition Metal Acetylides, TMAs, have been studied since the mid 1970s [6] when synthesis methods for these types of materials were first published [7]. I have concentrated on the properties of TMAs and their limiting mechanism is described in more detail in section 1.3.4.

1.3.1. Porphyrins

Porphyrins and closely related compounds are vital for many biological processes such as photosynthesis, and have been used as pigments for thousands of years. The molecule consists of four 'pyrrole-type' rings joined by four methine bridges. The structure of a zinc Porphyrin is shown in Figure 1-2.

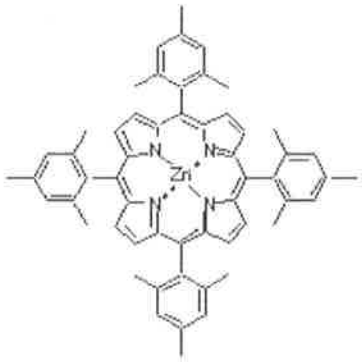

Figure 1-2: Molecular Structure of a teraphenyl zinc porphyrin

The central metal plays a significant role in the porphyrin limiting performance [8]. The ground state absorption spectrum of a porphyrin can be adjusted by altering the central atom and any side groups attached to the outer part of the molecule. However, to reduce the transmission of any threat laser to acceptable levels, porphyrin solutions are usually too highly coloured. Also, they usually have very poor performance in the red [9].

1.3.2. Phthalocyanines and Napthalocyanines

Phthalocyanines and napthalocyanines (Figure 1-4) have similar planar structures to porphyrins but with extra phenyl groups attached to the bridges. The best napthalocyanine to date is SiNc [10], shown in Figure 1-3, which has shown exceptional optical limiting behaviour when exposed to red or blue laser light [11]. Furthermore, the material is extremely stable, readily available and performs equally well in solid form (PMMA host).

The single largest drawback of SINC is its highly-coloured green appearance at the high concentrations required.

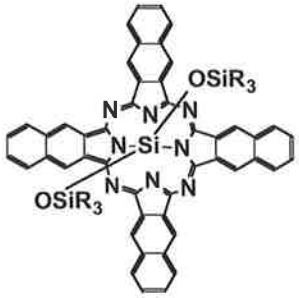

Figure 1-3: Structure of SiNc (Silicon, 2,3-naphthalocyanine bis(trihexylsilyoxide)).

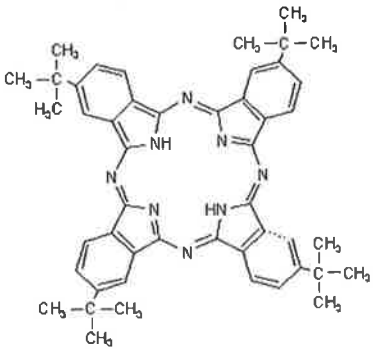

Figure 1-4: Structure of a phthalocyanine (2,9,16,23-Tetra-tert-butyl-29H,31H-phthalocyanine)

1.3.3. Fullerenes

Materials such as C_{60} (Figure 1-5) have been shown to exhibit optical limiting against nanosecond pulses at 532 nm [12]. C_{60} has a very flat ground state absorption spectrum resulting in little colouration and shows reasonable limiting behaviour [13], but has stability problems (albeit less than for Pt:ethynyl). Another major drawback to the use of C_{60} is its poor performance in solid hosts. A general rule of thumb is that the clamping levels of C_{60}/PMMA discs are twice as high as those of C_{60} in toluene solutions with the same photopic transmission [14],[15].

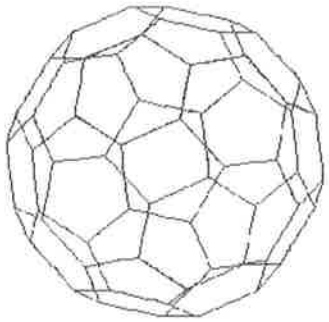

Figure 1-5: Structure of fullerene consisting of 60 carbon atoms linked together to form a truncated icosahedron, (C_{60}).

1.3.4. Transition Metal Acetylides (TMAs)

TMAs were first synthesised in the 1970s by Masai [16]. Since then there has been intense research into their nonlinear properties for optical limiting by many research groups [17], [18]. TMAs are one of the more promising classes of optical limiters and some have been found that limit strongly across much of the visible spectrum.

The TMAs I have investigated consist of a rigid backbone of highly conjugated atoms, usually phenyl and acetylide groups, although other ring structures such as thiophenes or napthalenes have been used. This backbone is interspersed with transition metals such as platinum or palladium. The high degree of conjugation allows electron delocalisation and the heavy metal increases spin-orbit coupling allowing the normally spin-forbidden triplet states to be accessed. High conjugation along the backbone delocalise the π-electron orbitals, lowering the energy gap to within the visible part of the spectrum. A direct S_0 to T_1 transition has been observed in several TMAs, which normally manifests itself as a shoulder in the ground state absorption spectrum, located approximately 100 nm red-shifted from the main peak (see absorption spectra in Chapter 2). The triplet manifold in these materials often consists of a long-lived (several μs) lower state, T_1 and much shorter lived higher energy states, T^*. If the energy gap between these two states is similar to that

of the incident laser photon energy then photons may be absorbed and reemitted in random phase and direction, reducing the transmitted energy.

A five-level model [14] is commonly used to describe the mechanism involved in optical limiting for TMAs. It includes the ground state (S_o), the first two excited singlet states (S_1 and S_2) and two excited triplet states (T_1 and T^*) as shown in Figure 1-6.

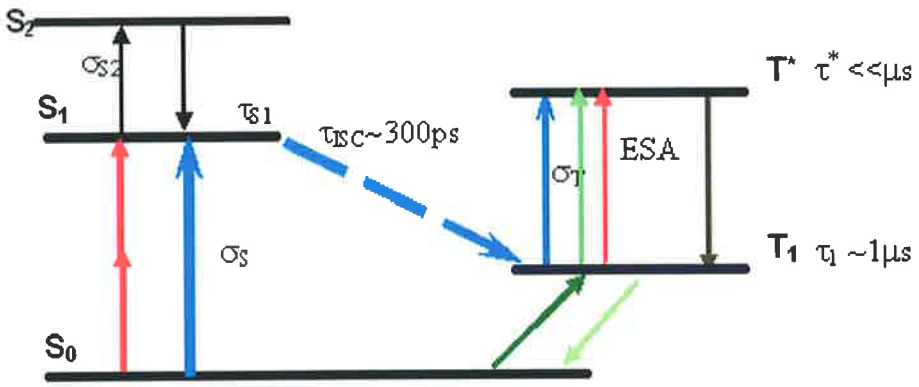

Figure 1-6: Diagram of the five-level model, showing absorption to the first excited singlet state (σ_S), Intersystem crossing (ISC) to the first excited triplet state (T_1) and then absorption to higher triplet states (σ_T).

An incoming photon of appropriate energy interacts with the ground state (S_0), exciting the molecules to one of the many vibration states within S_1. The molecule decays back to the ground state by two possible pathways,

1. radiative or non-radiative decay back to the ground state,
2. via intersystem crossing to the triplet state, (T_1).

For materials with strong spin-orbit coupling the second pathway can become the dominant decay mechanism, this leads to possible Excited State Absorption (ESA) if the gap between two triplet states (T_1 and T^*) is similar to the incoming laser photon energy. In principle S_1 to S_2 excited state absorption is possible, but does not contribute significantly

to nanosecond limiting in TMAs as the S_1 lifetime is less than 300 ps. Furthermore, since no limiting at 532 nm is observed in many TMAs for 30 ps pulses, it appears that either there is no transition available at 532 nm or that the S_2 lifetime is greater than 30 ps.

Many research groups have investigated the spatial extent of the lowest singlet and triplet states. It is generally accepted that while the singlet state is delocalised along much of the backbone [19], the triplet state is often confined to a small region of the molecule [20],[21],[18].

Investigations into the choice of spacer group inserted into the backbone have shown that it affects not only the singlet energy levels, but also the intersystem-crossing rate. However it has little effect on the singlet-triplet energy gap [20],[22].

DSTO Edinburgh in Adelaide has previously investigated the optical limiting performance of Pt:ethynyl [23], the structure of which is shown in Figure 1-7. Pt:ethynyl shows strong optical limiting, particularly at 532 nm however it has several draw backs, predominantly poor UV stability and solubility.

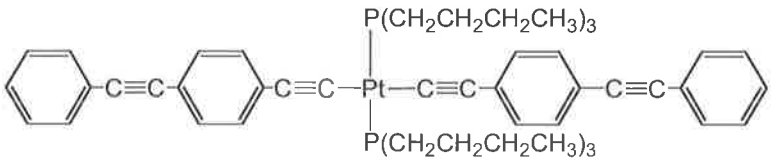

Figure 1-7: Structure of Pt:ethynyl, Bis((4-(phenylethynyl)phenyl) ethynyl) bis-(tributylphosphine) platinum(II)

For certain limiters absorption mechanisms are not uniform across the entire visible spectrum. With reference to Figure 1-6, it can be seen that S_0 to S_1 transitions can occur by

either one photon absorption in the blue or simultaneous Two-Photon Absorption (TPA) in the red [24].

Studies on Pt:ethynyl have shown that for this material there are three wavelength dependant excitation pathways from the ground state to the lowest triplet state:

- For wavelengths less that 500 nm, direct S_0 to S_1 absorption followed by almost complete, rapid intersystem crossing into T_1
- Between 500 and 540 nm, direct absorption from S_0 to T_1
- For wavelengths between 540 nm and 700 nm, two photon absorption from S_0 to S_1 followed by almost complete, rapid intersystem crossing into T_1

While Pt:ethynyl shows strong optical limiting across most of the visible spectrum, it suffers in the red, and for a practical application would require mixing with another limiter with much stronger limiting in this region.

1.4. Thesis Overview

While a considerable amount of research has been done into broadband optical limiting, there is still little understanding of the effects of individual components of the molecular structure on optical limiting. I have attempted to measure the effect of structural change on optical limiting by studying materials structurally similar to Pt:ethynyl.

Chapter 2 describes in more detail the theoretical background and the desired characteristics of an ideal limiter, the optical limiting test-bed and optical limiting results of the TMAs measured. Since there are several factors that might affect the optical limiting, I have measured the broadband optical limiting against nanosecond pulses for a wide range of TMAs. Some of the structural changes that I have studied include:

- central heavy atoms
- molecular length
- number of arms
- choice of solubilising groups
- terminal group (electron donator or withdrawer)
- choice of spacer.

Work has focused on determining which TMAs exhibit optical limiting and whether they can be used to achieve a clamping level below 1 μJ for a 70 % linear transmission at 532 nm. From these limiting results a short list of two sets of oligomers of Pt:ethynyl and a precursor, [4-(phenylethynyl)phenylethyne], PEPE, were chosen for detailed spectroscopic analysis. The two sets of oligomers differed by a terminal-acetylide group. While this was initially thought to only have a small impact on the energy level, structure and limiting, experimental and theoretical results proved otherwise.

In Chapter 3, I provide details of the spectroscopy experiments used to measure:

- luminescence spectra
- S_1 and T_1 lifetimes
- intersystem crossing rates
- single-photon absorption cross sections
- two-photon absorption cross sections.

Results of these experiments on the oligomers and PEPE are presented and briefly discussed in Chapter 4.

In Chapter 5 I use a computer model of the optical limiting testbed to investigate the effects of the parameters in 5-level model presented in Figure 1-6.

The predictions of this model are then compared with the measured limiting obtained for PEPE and both sets of oligomers for ns pulses in Chapter 6. As indicated above, an interesting pre-cursor material, PEPE, was also characterised. Response theory modelling of PEPE was performed by an associate using the DALTON quantum chemistry program. Results discussed in Chapter 6 show that PEPE consists of closely matched S_1 and T^* states. This facilitates singlet-triplet crossing, despite the absence of a heavy platinum atom, and results in a much longer T_1 lifetime and significant optical limiting. The structure of PEPE and its limiting are well described by the 5-level model, and thus PEPE can be used to validate the 5-level model.

I also discuss the spectroscopic measurements of the oligomers in more detail, and look at the common features of the most promising optical limiters. I will show that the optimum TMA has two platinum atoms and a terminal phenyl group. Several materials that fit this general description show promising optical limiting across the visible spectrum.

While I report the optical limiting performance of materials at 470, 532 and 630 nm in Chapter 2, much of my research is centred on understanding the limiting at 532 nm. In Chapter 7, however, I summarise the results and discuss the requirements for broadband optical limiting. I also discuss some future work that could be done to increase our understanding of these materials.

2. Optical Limiting of TMAs

As indicated in Section 1.3, the optical limiting of a large number of Pt:ethynyl-related TMAs was measured using a standard f/5 test-bed, which will be described in Section 2.1. In Section 2.2, I will discuss measurements, which are reported in Section 2.3, using Pt:ethynyl as a benchmark.

2.1. Optical Limiting Test-Bed

Optical limiting was measured using the standard f/5 test-bed [24], [25] shown in Figure 2-1. A similar test-bed has been used by several groups, [26], [17], [27], [28] as it mimics the optics of a human eye looking though a typical military optical sight of magnification 2.5 and f/5 aperture, and allows easy comparison with other optical limiting materials.

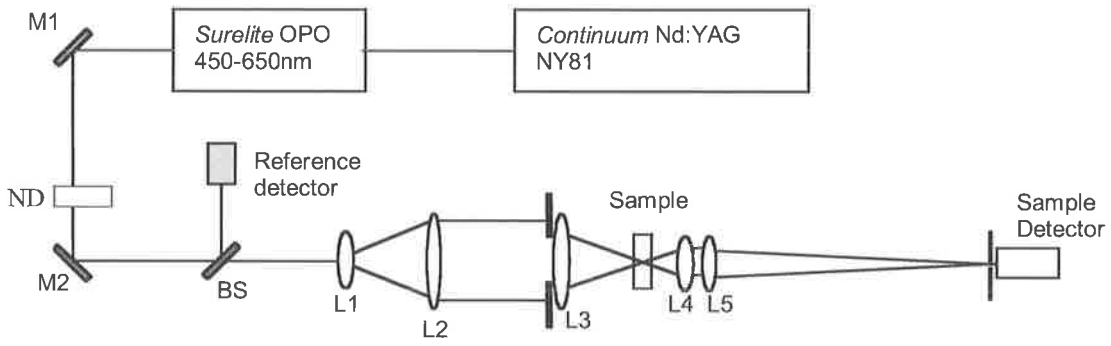

Figure 2-1: Optical limiting test-bed. M1 and M2 are mirrors, BS is a beam splitter and ND is two neutral density filter wheels.

The test-bed consists of a Continuum frequency-tripled Nd:YAG laser operating at 2 Hz pulse repetition and 6 ns (HW1/eM) pulse width, which pumps a Surelite Optical Parametric Oscillator (OPO). Laser wavelengths in 20 nm increments between 450 and

650 nm were used for the measurements, with the exception of 532 nm instead of 530 nm as this is the wavelength of a frequency doubled Nd:YAG laser.

The OPO output is reflected from mirror (M1) before passing through two neutral density filter wheels (ND) which attenuate the pulse energy to between 1 and 200 μJ, before being reflected from second mirror (M2). A beam splitter (BS) directs a small amount of energy into a reference detector. The transmitted beam is expanded using lenses L1 and L2, before passing through an aperture, creating a top-hat beam. Lens L3, then focuses the top-hat to a 200 μm diameter spot within the sample, which is in a 2 mm cuvette. The light transmitted through the sample is collimated by lens L4 and focused onto the sample detector by lens L5. The aperture at the detector is approximately 0.5 mm.

The two detectors were calibrated by recording their readings for various neutral density filters without a sample in position. This calibration factor was used to determine the energy of the pulse that would have been incident upon the sample detector in the absence of the limiter. A plot of transmitted energy against incident energy was then plotted at each wavelength to obtain a clamping level value, as shown in Figure 2-3. Calibration of the test-bed detectors using no sample, rather than a cuvette filled with solvent, means that the incident energy will always be slightly less than that calculated using the calibration factor, as it will not take into account reflection losses from the cuvette faces. While this would create a systematic error in the calculated transmission, it will have no effect on the comparison of the observed clamping levels reported in this chapter.

2.2. Optical Limiting and Pt:Ethynyl Benchmark

All of the TMAs I studied have similar ground state absorption spectra to that shown for Pt:ethynyl in Figure 2-2 and 2-3, with a strong absorption maximum in the blue/UV region

(380 nm for Pt:ethynyl). Some TMAs also have a "shoulder", usually located around 500 nm (520 nm for Pt:ethynyl) associated with the spin-forbidden S_0 to T_1 transition. The ground state absorption of materials in subsequent sections will therefore be characterised by the wavelength of the absorption maxima (λ_{max}) and the wavelength and strength of any shoulder. The linear transmission values quoted throughout this thesis were obtained using a spectrometer unless otherwise stated.

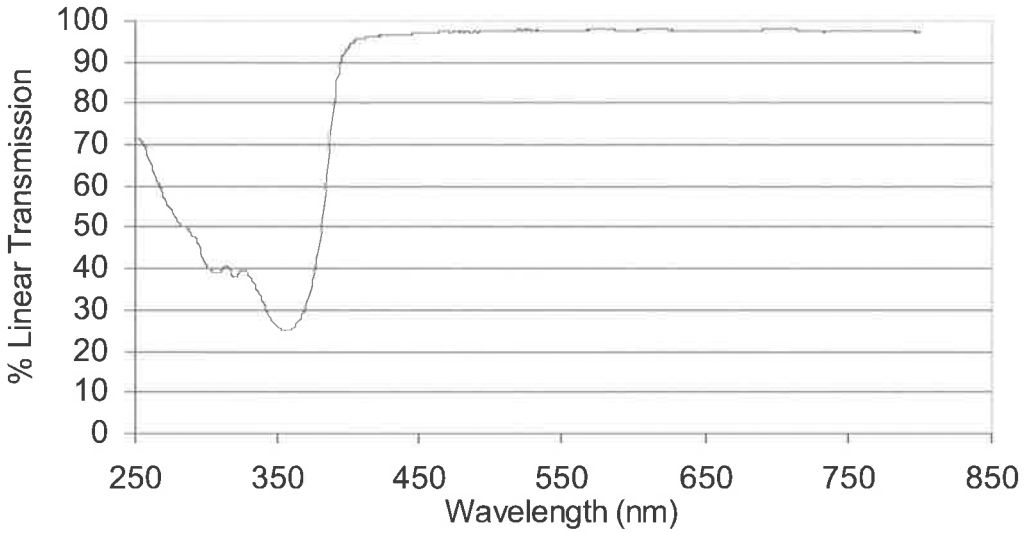

Figure 2-2: Transmission spectrum of a dilute Pt:ethynyl solution in DCE.

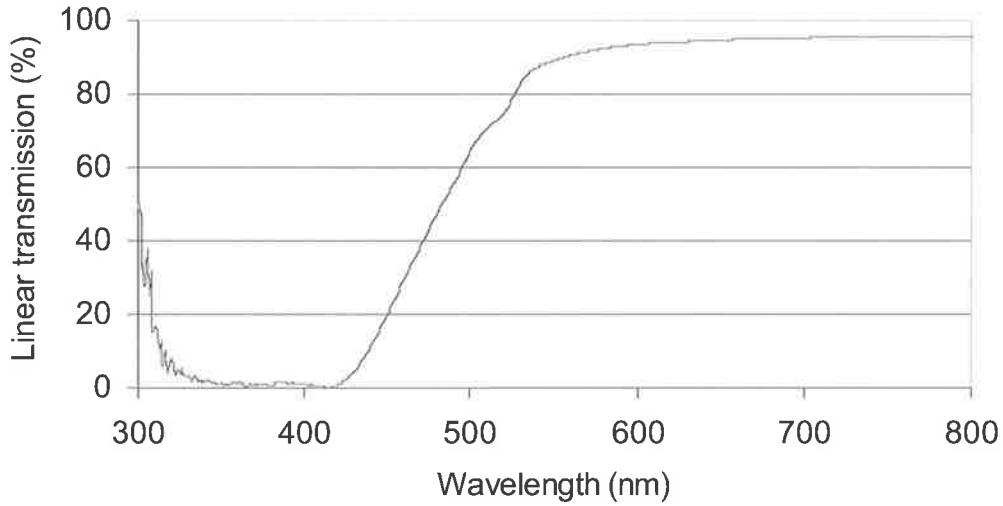

Figure 2-3: Transmission spectrum of a concentrated Pt:ethynyl solution in THF.

For small incident energies, the transmitted energy is proportional to the incident energy. As the incident energy increases, the transmitted energy levels off and clamps, as shown in

Figure 2-4. At very high incident energy levels the sample is damaged causing black deposits to form on the cuvette face.

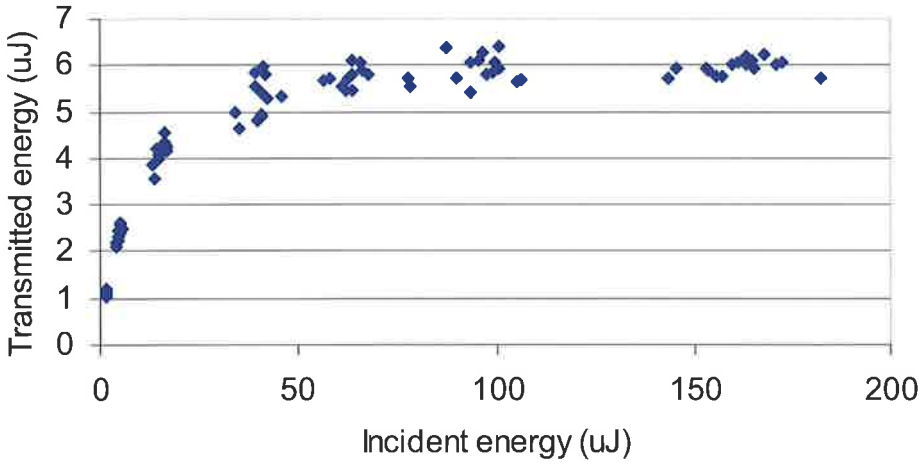

Figure 2-4: Transmitted energy as a function of incident energy at 532 nm for a Pt:ethynyl solution with 94 % linear transmission at 532 nm.

A plot of the clamping level for Pt:ethynyl as a function of linear transmission at 532 nm (Figure 2-5), shows that clamping level increases semi-logarithmically as the linear transmission increases.

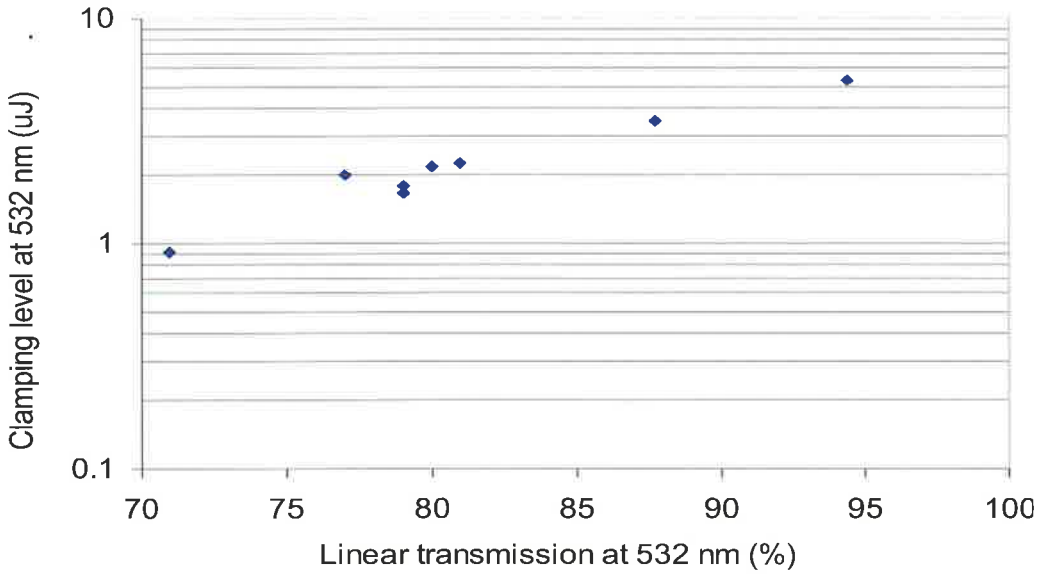

Figure 2-5: Clamping level at 532 nm as a function of linear transmission at 532 nm for Pt:ethynyl solutions.

The ideal optical limiter has a low clamping level and high linear transmission at 532 nm, placing it in the bottom right corner of Figure 2-5. It also provides broad-band protection, with low clamping levels and high linear transmission across the visible part of the spectrum.

A plot of the clamping level at 532 nm against linear transmission at 532 nm for materials from different classes of optical limiters is shown in Figure 2-6. Of the five materials shown, Pt:ethynyl shows superior optical limiting, so I have concentrated my research on TMAs.

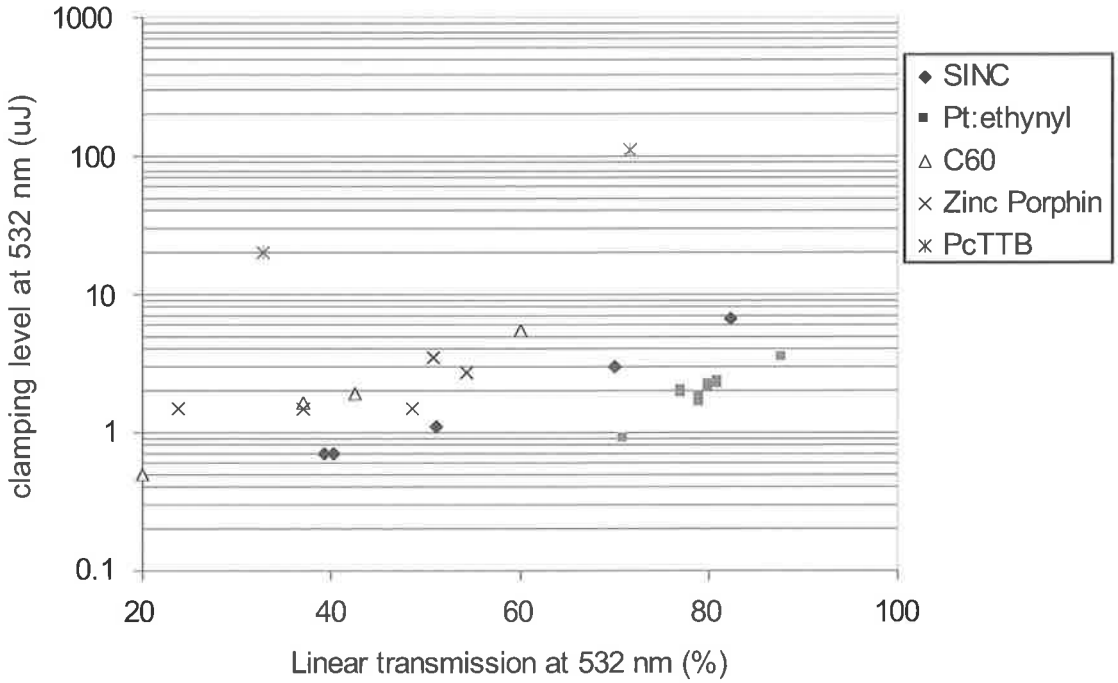

Figure 2-6: Clamping level at 532 nm as a function of percentage linear transmission at 532 for different classes of optical limiters.

The wavelength dependence of the clamping level for a Pt:ethynyl solution is shown in Figure 2-7. Strong limiting in the blue, where there is strong linear absorption and weaker

limiting in the red, where there is little, if any linear absorption is normally observed in TMAs as the optical limiting follows the linear absorption spectrum.

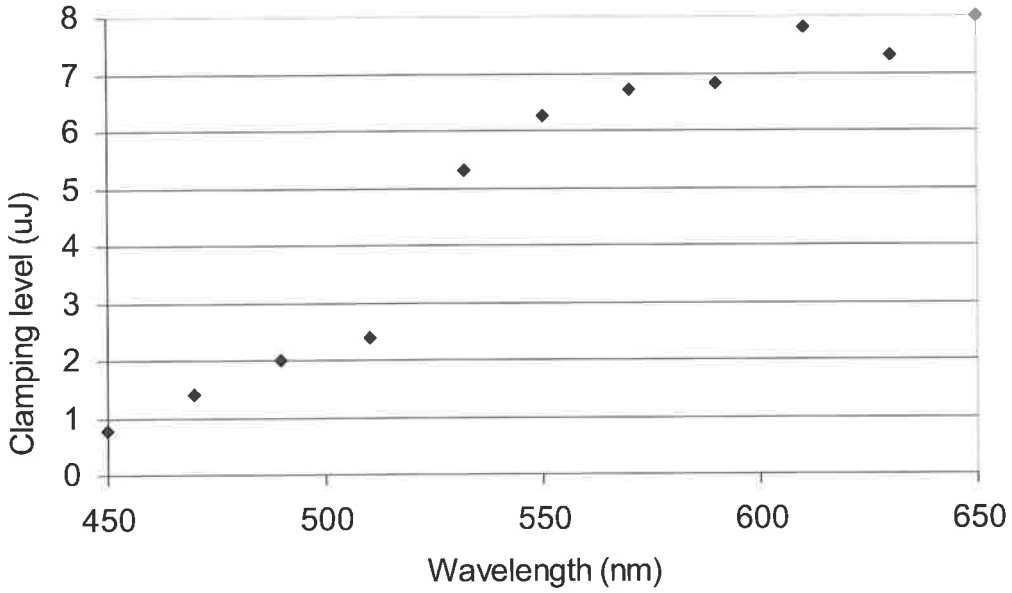

Figure 2-7: Wavelength dependence of the clamping level of a DCE solution of Pt:ethynyl (94 % transmission at 532 nm).

I have concentrated much of my work at 532 nm as this is both in the centre of the visible spectrum and a technologically significant wavelength. However, I also present clamping levels at 470 nm and 630 nm to give an indication of limiting in the blue and red regions of the spectrum. All clamping levels will be plotted against the linear transmission at 532 nm, as this is defined by the sample concentration but is more significant than concentration in any practical limiting application. In a diffraction limited system the intensity at the focus in the sample is proportional to $1/\lambda^2$, and thus one would expect the clamping level to be proportional to λ^2. `However, the observed dependence is much stronger, implying that other factors such as stronger linear absorption at shorter wavelengths are more important.

In a final application it is likely that "photopic transmission" may be used as the independent variable. Photopic transmission is the weighted average of the limiter

transmission across the spectral response region of the sensor. For most TMAs the photopic transmission is approximately 2 or 3 % less than the linear transmission at 532 nm.

2.3. Optical Limiting of TMA Materials

The molecular structures of the materials investigated are shown in Appendix A[1]. The materials tested have been divided into groups of similar structure. The materials studied are based on Pt:ethynyl, with each group having a small but significant alteration to the structure:

- Altering the heavy metal used (Section 2.3.1),
- Altering the solubilising group (Section 2.3.2),
- Using electron donors or withdrawers in the terminal position (Section 2.3.3),
- Altering the number of repeat units to form oligomers (Section 2.3.4),
- Altering the spacer used in a series of polymers (Section 2.3.7),
- Altering the number of arms. (Section 2.3.8).

Ground state absorption properties and the optical limiting at 470, 532 and 630 nm is presented for each group. I also studied two materials that have similar lengths to those materials that showed promising limiting, as reported in Section 2.3.5, and a precursor of Pt:ethynyl, PEPE, which is reported in Section 2.3.6.

2.3.1. Effect of Altering the Metal

It is well known that heavier metals increase the spin-orbit coupling [29], but it was not initially known how this would affect the optical limiting. A series of polymers using

1

nickel, palladium or platinum as the metal, M, as shown in Figure 2-8, were tested. Only group VII metals were used as they have the same number of electrons in the outer shell leading to similar square planar structures. The ground state absorption spectra features for these polymers are listed in Table 2-1 and the wavelength dependence of the clamping levels is shown in Figure 2-9.

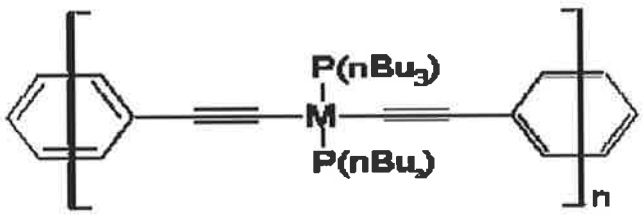

Figure 2-8: Structure of Polymers with different metal, M is Ni, Pd or Pt.

Material	λ_{max} (nm)	Shoulder	Shoulder wavelength (nm)
M=Ni	331	none	-
M=Pd	349	none	-
M=Pt	360	strong	504

Table 2-1: Ground state absorption properties of polymers with different metals.

Linear transmissions at 532 nm for saturated solutions of the Ni, Pd and Pt polymers are 65, 87, and 69 percent respectively. The ground state absorption spectra for these materials show strong absorption in the UV with little absorption elsewhere. Only the platinum polymer showed signs of a shoulder, indicating significant spin-orbit coupling. This is expected, as platinum is the heaviest of the metals investigated.

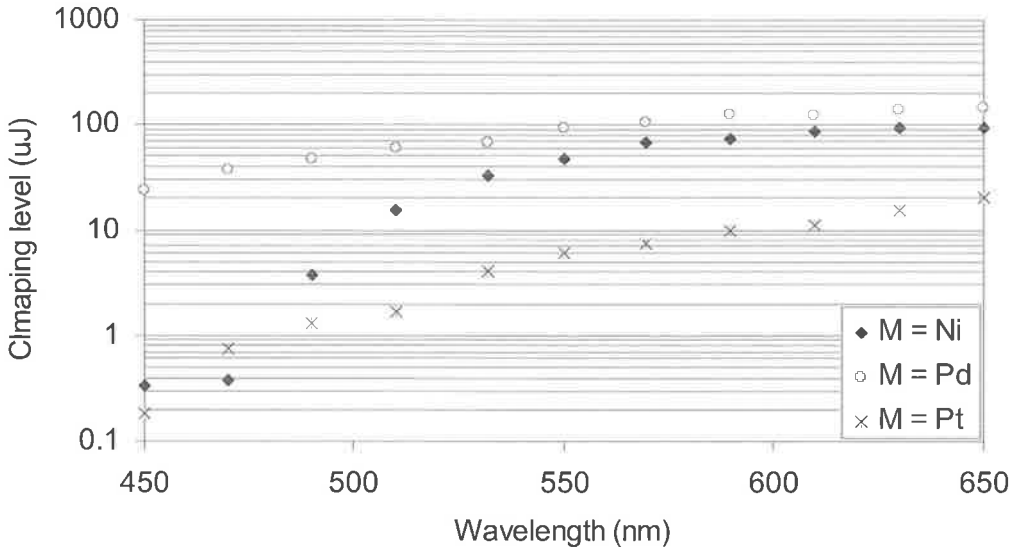

Figure 2-9: Clamping level as a function of wavelength for Ni, Pd and Pt polymers. (Linear transmissions at 532 nm are 65%, 87% and 75% for Ni, Pd and Pt polymers.)

It can clearly be seen from Figure 2-9 that the platinum material has superior limiting. The platinum polymer has a higher linear transmission than the nickel polymer yet has clamping levels up to 8 times lower. The palladium polymer has even higher clamping levels, although it should be noted that its linear transmission at 532 nm is 87 %.

A plot of clamping level at 532 nm against linear transmission at 532 nm (Figure 2-10) shows that the platinum material has a much better clamping level for a given transmission at 532 nm. These results reinforce the general understanding that platinum is the best of the group VII metals for optical limiting as it is heaviest and thus produces the largest spin-orbit coupling. An increase in spin-orbit coupling results in a more accessible triplet manifold, which is a key component in optical limiters.

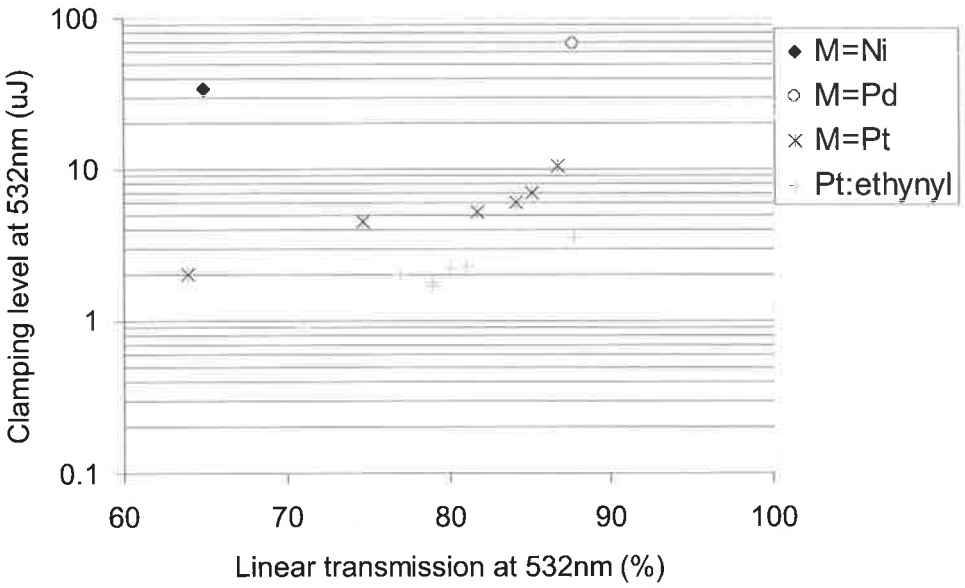

Figure 2-10: Clamping level as a function of linear transmission for the metal polymers and Pt:ethynyl.

2.3.2. Pt:Ethynyl with Different Solubilising Groups

Altering the solvent in which an optical limiter is dissolved can have a large effect on the clamping level [30],[29] as discussed further in Section 2.4. I thus expected that changing the solubilising group attached to the platinum atom might have a similar effect. Furthermore changing the solubilising group may improve the solubility of Pt:ethynyl, thereby solving its poor solubility problem. All these materials were dissolved in chloroform with the exception of R=P(n-Bu_3) material which was dissolved in Dichloroethane (DCE).

For convenience the structure of Pt:ethynyl is shown again in Figure 2-11. The Pt:ethynyl investigated by Staromlynska [25] and has R=P(n-Bu_3).

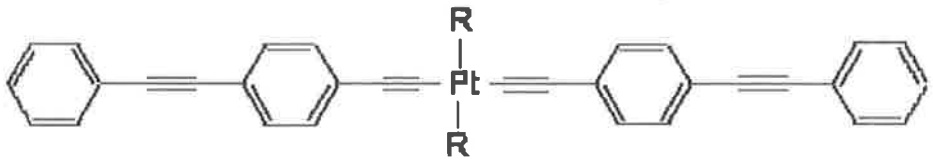

Figure 2-11: Structure of Pt:ethynyl with solubilising groups R=P(n-Bu3), R=Ph2Me, R=PMe2Ph, R=P(m-tol), R=PEt3 and R=PPh3.

The ground state absorption features of these materials are listed in Table 2-2 and the clamping levels at 532, 470 and 630 nm are shown in Figures 2-12 to 2-14.

R group	λ_{max} (nm)	Shoulder Strength	Shoulder wavelength (nm)
PPh_2Me	347	Weak	506
PMe_2Ph	313	Very weak	414
$Pet_{3\neq}$	-	-	-
PPh_3	371	None	-
P(m-tol)	316	Very strong	365
P(n-Bu_3)	380	Strong	520

Table 2-2: Ground state absorption properties of Pt:ethynyl with different solubilising groups.

The ground state spectra show strong absorption in the UV with λ_{max} values between 313 and 380 nm. As is the case for most TMAs, there is negligible absorption in the visible, although there are strong shoulders for both the P(n-Bu_3) and P(m-tol) materials and a small shoulder for PPh_2Me and PMe_2Ph, with no visible shoulder observed for PPh_3.

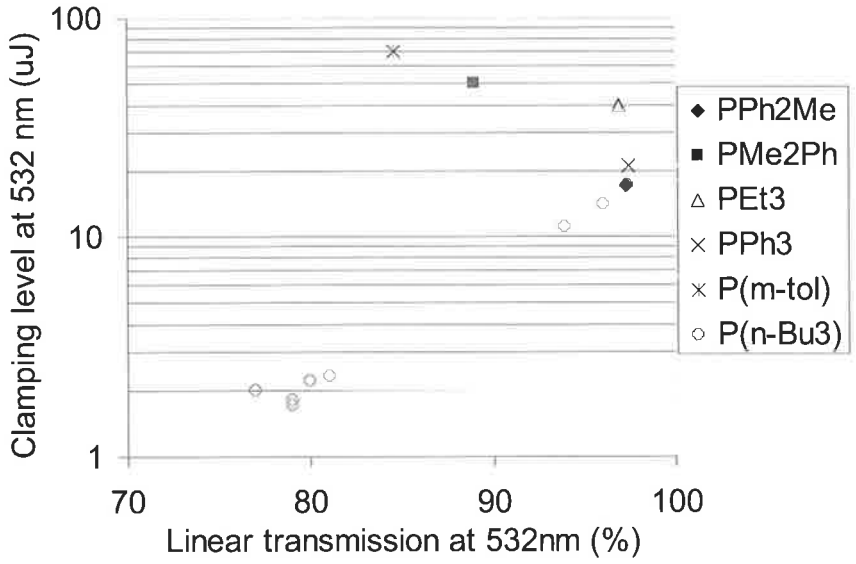

Figure 2-12 : Clamping level at 532 nm as a function of linear transmission at 532 nm for different solubilising group materials.

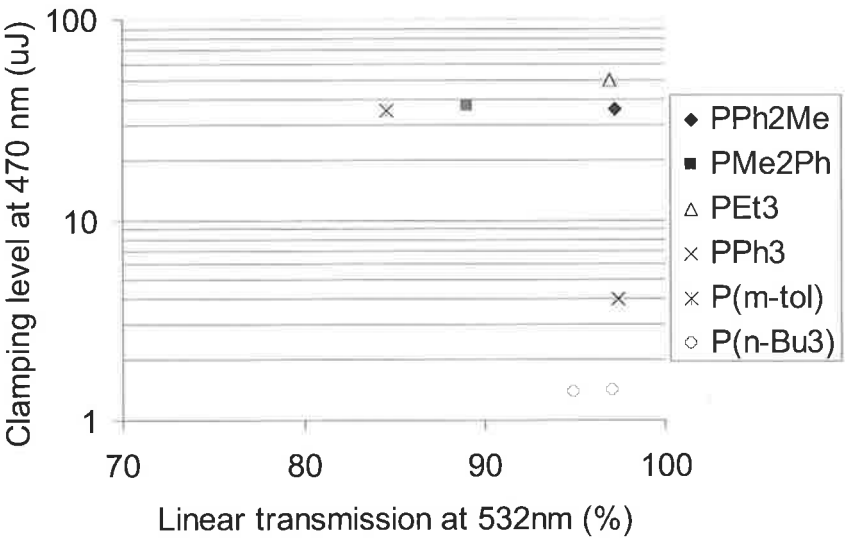

Figure 2-13 : Clamping level at 470 nm as a function of linear transmission at 532 nm for different solubilising group materials.

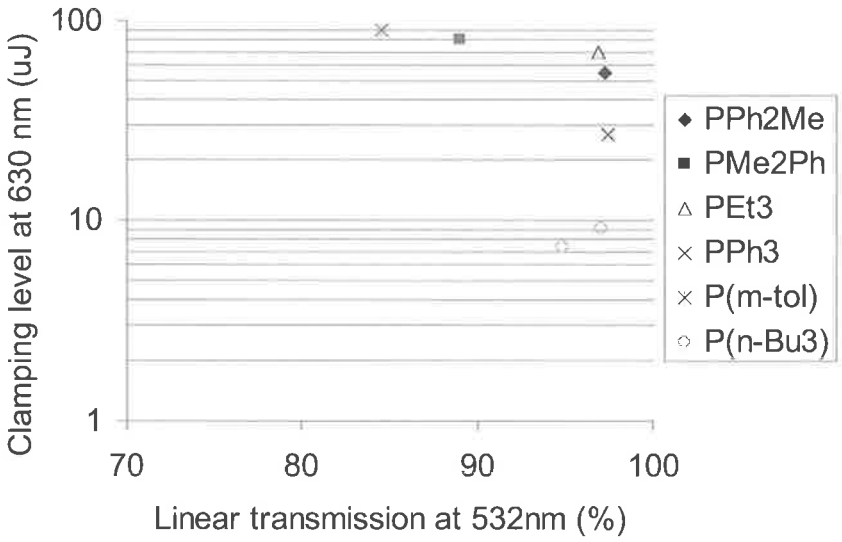

Figure 2-14 : Clamping level at 630 nm as a function of linear transmission at 532 nm for different solubilising group materials.

At 532 nm, only the PPh_2Me and PPh_3 materials show comparable clamping values to the P(n-Bu_3) material. Since PPh_2Me shows some signs of a shoulder at 506 nm, it is perhaps unsurprising that this material shows better limiting at 532 nm than most of the other materials. However, it is interesting that PPh_3 shows good limiting although no shoulder was observed. The population of the triplet states may be due to fortuitous alignment of energy levels enabling intersystem crossing in the absence of apparent spin-orbit coupling.

At 470 nm, as Figure 2-13 shows, the PPh_3 still shows comparable limiting to P(n-Bu_3), while the other materials perform much worse.

It is notable that the material with the strongest shoulder, P(m-tol), is the poorest limiter, even at 630 nm where one might have expected two-photon absorption to provide a pathway into S_1. (Recall that two-photon absorption is an important process in limiting in Pt:ethynyl at 630 nm.) Whether this degraded limiting is due to a disruption of the inter-system crossing, a decreased T_1 lifetime and/or a decreased excited state cross-section is

unclear. At 630 nm only P(n-Bu_3) shows appreciable limiting, indicating that the two-photon absorption for the other solubilising groups has decreased significantly.

None of the materials with different solubilising groups come anywhere near being as good as the original P(n-Bu_3) materials and so have not been studied further. Figure 2- 12 shows that for solutions of maximum solubility, modified solubilizing groups have higher linear transmission at 532 nm. This indicates that the solubility has actually decreased.

2.3.3. Pt:Ethynyl with Different Terminal Groups

Optical limiting occurs in materials that have highly conjugated bonds and thus expected to be strongly affected by electron delocalisation. It was expected that by terminating the backbone with electron donors (CO_2Me, OH, I and NH_2), as shown in Figure 2-15, the electron delocalisation might increase. This may affect the energy of the excited states, (causing a red shift of the absorption maxima) which would affect the intersystem crossing and absorption cross sections. The effect of an electron withdrawing terminal group, (NO_2) was also tested. All materials were dissolved in dichloromethane (DCM).

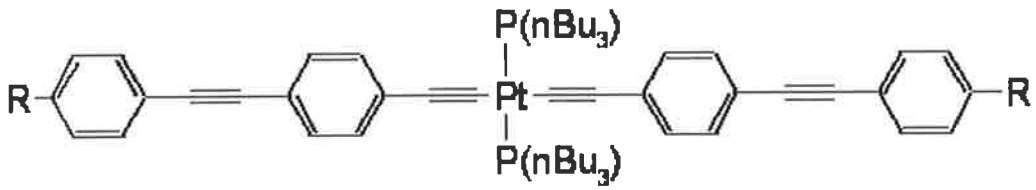

Figure 2-15: Pt:ethynyl with electron donating (R=OH, NH2, I, CO2Me) and withdrawing, R=NO_2 terminal groups.

The ground state absorption spectral features are shown in Table 2-3 and the clamping levels at 532, 470 and 630 nm are shown in Figures 2-16 to 2-18.

The ground state spectra show absorption maxima ranging from 336 nm for R=NH_2 to 394 nm for R=OH and are not in the predicted locations. All materials show very little absorption elsewhere in the spectrum. Only the R=H, CO_2Me and NH_2 materials show any shoulder and those of CO_2Me and NH_2 are very weak.

R group	λ_{max} (nm)	Shoulder strength	Shoulder wavelength (nm)
H	380	strong	520
CO_2Me	357	Very weak	685
I	367	none	-
OH	394	none	-
NH_2	336	Very weak	405
NO_2	367	none	-

Table 2-3: Ground state absorption properties of Pt:ethynyl with electron donor or withdrawer terminal groups.

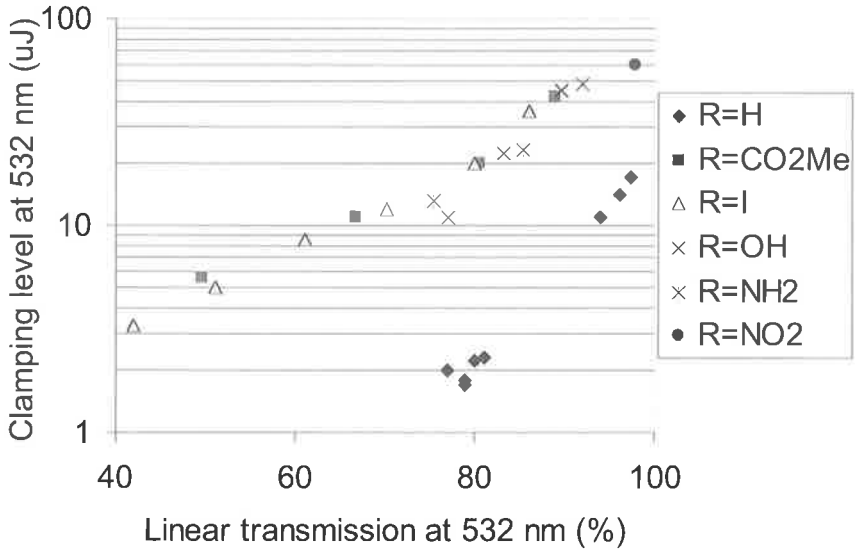

Figure 2-16: Clamping level at 532 nm as a function of linear transmission at 532 nm for various electron donating and withdrawing terminal groups.

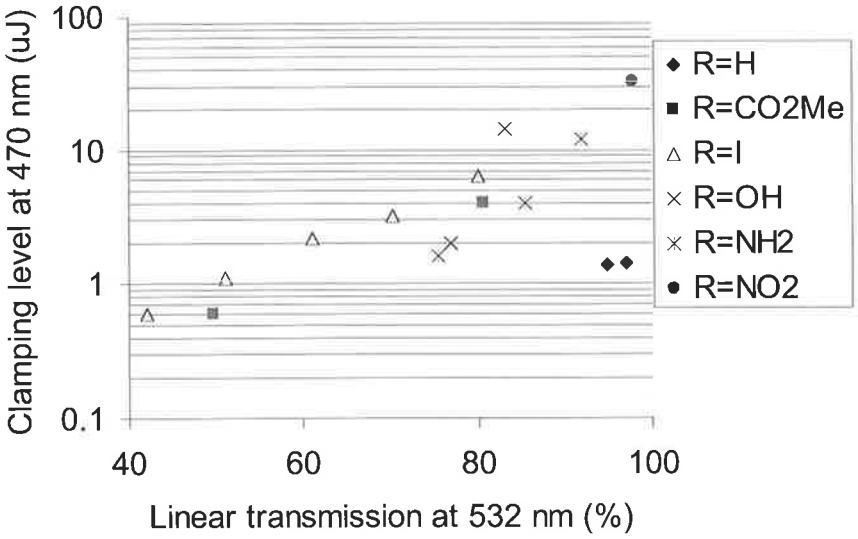

Figure 2-17 Clamping level at 470 nm as a function of linear transmission at 532 nm for various electron donating and withdrawing terminal groups.

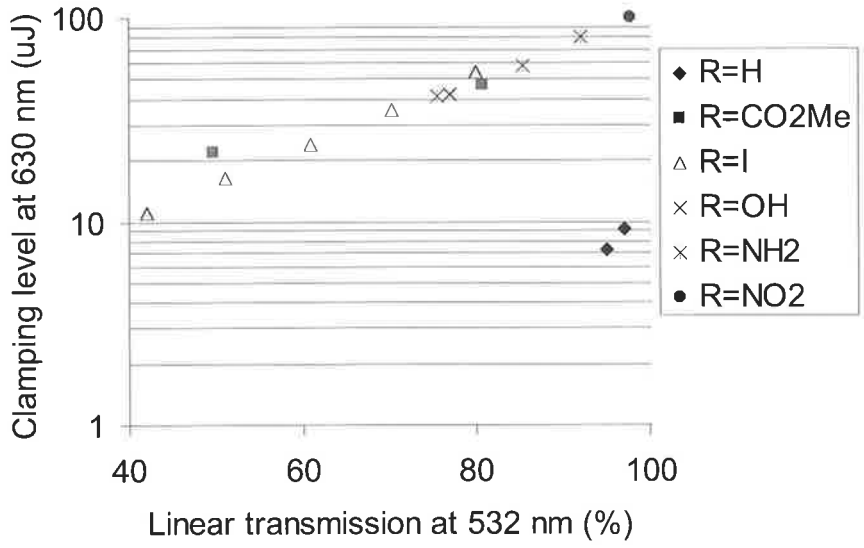

Figure 2-18: Clamping level at 630 nm as a function of linear transmission at 532 nm for various electron donating and withdrawing terminal groups.

Clamping levels at 532 and 630 nm consist of roughly two lines, one for the neutral R=H material and another for all the other terminal groups. It is surprising that all these materials lie along the same line as it implies that the energy level structure for Pt:ethynyl is special and these groups disrupt it. Also, all of the modified terminal group materials show significantly worse limiting at 630 nm than the original R=H group, indicating a

decrease or possibly absence of two-photon absorption at longer wavelengths for altered terminal group materials.

At 470 nm there is much more spread in clamping levels than was observed at 532 nm, again the R=H is the best material. R=NH_2 shows some improvement over the other materials but is still very poor. It is clear that adding electron donors or withdrawers in the terminal position does not improve the limiting at any wavelength.

2.3.4. Oligomeric Compounds of Pt:Ethynyl

Two sets of oligomers were tested, one with terminal-phenyl groups and another with terminal-acetylide groups, as shown in Figure 2-19. The effect of both the overall molecular length and the additional terminal-acetylide group was investigated. These oligomers proved to be very interesting and were studied further to determine the parameters required for the five level models, (see Chapters 3 and 4 for more details). Due to synthesis problems the tetramer and pentamer of the terminal-acetylide oligomers were not produced. All of these materials were dissolved in DCE.

Figure 2-19: a) Terminal-phenyl oligomers. b) Terminal-acetylides oligomers.

As discussed in Chapter 1, the ideal optical limiter has a broad ground-state absorption in the visible with a much stronger excited-state absorption cross section. Increasing the effective conjugation length red-shifts and broadens both the ground-state and excited-state absorption maxima [31]. Further, while the singlet state is usually delocalised along much

of the molecule, the triplet state is localised to only a few repeat units [22]. This would suggest that increasing the number of repeat units past the number across which the triplet states extends should have a stronger effect on the singlet states than on the triplet states.

2.3.4.1. Oligomers with Terminal-Phenyl Groups

The ground state absorption spectral features are listed in Table 2-4 and the clamping levels at 532, 470, and 630 nm are shown in Figures 2-21 to 2-23. Figure 2-20 shows the change of λ_{max} and shoulder wavelength with number of repeat units.

n	λ_{max} (nm)	Shoulder strength	Shoulder wavelength (nm)	Clamping level ranking at 532 nm
1	336	weak	482	3
2	359	weak	505	1
3	362	weak	507	2
4	364	weak	509	4
5	370	weak	511	5

Table 2-4: Ground state absorption properties for terminal-phenyl oligomers.

The ground absorption state spectra of the oligomers show absorption peaks located between 330 and 370 nm and signs of a weak shoulder near 500 nm. These features red shift as the number of repeat units increases as expected. Figure 2-20 illustrates that the decrease in energy gap is inversely proportional to the number of repeat units squared as observed by Liu et al[31]. The clamping level ranking is based upon the clamping level at 532 nm.

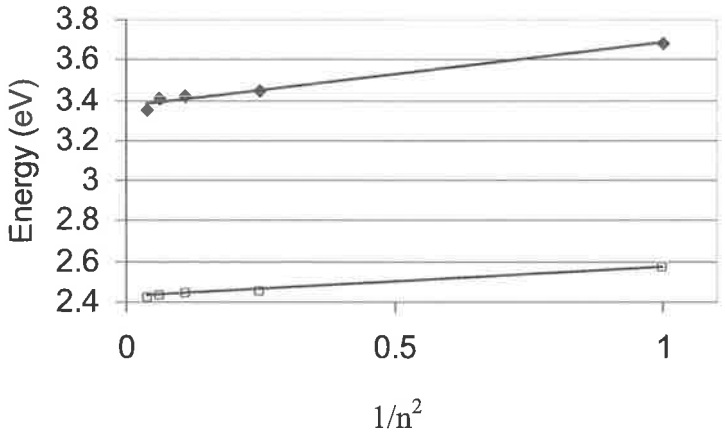

Figure 2-20: Transition energy gap against the inverse square of the number of repeat units. ♦ is the S_0 to S_1 energy gap, □ is the S_0 to T_1 energy gap.

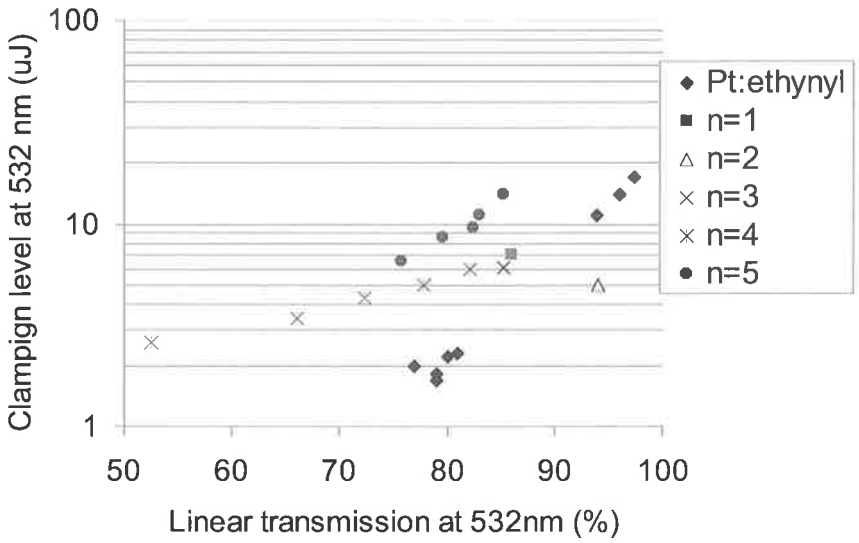

Figure 2-21: Clamping level at 532 nm as a function of linear transmission at 532 nm for terminal-phenyl oligomers.

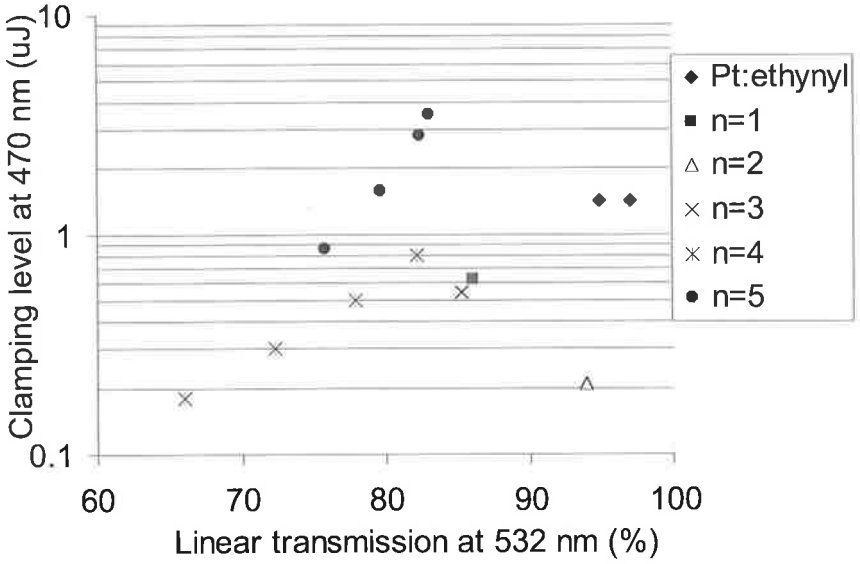

Figure 2-22: Clamping level at 470 nm as a function of linear transmission at 532 nm for terminal-phenyl oligomers.

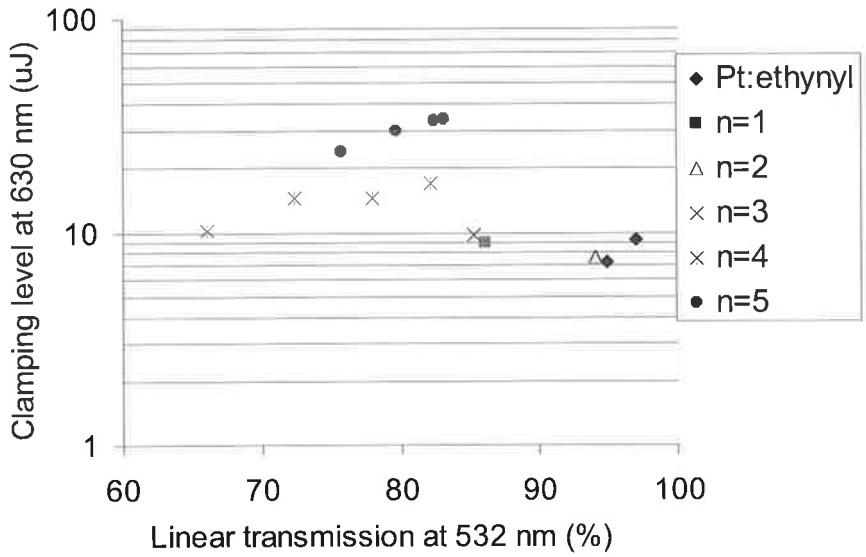

Figure 2-23: Clamping level at 630 nm as a function of linear transmission at 532 nm for terminal-phenyl oligomers.

The dimer has a significantly lower clamping level than Pt:ethynyl at 470 nm and 532 nm, but slightly higher level at 630 nm. The improved limiting at 532 nm is perhaps the more surprising feature given that the S_0 to T_1 absorption shoulder, is much weaker and occurs at a shorter wavelength than for Pt:ethynyl. This would suggest that the presence of a

shoulder indicates triplet state accessibility and the location and strength of the shoulder are not important.

It is also notable that the limiting of these oligomers at 630 nm is worse than for Pt:ethynyl. Recall that two-photon absorption is the primary mechanism for limiting at 630 nm in Pt:ethynyl [32]. It would seem that the two-photon absorption coefficient is smaller in these oligomers.

Clearly these oligomers, particularly the dimer, could provide useful insights into optical limiting via excited state absorption in Pt:ethynyl compounds. The results on spectroscopic and pump-probe measurements of these materials will therefore be presented in Section 4.1 and discussed in Chapter 6.

2.3.4.2. Oligomers with Terminal-Acetylide Groups

The ground state absorption spectral features of oligomers with terminal-acetylides are listed in Table 2-5 and the clamping levels at 532, 470 and 630 nm are shown in Figures 2-24 to 2-26.

n	λ_{max} (nm)	Shoulder strength	Shoulder wavelength (nm)	Clamping ranking at 532 nm
1	373	weak	504	4
2	375	weak	506	1
3	382	weak	505	3
n	366	weak	504	2

Table 2-5: Ground state absorption properties of oligomers with terminal-acetylides.

The ground state spectra of the terminal-acetylide oligomers show similar structure to terminal-phenyl oligomers; however the absorption maxima's of the oligomers with terminal-acetylide bonds are red-shifted by approximately 30 nm with little shift of the shoulder locations. The singlet red-shift is much larger than that observed when going from the monomer to the polymer within each set of oligomers, and thus terminal-acetylide groups clearly have a large effect on the singlet states. The polymer λ_{max} is quite low, possibly indicating that the material is bending or twisting our of a rigid rod shape; thus decreasing the effective conjugation length.

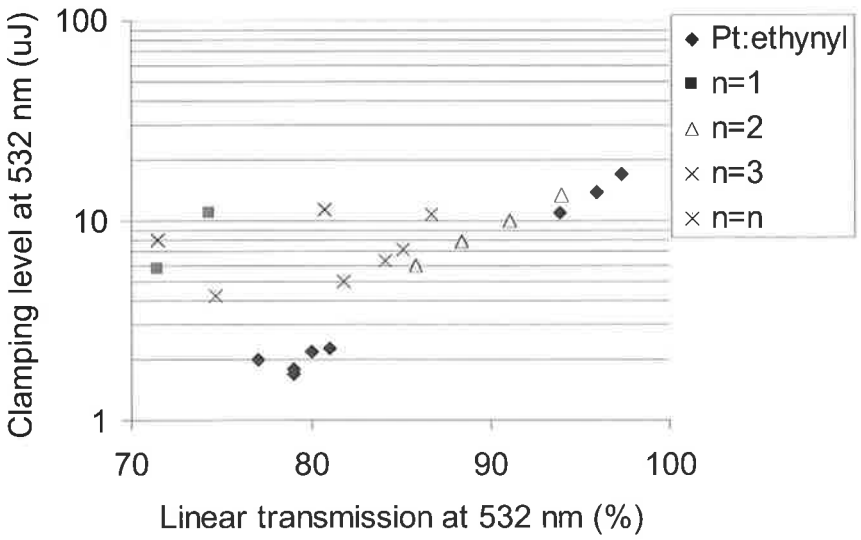

Figure 2-24: Clamping level at 532 nm as a function of linear transmission at 532 nm for terminal-acetylide oligomers.

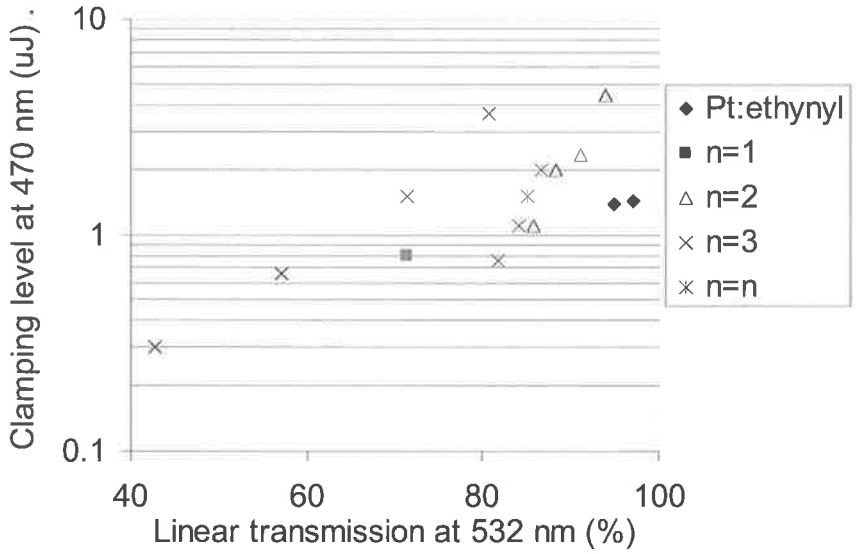

Figure 2-25: Clamping level at 470 nm as a function of linear transmission at 532 nm for terminal-acetylide oligomers.

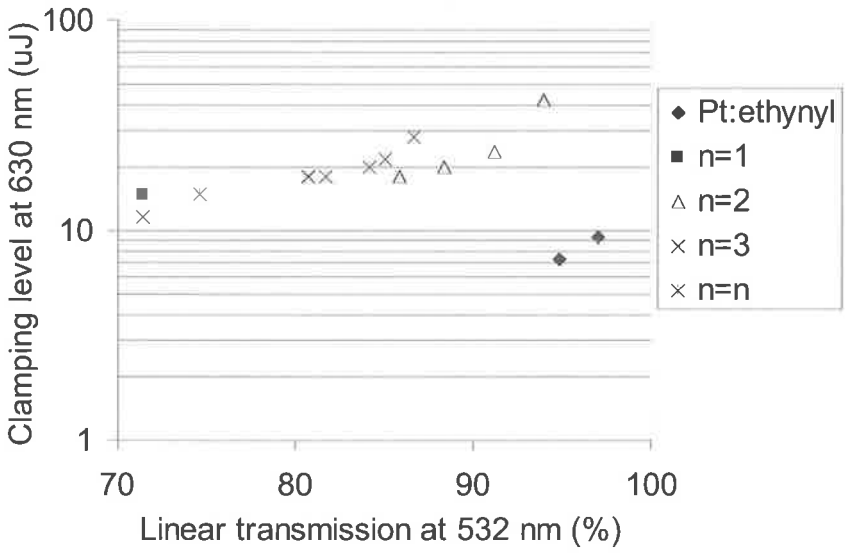

Figure 2-26: Clamping level at 630 nm as a function of percentage linear transmission at 532 nm for terminal-acetylide oligomers.

Of the terminal-acetylide oligomers all of the materials perform worse than Pt:ethynyl. This poor performance was consistently observed across the spectrum. Despite their poorer limiting behaviour, I will report results of spectroscopic and pump-probe measurements on these materials in Section 4.2 and discuss in Section 5.2.

2.3.5. Di-Platinum Ethynyl and Tri-Platinum Ethynyl

The optical limiting measurements described in Section 2.3.4 indicated that materials with two or three repeat units gave the best optical limiting. In order to explore this feature further, two new materials with extra phenyl-ethynyl groups (Figure 2-27) were synthesised and tested for optical limiting. These two materials are effectively the dimer and trimer of Pt:ethynyl.

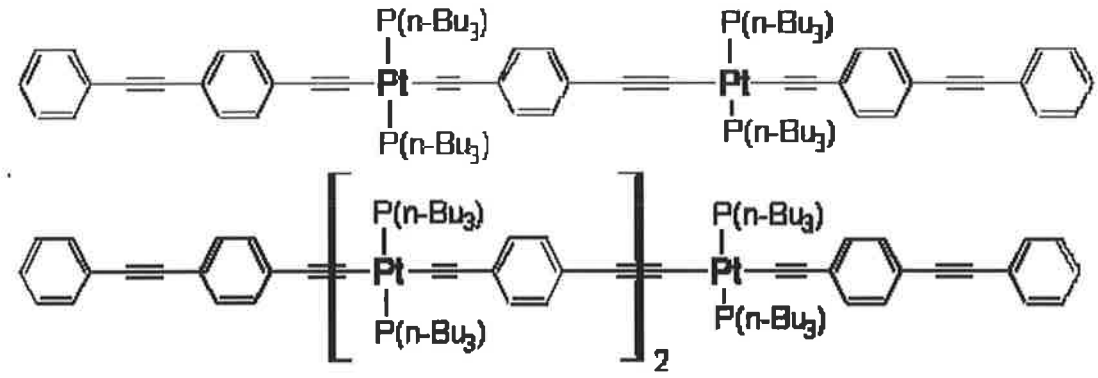

Figure 2-27: Structure of Di-platinum ethynyl, and Tri-platinum ethynyl.

The ground state absorption features are listed in Table 2-6 and clamping levels at 532, 470 and 630 nm are plotted in Figures 2-28 to 2-30. I have also included clamping levels of the dimer and trimer oligomers and Pt:ethynyl to facilitate comparison.

Material	λ_{max} (nm)	Shoulder strength	Shoulder wavelength (nm)
Di-platinum ethynyl	368	strong	462
Tri-platinum ethynyl	374	weak	504
Pt:ethynyl	380	Strong	520

Table 2-6: Ground state absorption properties of Di-platinum ethynyl and Tri-platinum ethynyl.

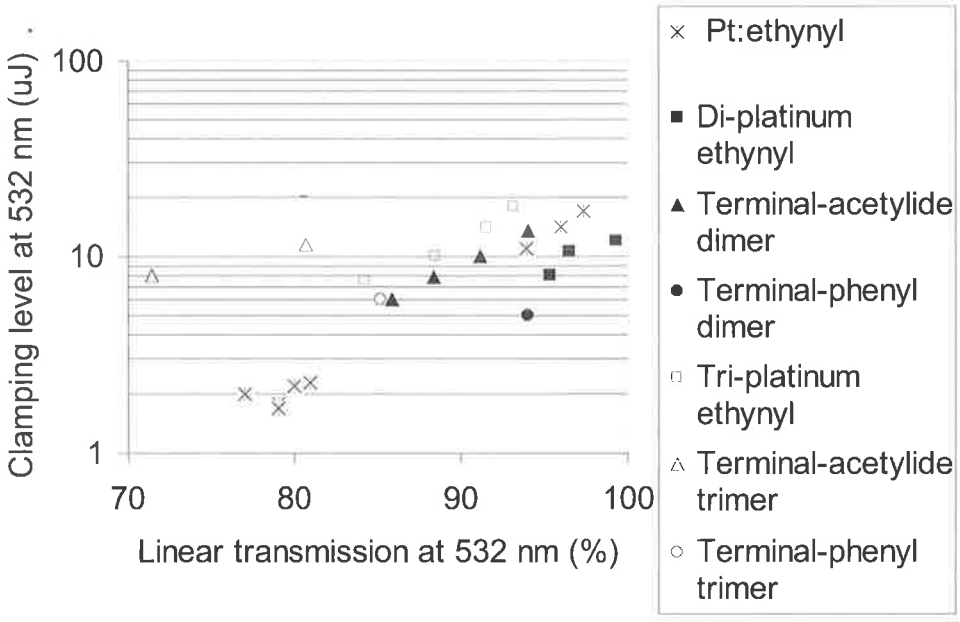

Figure 2-28: Clamping level of various di and tri oligomers and Pt:ethynyl at 532 nm as a function of linear transmission at 532 nm.

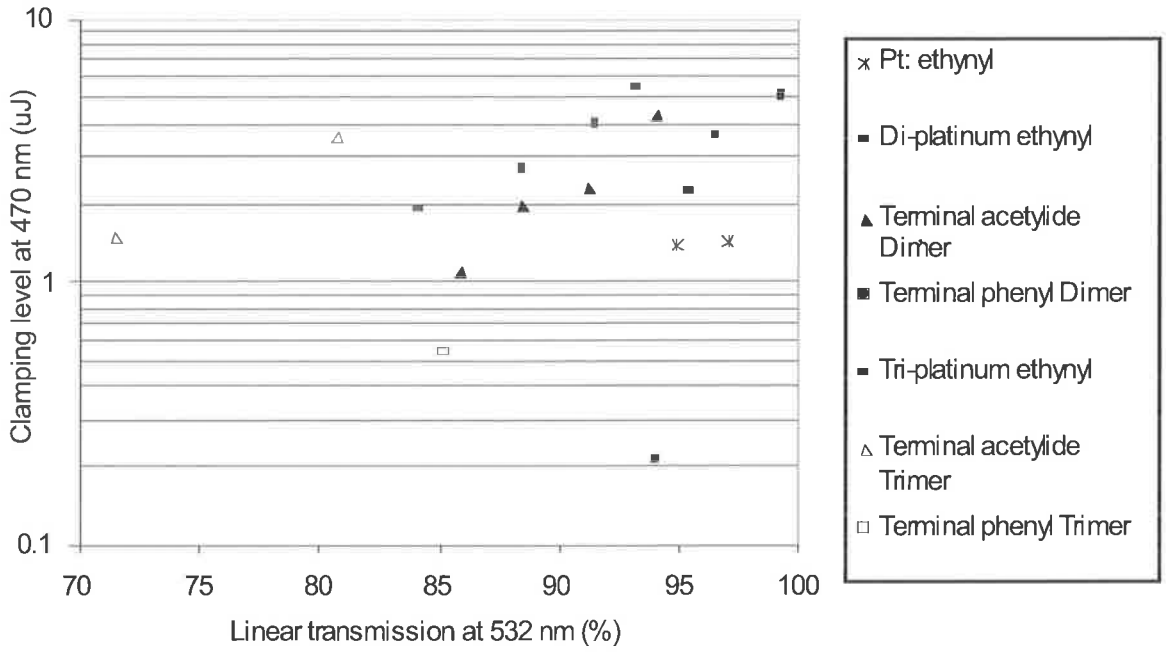

Figure 2-29: Clamping level of various di and tri oligomers and Pt:ethynyl at 470 nm as a function of linear transmission at 532 nm.

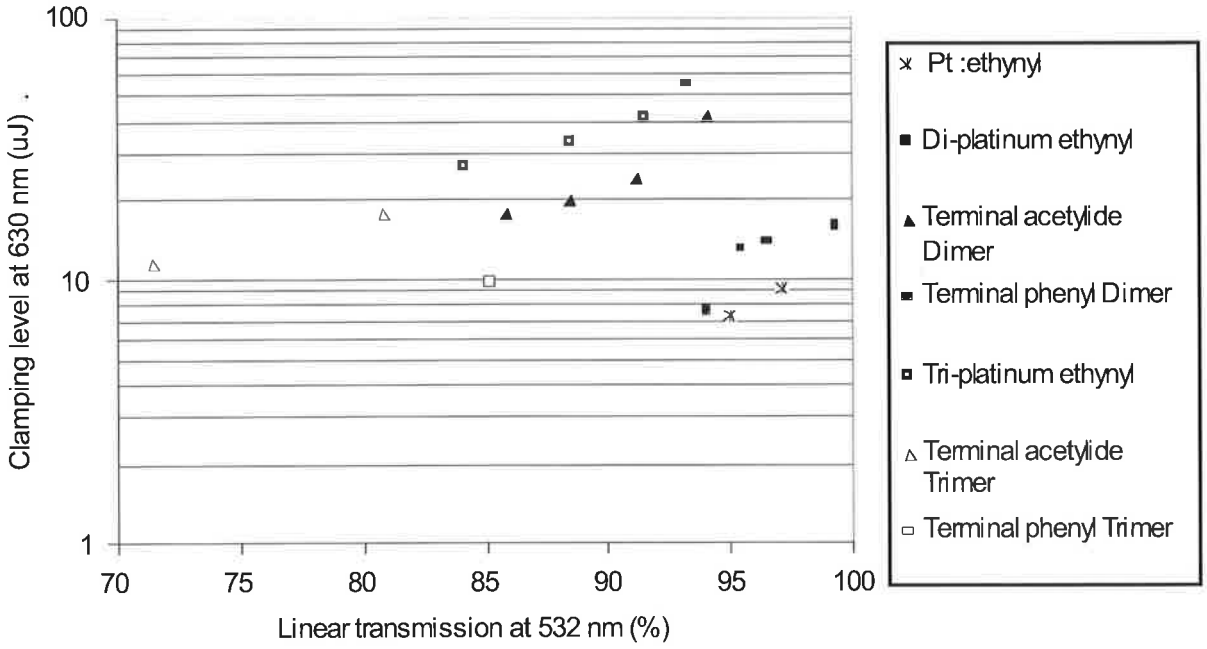

Figure 2-30: Clamping level of various di and tri oligomers and Pt:ethynyl at 630 nm as a function of linear transmission at 532 nm.

Figure 2-28 shows that there is little difference between di-platinum ethynyl and the terminal-phenyl dimer described in Section 2.3.4.1. Both of these perform better than Pt:ethynyl, while the terminal-acetylide dimer is worse than Pt:ethynyl. Tri-platinum ethynyl performs slightly better than the terminal-phenyl trimer which is also better than the terminal-acetylide trimer. This shows that oligomers ending with terminal-phenyl groups show superior performance at 532 nm. All of the oligomers show worse limiting than Pt:ethynyl at 630 nm, however the terminal-phenyl dimer is only slightly worse, indicating that this material is likely to have a significant two-photon absorption, which most of all the other materials tested do not. This will be discussed further in Chapter 6.

2.3.6. Precursor, PEPE

In order to investigate if a Pt:ethynyl precursor would show signs of limiting, a precursor that consisted of one arm of Pt:ethynyl, shown in Figure 2-31, was synthesised and tested.

This material showed much promise as an optical limiter considering the lack of heavy atom and was fully investigated, including some theoretical modelling performed by an associate.

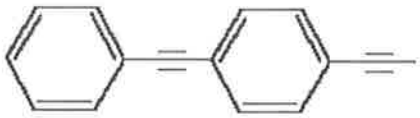

Figure 2-31: Structure of PEPE (phenyl ethynyl phenyl ethynyl).

The ground state absorption spectrum (Figure 2-32) is very similar to TMAs and shows strong ground state absorption located at 350 nm.

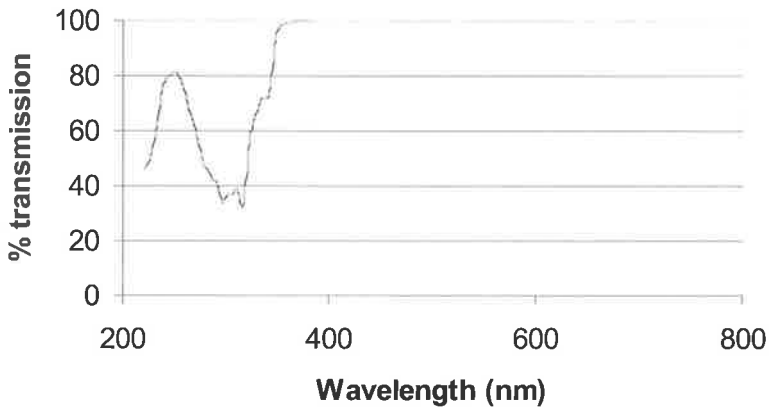

Figure 2-32: Ground state spectrum of PEPE in DCM.

This materials optical limiting shows the normal pattern for TMAs with strong limiting in the blue, reasonable limiting in the green and much poorer limiting in the red, as shown in Figure 2-33.

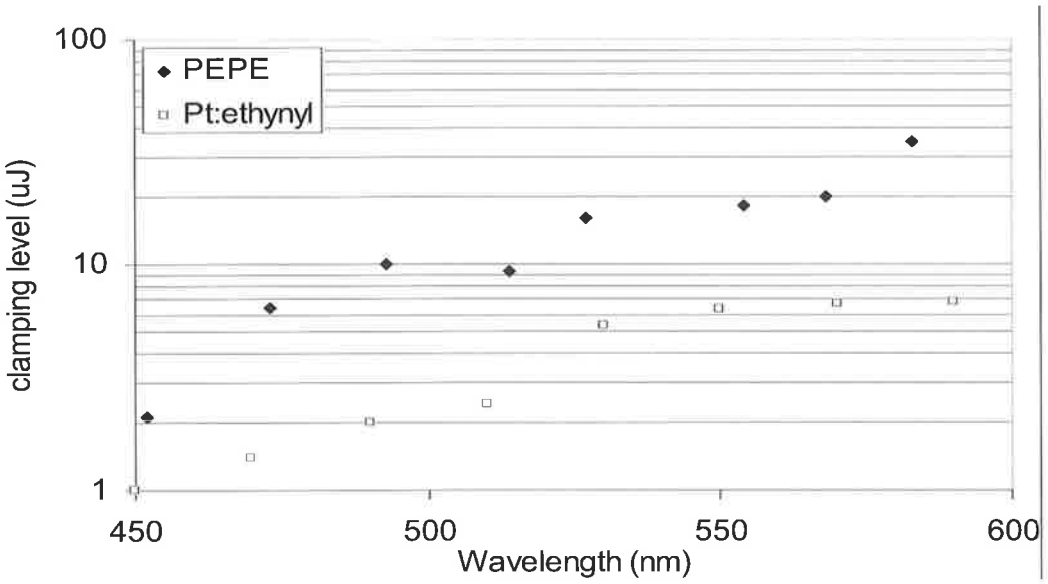

Figure 2-33: Clamping level against wavelength for PEPE, (66 % transmission at 532 nm) and Pt:ethynyl (94.4% transmission at 532 nm).

Although the clamping level of PEPE is still significantly higher than Pt:ethynyl it was surprising to see any limiting at all, as the common understanding of limiting is that a material requires a heavy metal (such as platinum) to provide spin-orbit coupling and thus access to the triplet state. The results of spectroscopic, pump-probe, two-photon absorption measurements are reported in Section 4.3, and used to explain the limiting of this material in Section 6.1.

2.3.7. Poly Pt:Ethynyl with Different Spacer Groups

Variation of the spacer group has been shown to affect optical limiting [19], [32]. I looked at spacers consisting of electron donors attached to a phenyl ring as well as groups such as anthracene and naphthalene as the spacer group as shown in Figures 2-34 and 2-35. Increasing the distance between platinum atoms by using a diyne was also investigated. The ground state absorption spectral features of a Pt:ethynyl polymer with different spacer

groups are listed in Table 2-7 and the clamping levels at 532, 470 and 630 nm are shown in Figures 2-36 to 2-38.

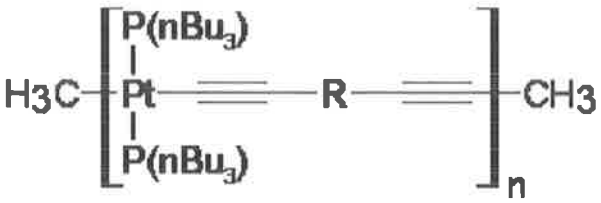

Figure 2-34: Structure of materials with various spacer group R.

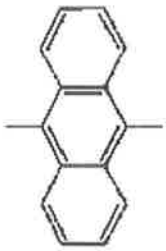

a) R= Anthracene

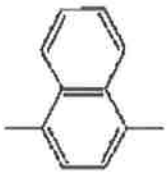

b) R= Naphthalene

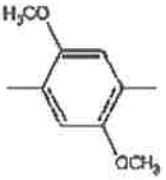

c) R= Dimethoxy-phenyl

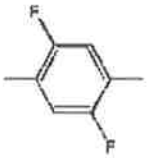

d) R= Difluro-phenyl

e) R= Diyne

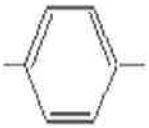

f) R= Phenyl

Figure 2-35: Structure of spacer groups used.

R group	λ_{max} (nm)	Shoulder strength	Shoulder wavelength (nm)
Anthracene	485	Very strong	554
Napthalene	408	Medium	456
Dimethoxy-phenyl	402	None	-
Difluro-phenyl	356	Weak	509
Diyne	399	None	-
Phenyl	360	Strong	504

Table 2-7: Table showing absorption properties of materials with various spacer groups.

Of the six different spacer groups synthesised the ground state spectra for the R=Anthracene, R=Phenyl, R=Difluro-phenyl and R=Naphthalene show distinct shoulders. The other materials show no features other than absorption maxima at short wavelengths.

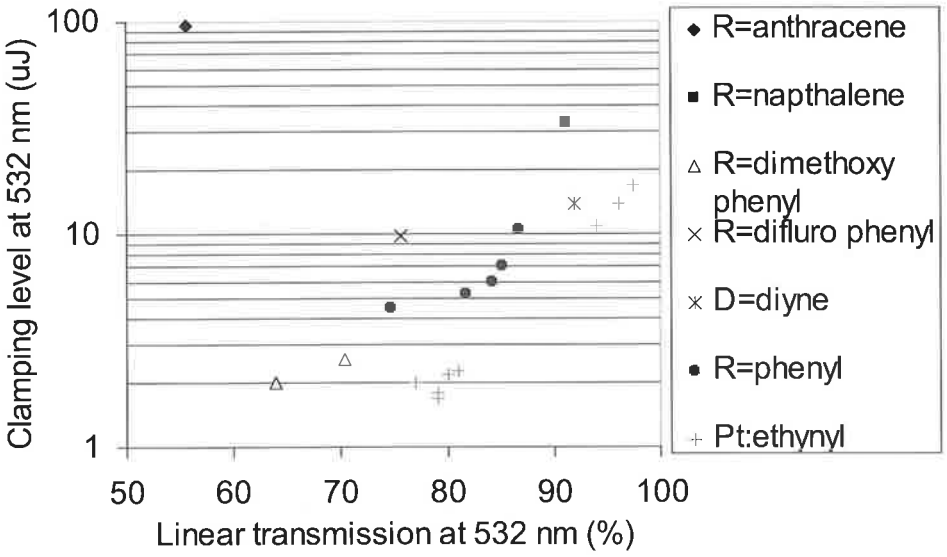

Figure 2-36: Clamping level at 532 nm as a function of linear transmission at 532 nm for various spacer group materials.

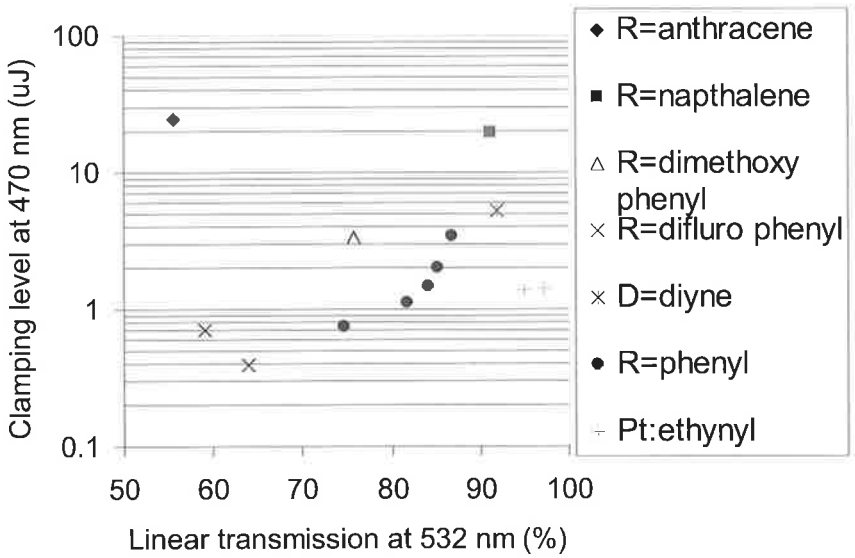

Figure 2-37: Clamping level at 470 nm as a function of linear transmission at 532 nm for various spacer group materials.

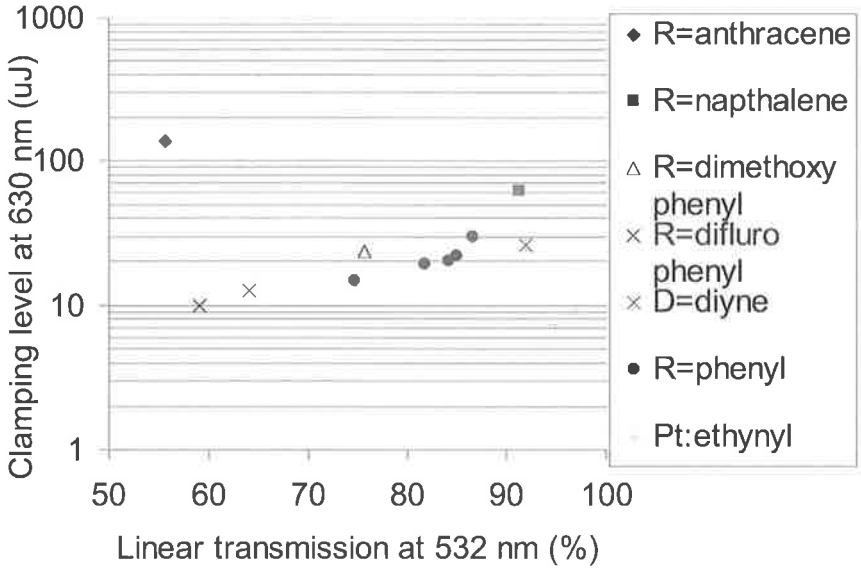

Figure 2-38: Clamping level at 630 nm as a function of linear transmission at 532 nm for various spacer group materials.

All of the polymers with modified spacer groups show higher clamping levels than Pt:ethynyl, but since most polymers have similar clamping levels, the poor limiting is due mostly to polymerisation.

2.3.8. Number of Arms

Given that Pt:ethynyl and materials of about two repeat units in length appear to be superior optical limiters, an attempt was made to synthesise a material with similar conjugation length, but with more delocalised electrons and heavy metal centres. The increased number of heavy metal centres should increase the number of high spin-orbit coupling sites, thus increasing triplet state absorptions. This was achieved by increasing the number of "arms" to a central phenyl ring as shown in Figure 2-39.

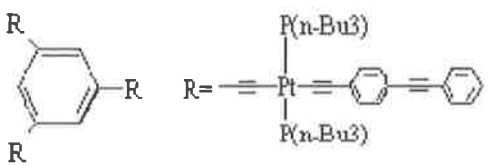

Figure 2-39: Structure of three-arm TMA.

The ground state absorption spectrum of this material is shown in Figure 2-40, similar to that of Pt:ethynyl. The clamping level as a function of wavelength is shown in Figure 2.41.

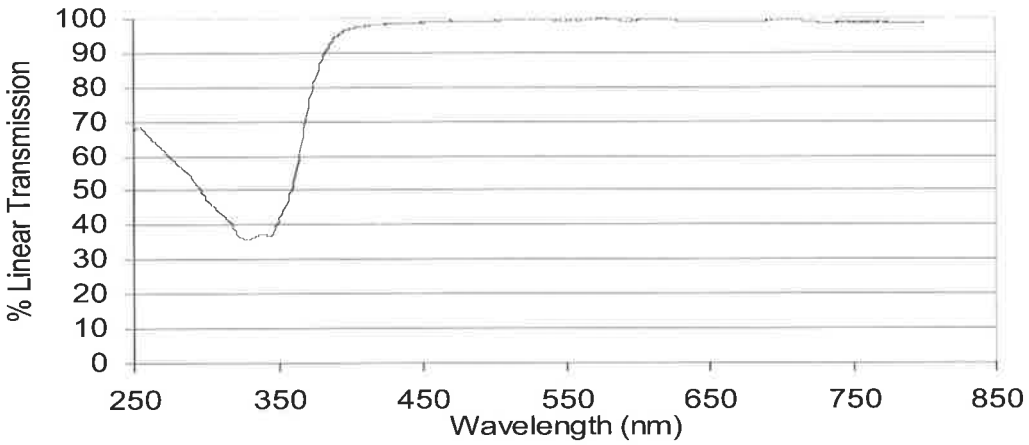

Figure 2-40: Ground state spectra of three arm material.

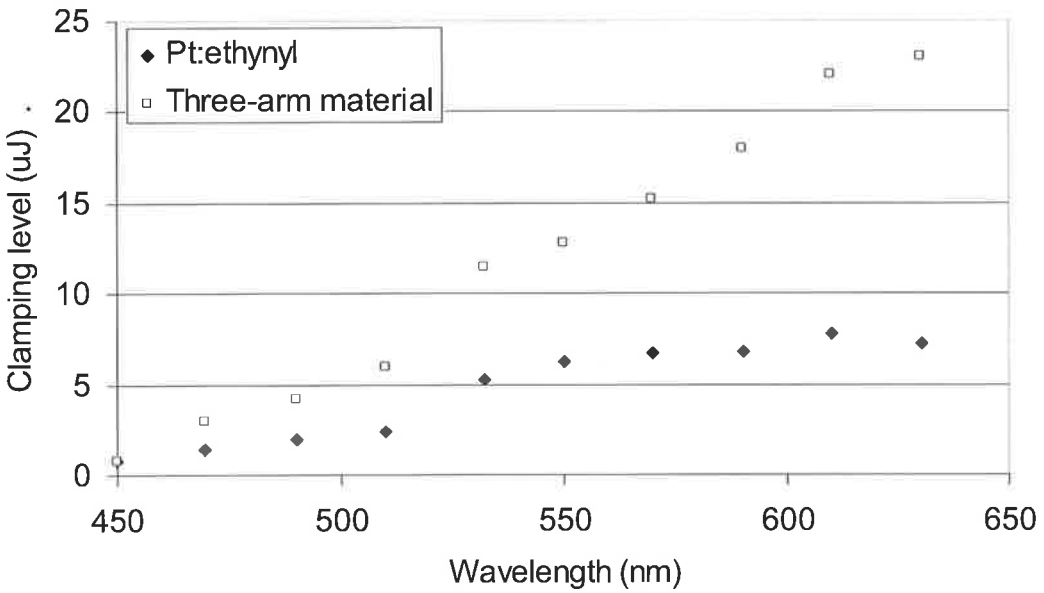

Figure 2-41: Clamping level against wavelength for three-arm TMA (92 percent linear transmission at 532 nm) and Pt:ethynyl (94 percent linear transmission at 532 nm).

The three-arm material shows significantly worse optical limiting than Pt:ethynyl at all wavelengths.

2.4. Solvent Effects

As mentioned previously the choice of solvent is known to affect optical limiting [27], [30], [33]. In order to investigate the solvent effect on TMAs a small solvent study was conducted.

During this study samples of four materials, R=I and R=NO_2 terminal groups (Section 2.3.3), the terminal-phenyl trimer (Section 2.3.4), and di-platinum-ethynyl (Section 2.3.5) were dissolved in four different solvents (Toluene, THF (Tetrahydrofuran), Dioxane and DCM or DCE) and the optical limiting at 532 nm was measured. The results are plotted in Figures 2-42 to 2-45. These materials were selected as they represent the different groups investigated. Time constraints ruled out investigating the solvent effect on each material, so only one material from each group was selected. In order to also measure qualitatively the solubility of these materials, solutions were made up to close to the maximum solubility rather than constant linear transmission

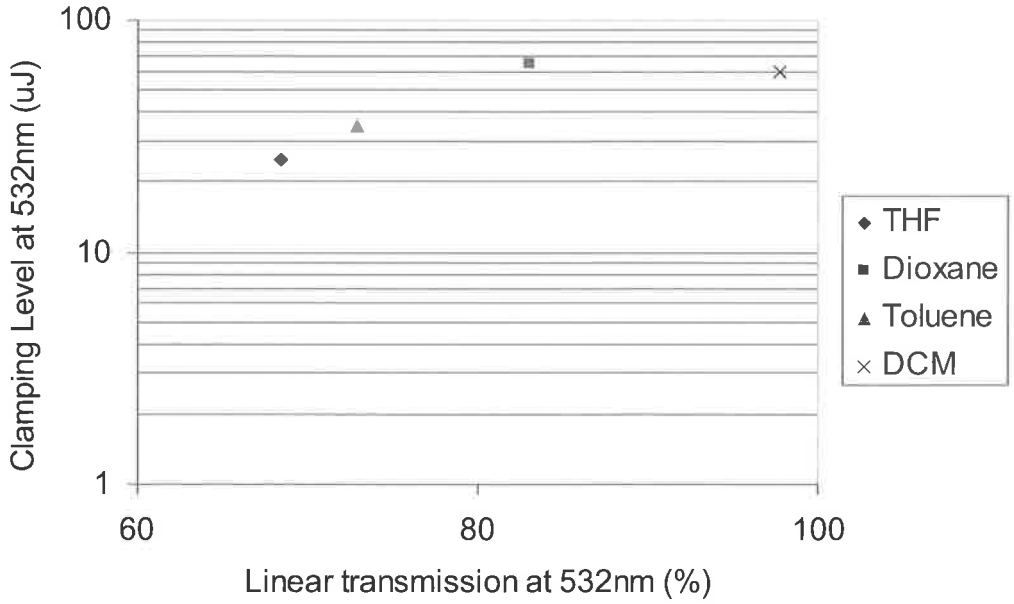

Figure 2-42: Clamping level at 532 nm as a function of linear transmission at 532 nm for solutions of R=NO2 as the terminal group in various solvents.

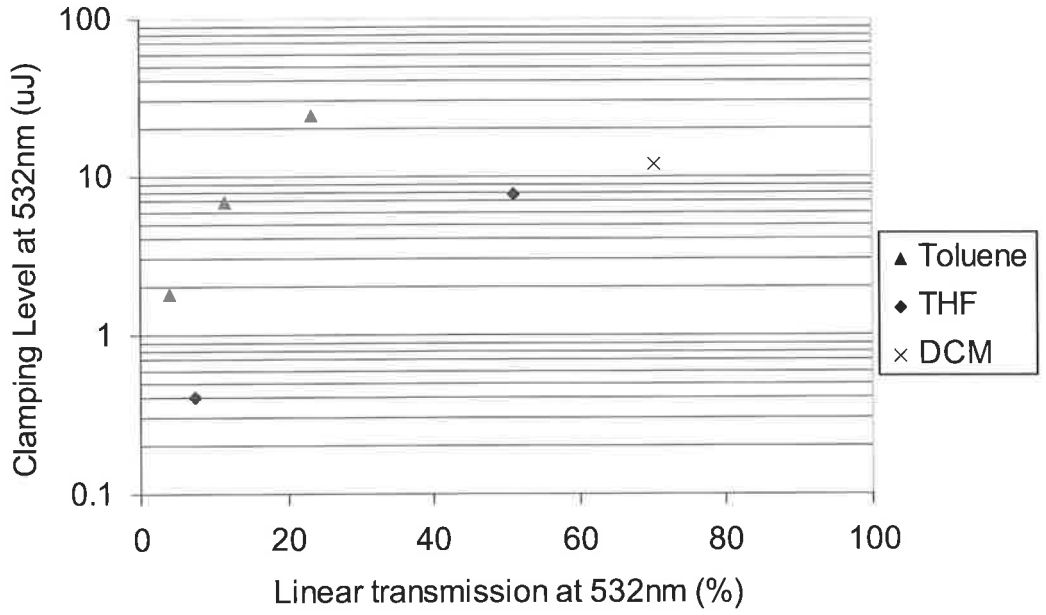

Figure 2-43: Clamping level at 532 nm as a function of linear transmission at 532 nm for solutions of R=I as the terminal group in various solvents.

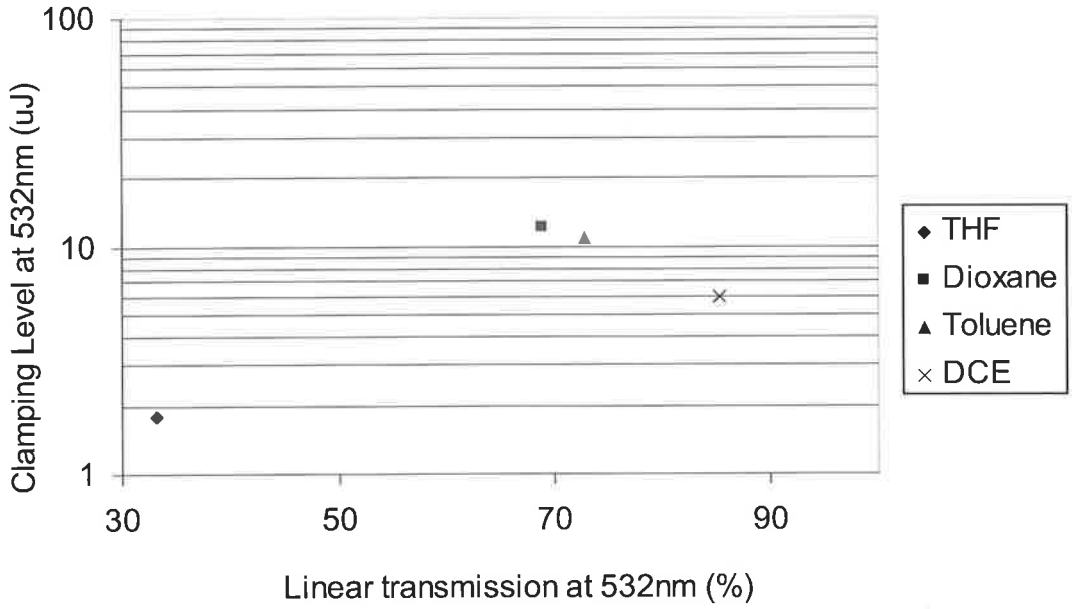

Figure 2-44: Clamping level at 532 nm as a function of linear transmission at 532 nm for solutions of terminal-phenyl trimer in various solvents.

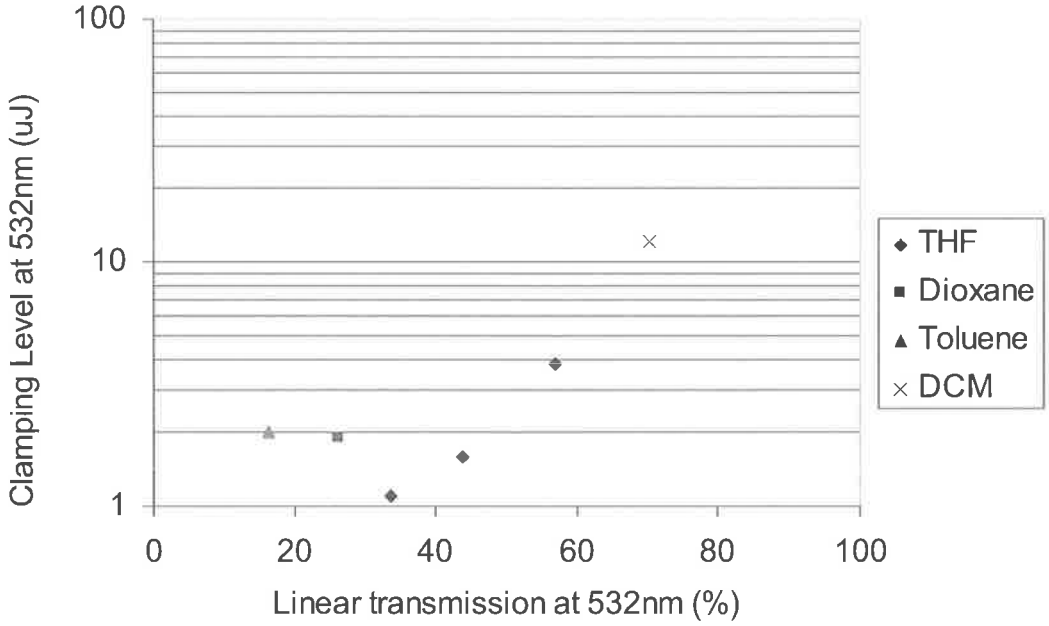

Figure 2-45: Clamping level at 532 nm as a function of linear transmission at 532 nm for solutions of di-platinum ethynyl in various solvents.

It can be seen that for some TMAs the choice of solvent can have a large effect on the clamping level and ground state spectra, while for other materials there is little solvent effect. As it is very time consuming and expensive to test each material in a range of solvents it was decided to test each material in an appropriate solvent (usually DCM or DCE) and only investigate materials that warranted further solvent studies at a later stage.

2.5. Summary of Limiting Results

Of all the materials that were tested for optical limiting only the terminal-phenyl dimer and di-platinum ethynyl show improved limiting at 532 nm compared to Pt:ethynyl. A terminal phenyl group seems to be a strong factor in the optical limiting of a TMA. Optimum molecular lengths of the better performing materials are also very similar.

Many of the TMAs tested showed very poor limiting, especially at 630 nm, and many of the changes that were investigated proved to be fruitless. It has been observed that in many of the materials I have discussed in this chapter, the shoulder strength, which had initially

been thought to be a good indicator of limiting ability may in fact hinder optical limiting. A shoulder in the ground state absorption spectrum is an indication of triplet state accessibility, and thus materials with very strong shoulders may have significantly reduced T_1 lifetime. It is also possible that the energy levels of higher singlet and triplet states may have shifted decreasing limiting performance. A summary of the limiting results for each group is presented below in Table 2-8.

Group	Effect in blue	Effect in green	Effect in red
Altering Metal	worse	worse	worse
Solubilising group	worse	PPh_2Me same, rest worse	worse
Terminal group	worse	worse	worse
Terminal-phenyl oligomers	N=2 better	N=2 better	worse
Terminal-acetylide oligomers	worse	N=2 marginally better	worse
Di and Tri Pt:ethynyl	N=2 better	N=2 better	worse
PEPE	worse	worse	worse
Spacer group	worse	worse	worse
Number of arms	worse	worse	worse

Table 2-8: Effect of various structural changes on optical limiting performance.

To find out the reasons for these results requires detailed and time consuming measurement of the excited state parameters used to construct a five-level model. As time constraints ruled out performing these measurements on all materials, I decided to concentrate on the two sets of oligomers and the precursor material. Investigation of the precursor material will help to determine why it shows limiting behaviour and will enable

validation of the 5-level model that can then be used to investigate the limiting of Pt:ethynyl and the oligomers.

The techniques used to measure the parameters in the 5-level model are described in Chapter 3, and the measurements presented in Chapter 4.

3. Spectroscopic Measurement Techniques

This chapter describes the techniques used to measure the parameters needed to construct a five-level model for each of the two sets of oligomers and the precursor. The results of the spectroscopic measurements are presented in Chapter 4.

Time resolved luminescence spectroscopy (Section 3.1) was used to determine the wavelengths of the transitions from the lowest singlet and triplet states to the ground state ($\lambda_{S1\text{-}S0}$ and $\lambda_{T1\text{-}S0}$), and T_1 lifetimes, τ_{T1}. S_1 lifetimes, τ_{S1}, were measured by recording the fluorescence decay rate at room temperature (Section 3.2). The ground state and excited state absorption cross sections at 532 nm were obtained from the ground state absorption spectrum and pump-probe experiments (Section 3.3). Section 3.4 describes how the broadband excited state absorption spectra were determined. The technique used to determine the S_0 to S_1 two-photon absorption coefficient at 532 nm, is described in Section 3.5. The triplet yield was assumed to be 100 percent, based on previous experiments with Pt:ethynyl. The actual value is unimportant, provided that it is non-zero, as the excited state absorption cross-section is calculated assuming a percentage triplet yield. Thus, if the triplet yield is assumed to be 50% then the excited state absorption cross-section would be double that otherwise calculated. This change would have no effect on the numerical 5-level model.

3.1. Time Resolved Spectroscopy

The $S_1 \rightarrow S_0$ and $T_1 \rightarrow S_0$ energy gaps and the T_1 lifetime at low temperatures were measured using time resolved spectroscopy. At room temperature the dominant $T_1 \rightarrow S_0$ decay path is non-radiative, resulting in extremely weak phosphorescence signals that cannot normally be discerned. Samples were thus cooled to approximately 17 K to enhance the phosphorescence strength.

The TMA sample was prepared by spin coating a thin layer onto a thermally conducting copper disc. This disc was placed inside the cryostat, and cooled to about 17 K.

The sample was pumped with 355 nm, 30 ps pulses, as shown in Figure 3-1, causing excitation into S_1. The material then decays back to the ground state directly and via T_1. Luminesce resulting from this decay was collected by a series of lenses (L1 and L2) and focused into a SPEX 0.22m Optical Multi-channel Analyser (OMA).

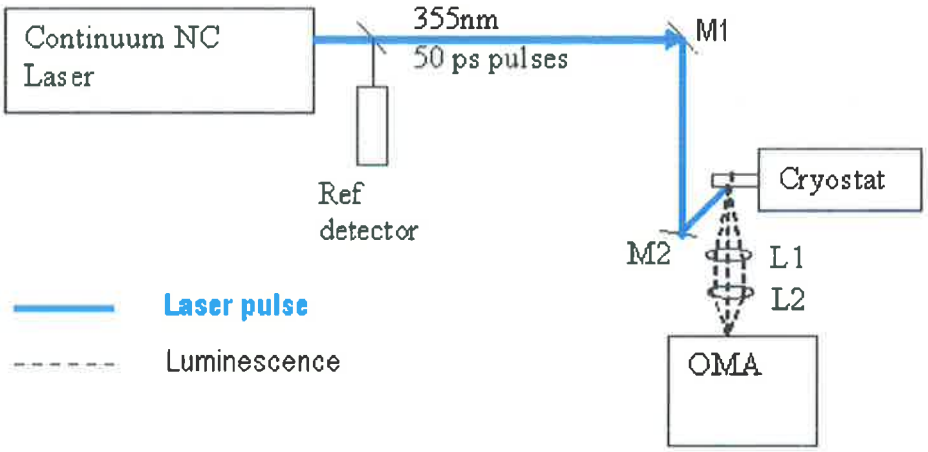

Figure 3-1: Schematic of the time-resolved spectroscopy measurement systems, L1 has focal length of 76 mm, L2 has focal length 100 mm.

The OMA separates luminescence wavelengths by use of a grating. It could be operated in either cw mode, which collects a spectrum for 15 ms, or in one of two gated modes. In the first gated mode, the integration time could be varied between 20 ns and 3.5 μs and delayed by up to several milliseconds. In the second gated mode, spectra were repeatedly collected and then read-out with each cycle taking 10.24 ms.

Most TMAs that I measured had a fast fluorescence at short wavelengths and a much slower phosphorescence above 500 nm. The luminescence collected using a 15 ms

integration time with no time delay, (shown in Figure 3-2 as 'long gate'), shows a broad peak located around 426 nm and a much sharper peak at 512 nm (with some subsidiary structure above 512 nm). When the integration time is reduced to 70 ns ('short gate') most of the 512 nm peak disappears, leaving the 426 nm peak unchanged. Increasing the integration time to 1 μs and delaying the integration by several microseconds ('delayed gate' in Figure 3-2), the 426 nm peak disappears but the 512 nm peak remains unchanged. This indicates that the 426 nm peak is due to the short lived S_1 to S_0 fluorescence and the 512 nm peak is due to the long-lived T_1 to S_0 phosphorescence. This pattern of a short-lived peak at shorter wavelengths (S_1 to S_0) and a much longer-lived red-shifted peak (T_1 to S_0) was observed for all of the TMAs studied. For most of the materials the S_1 to S_0 decay was much faster than the minimum 20 ns integration time. To accurately measure the S_1 lifetime a Cordin streak camera was used as described in section 3.2.

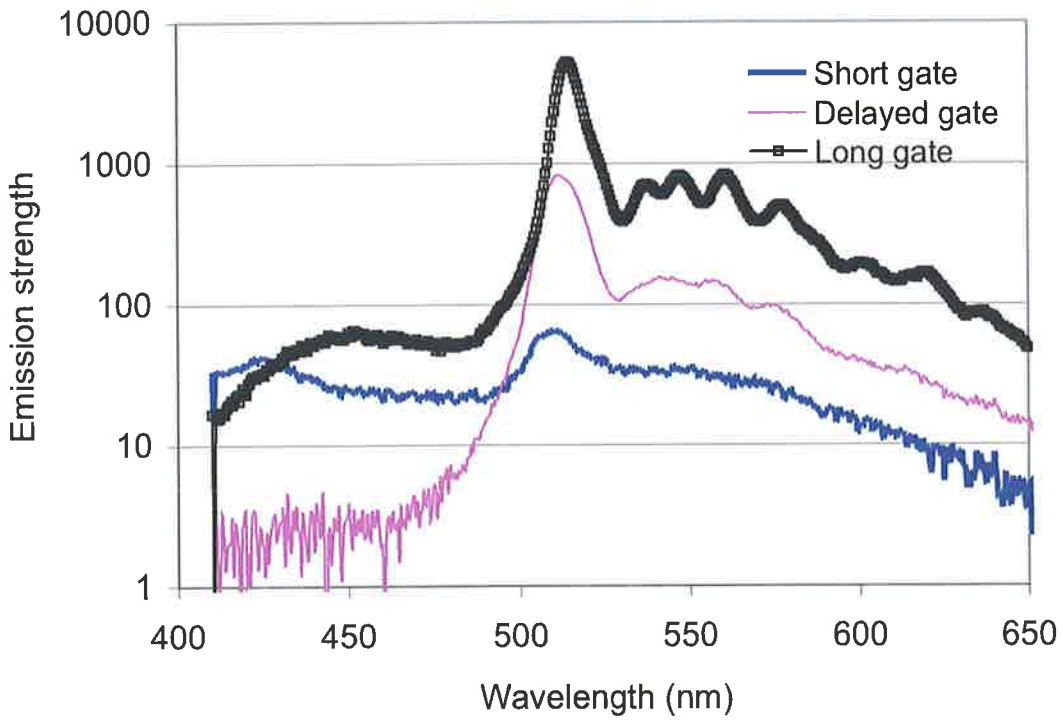

Figure 3-2: Luminescence for a TMA, showing a short lived fluorescence peak at 426 nm and a much longer lived phosphorescence peak at 512 nm. Long gate is 15 ms long with no delay, Short gate is 70 ns long with no delay, and Delayed gate is 1 μs long, 1μs after the excitation pulse.

The phosphorescence lifetime was determined by averaging the peak over many pulses as a fixed delay then repeating for many delays. The following result is for the terminal-phenyl tetramer a typical decay curve is shown in Figure 3-3. Phosphoresce decays were assumed to decay exponentially,

$$\text{Intensity} = \exp(-t/\tau), \qquad \textbf{3-1}$$

where the lifetime, (τ), is the time, (t), taken for the intensity to decrease to 1/e.

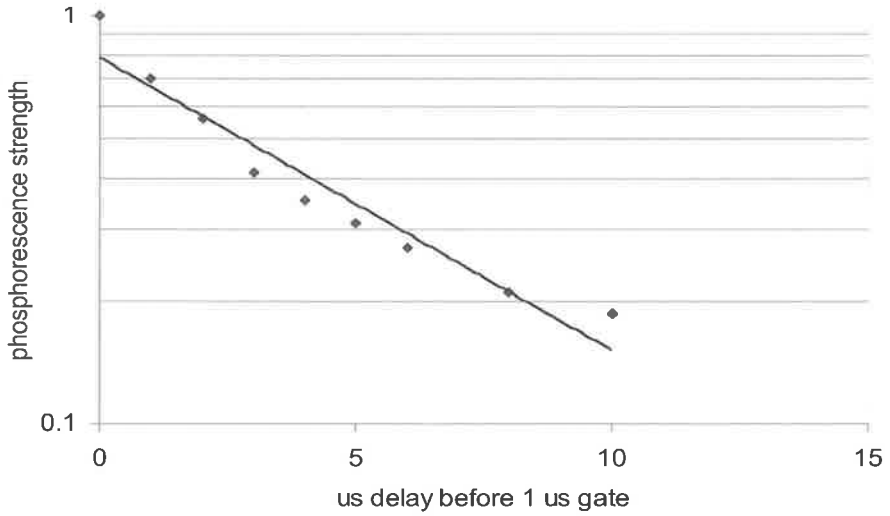

Figure 3-3: Example of phosphorescence decay and a fit to the data.

3.1.1. Phosphorescence Decay Rate of PEPE

Theoretical calculations predicted the lifetime of an isolated PEPE molecule to be 16 seconds. The phosphorescence decay was therefore recorded using the second gated mode, which integrates the phosphorescence for 5.12 ms every 10.24 ms, giving the data plotted in Figure 3.4. The first two data points were contaminated by short lived fluorescence and thus were ignored when producing the decay curve shown in Figure 3-4, which has τ=30 ms and includes the effect of the 5.12 ms integration time.

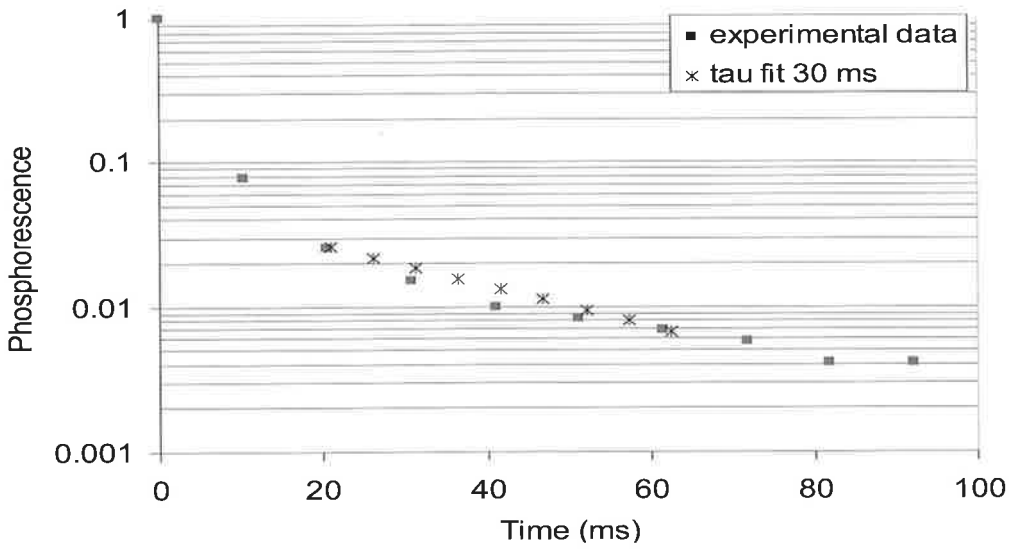

Figure 3-4: Phosphorescence decay at 455 nm ■ and fitted data * for PEPE at 17 K.

3.2. *Intersystem Crossing Rate*

At 17 K, the $T_1 \rightarrow S_0$ phosphorescence dominates the luminescence spectra, while at 300 K it is almost non-existent. The energy emitted by the $S_1 \rightarrow S_0$ decay curve on the other hand remains relatively constant. Thus we can assume that intersystem crossing from S_1 to T_1 is the dominant S_1 decay path at both 17 and 300 K.

The intersystem crossing rate was determined by recording the decay of the emission due to the $S_1 \rightarrow S_0$ fluorescence using a streak camera. The sample was spun onto a copper disc and positioned so that after irradiation with a 30 ps, 355 nm pulse the fluorescence was imaged at a Cordin streak camera (see Figure 3-5). Lifetimes of less than a half nanosecond were recorded for all the materials tested. (See Sections 4.1.2 and 4.2.2 for oligomer results and 4.3.2 for PEPE results.)

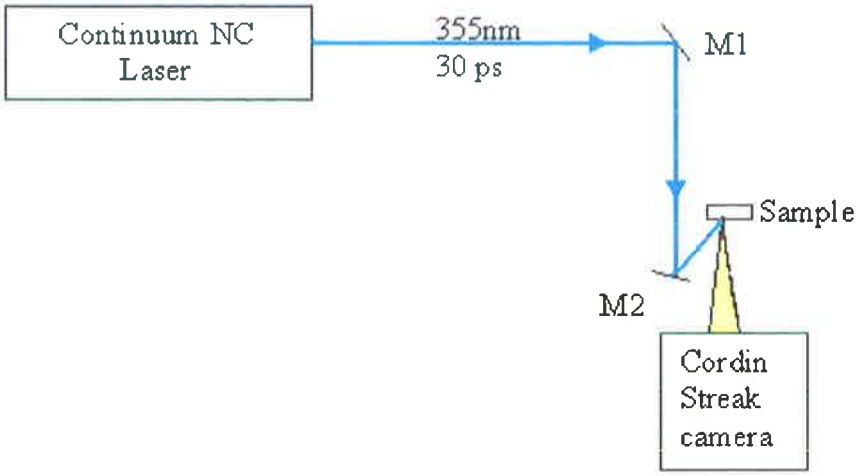

Figure 3-5: Intersystem crossing rate experiment set-up. M1 and M2 are mirrors.

3.3. Absorption Cross Sections

3.3.1. Ground State Absorption Cross Section

A known concentration DCE solution of the material to be tested was filtered and placed in a 2 mm cuvette, in general dilute solutions were used when measuring the absorption cross section to minimise the likelihood of material being trapped in the filter and overestimating the concentration. While material may have been lost during filtering, particularly for the more concentrated solutions, the actual value of the concentration is unimportant for this study as all limiting measurements are plotted as a function of measured linear transmission rather than concentration. Furthermore, while the nominal concentration is used to convert the measured absorption coefficients to cross-sections, the absorption coefficients are the important parameters for the 5-level model and thus its predictions are unaffected by uncertainty in the concentration. Absorption spectra were recorded at room temperature using a Varian Cary 5E UV-VIS-NIR spectrometer.

The ground state absorption cross section, σ_S is the ratio of the ground state absorption coefficient, α_S, to the density of molecules in the ground state, N_0:

$$\acute{o}_S = \frac{\acute{a}_S}{N_0} \qquad \textbf{3-2}$$

The ground state absorption coefficient is calculated from the ground state transmission, T_{lin}, and the path-length, L, of the sample:

$$\acute{a}_S = \frac{-\ln(T_{lin})}{L} \qquad \textbf{3-1a}$$

The density of molecules in the ground state, N_0, can be calculated using:

$$N_0 = \frac{N_A C}{1000} \qquad \textbf{3-2}$$

where N_A is Avogadro's number (6.02×10^{23} molecules/mol), and C is the concentration of the solution (mol/L).

3.3.2. Excited State Absorption Cross Sections

The excited state absorption cross section at 532 nm was determined using a pump-probe experiment. In this experiment a filtered, DCE solution of the material in a 2 mm cuvette was pumped with a 30 ps, 532 nm high intensity (pump) beam, populating the S_1 state. This was followed by intersystem crossing to T_1. Approximately 800 ps later a weaker, probe beam was passed through the pumped region of the sample as shown in Figure 3-6. As the probe beam was delayed by much less than the T_1 lifetime, absorption of the probe beam consisted of both ground state (S_0 to S_1) and excited state (T_1 to T^*) components. By measuring the drop in transmission of the probe beam when the pump beam was applied the triplet state absorption cross section at 532 nm can be calculated.

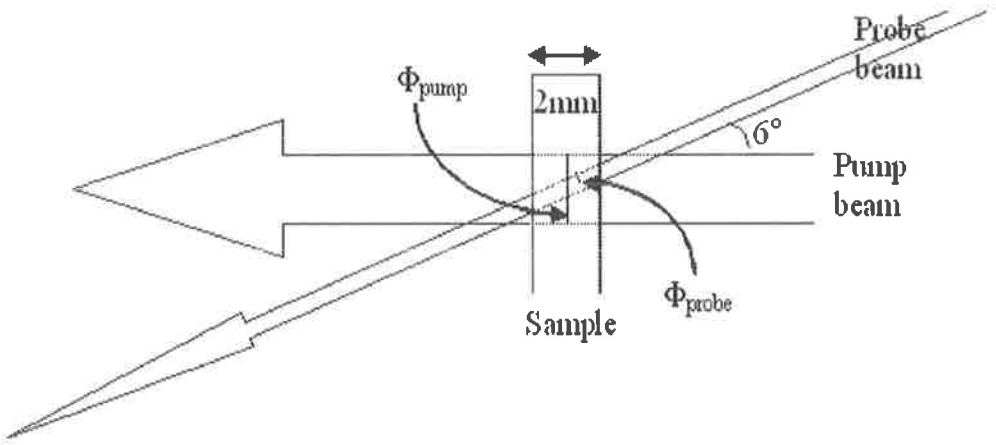

Figure 3-6: Pump-probe beam interaction, Φpump =210 μm, Φprobe =120 μm

The layout of the pump-probe experiment is shown in Figure 3-7. The pump beam was focussed by L1 to a waist diameter of 210 μm, while the probe beam, which was orthogonally polarised and delayed with respect to the excitation beam was focussed by L2 to a waist diameter of 120 μm. Care was taken to ensure that the probe beam was well contained within the pumped region of the sample. The energy of the pump and reference beams were measured using RJP 735 pyrometers. The energy of the probe beam was measured using a more sensitive RJP 765a silicon energy detector.

The incident pump energy, $E_{pump\ incident}$ was calculated by recording the pump and reference detector values, when a cuvette filled only with solvent was in the sample position. The reference detector reading was used to calculate $E_{pump\ incident}$ during the pump-probe experiment. This method was also used to calculate $E_{probe\ incident}$ using the same reference detector. By calibrating the reference detector with a solvent only cuvette in place, reflections form the cuvette faces can be ignored when calculating σ_T.

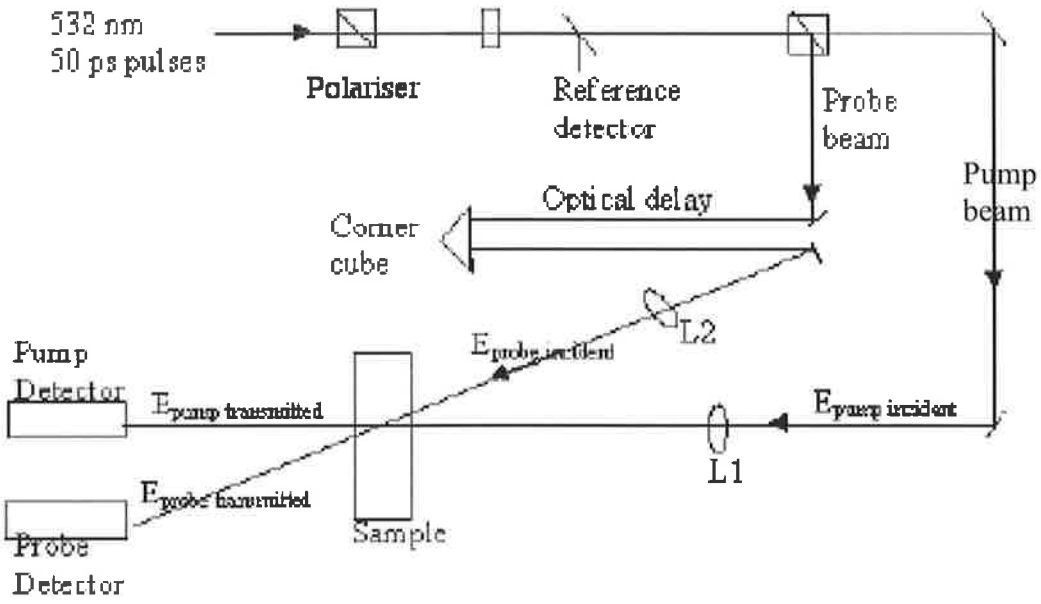

Figure 3-7: Pump-probe experimental set up. Focal length of L1 is 76 mm, focal length of L2 is 150 mm, optical delay is 24 cm (800 ps).

The population density of the triplet state, N_T, was calculated using

$$N_T = \frac{E_{pump\ absorbed}}{E_{532nm\ photon} \cdot V_{pump}} \qquad \textbf{3-4}$$

where $E_{532\ photon}$ is the energy of a 532 nm photon and V_{pump} is the volume of the sample the pump beam passes through.

When measuring the pump energy absorbed, care was taken to ensure that the pump energy was low enough that the sample was not limiting and thus it could be assumed that for each 532 nm pump photon absorbed there was one molecule excited to T_1. To confirm this, the ground state absorption cross-section was calculated, as described in Section 3.3.1, and compared to the value determined in the spectrometer.

The probe beam absorbed when the pump beam was applied is composed of ground state (linear) and excited state components, thus,

$$E_{\text{probe beam transmitted}} = E_{\text{probe}_{\text{incident}}} T_{\text{linear}} T_{\text{nonlinear}} \quad \textbf{3-5}$$

where $T_{\text{linear}} = e^{-\alpha_S L}$ is the ground state transmission, $T_{\text{nonlinear}} = e^{-\acute{a}_T L}$ is the excited state transmission, α_S is the $S_0 \rightarrow S_1$ absorption coefficient, α_T is the $T_1 \rightarrow T^*$ absorption coefficient and L is the interaction length. Inserting these relationships into Equation 3-6 gives

$$E_{\text{probe}_{\text{pump beam transmitted}}} = E_{\text{probe}_{\text{incident}}} e^{-\acute{a}_S L} e^{-\acute{a}_T L} \quad \text{3-6}$$

Dividing both sides by the incident probe energy and taking natural logs of both sides:

$$\acute{a}_S + \acute{a}_T = \frac{-\ln\left(\frac{E_{\text{probe}_{\text{pump beam transmitted}}}}{E_{\text{probe}_{\text{incident}}}}\right)}{L} \quad \text{3-7}$$

Rearranging for α_T gives:

$$\acute{a}_T = \frac{-\ln\left(E_{\text{probe pump beam transmitted}} \Big/ E_{\text{probe incident}}\right)}{L} - \acute{a}_S \quad \textbf{3-8}$$

σ_T can then be calculated using:

$$\acute{o}_T = \frac{\acute{a}_T}{N_T} \quad \textbf{3-9}$$

The calculation for one of the oligomers is shown in appendix D, and results are presented in Chapter 4.

This process was repeated several times and the excited state cross section values were averaged to find the final value for each material. The standard error was calculated using the formula:

$$\text{standard error} = \frac{\text{standard deviation}}{\sqrt{n}} \quad \text{3-10}$$

$$\text{standard error} = \frac{\sqrt{n\sum x^2 - \left(\sum x\right)^2}}{n^2(n-1)} \quad \text{3-11}$$

where n is the number of points from which the average excited state absorption was calculated, which was always greater than 8.

3.4. Broadband Excited State Absorption Cross Sections

Broadband excited state absorption cross sections were determined using a white-light spectrometer at DSTL in Malvern, UK. Unfortunately equipment failures resulted in only a few of the materials being measured and the cross sections were not calibrated. However the relative shapes of the excited state absorption curves for several materials were collected and later calibrated using the excited state absorption cross sections calculated as described in section 3.3. Broadband excited cross sections are shown in Sections 4.1.4 and 4.2.4

The experimental set-up is described in detail by J Robertson [34] and will only briefly be described below. It employs the same principles as the pump-probe method described above however the probe pulse consists of a broadband (white) beam that is able to probe the wavelength dependence of the T_1 to T^* absorption.

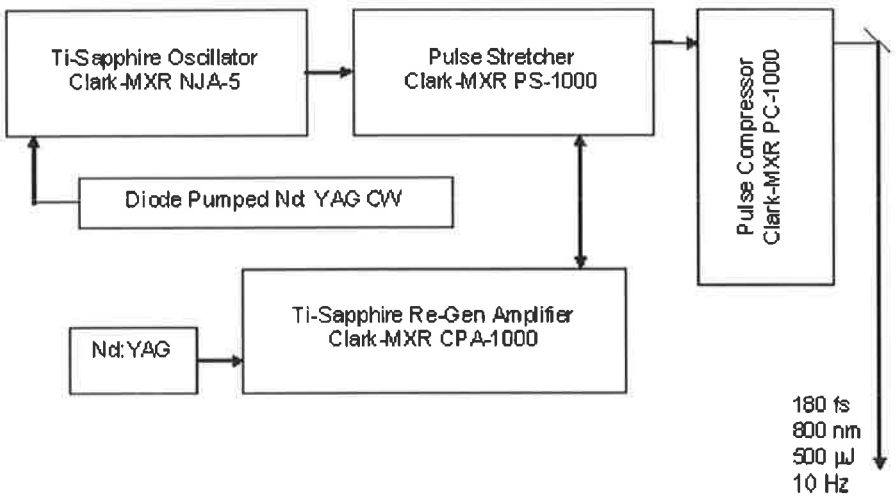

Figure 3-8: Laser system used to generate 180 fs pulses at 10 Hz

A Millennium V CW laser was used to pump a Ti-sapphire oscillator (Clark-MXR, NJA-5). To avoid damage to optical components, the femtosecond pulse was stretched using a (Clark-MXR PS-1000. pulse stretcher) before being amplified by a Ti-Sapphire regenerative amplifier (Clark CPA-1000). This technique is known as chirped pulse amplification. The beam was then compressed using a pulse compressor (Clark-MXR PC-1000). This system produces 180 fs, 500 μJ pulses at 10 Hz which were used for both the pump and probe beams as shown in Figure 3-9.

Figure 3-9 shows the pump and probe beam paths. The pulse was first split into the pump and probe beams using a beam splitter. The pump beam was passed through a SHG crystal to produce 400 nm pulses as TMAs show strong absorption at 400 nm and very little if any ground state absorption at 800 nm. This pump beam was then polarized and focused into the cuvette containing the sample dissolved in THF.

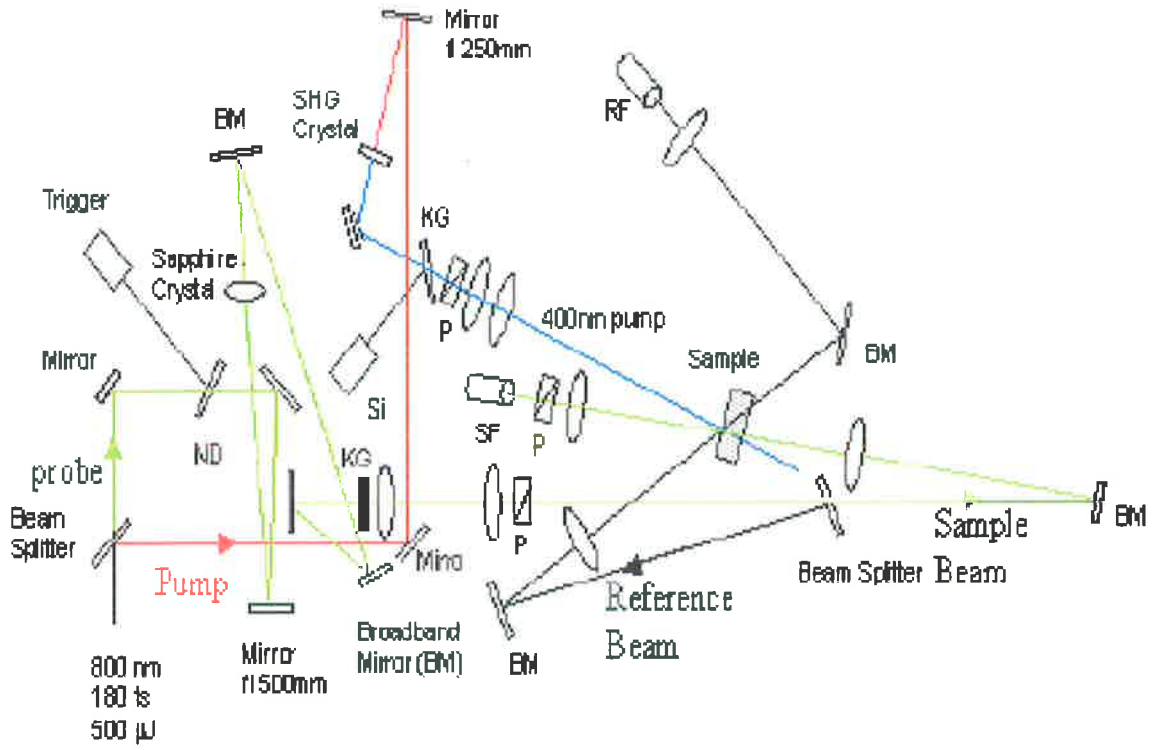

Figure 3-9: White light femtosecond spectroscopy system.

The probe beam passes through a Sapphire crystal which turns it into a white light continuum before passing through the sample. In this experimental setup there was some optical cross talk between the reference and signal detector fibres. Thus several sets spectra were collected so that the cross talk components could be removed. A series of ground state (files 1- 3) and excited state (files 4-6) transmission spectra were recorded as detailed in Table 3-1. Each file consisted of an average of 1000 spectra.

File name	Experimental details	Description
File 1	Both fibres, sample present, no pump beam	Ground state transmission of probe reference beam and signal beam
File 2	Reference fibre only, signal fibre blocked, sample present, no pump beam	Signal fibre cross talk due to reference exposure
File 3	Signal fibre only, reference fibre blocked sample present, no pump beam	Reference fibre cross talk due to signal exposure
File 4	Both fibres, sample present, with pump beam	Excited state probe beam transmission
File 5	Reference fibre only, signal fibre blocked sample present, with pump beam	Signal fibre cross talk due to reference exposure
File 6	Signal fibre only, reference fibre blocked sample present, with pump beam	Reference fibre cross talk due to signal exposure

Table 3-1: Files collected during white light spectroscopy experiments.

Cross talk between the reference and signal fibres was removed using the following data manipulation:

1. Remove cross talk from the reference to the signal detectors..... Test = (file 1)-(file2)
2. Remove cross talk from the signal to the reference detectors.....Test1 = (file 1) – (file 3)
3. Calculate ground state absorption..... Ground= Test/ Test 1

4. Remove cross talk from the reference to the signal detectors..... Test 2 = (file 3) – (file 4)
5. Remove cross talk from the signal to the reference detectors..... Test 3 = (file 3) –(file 5)
6. Calculate excited state absorption ..... Excited =Test 2/Test 3
7. Calculate excited state to ground state transmission ..... $T_{excited}/T_{ground}$=Excited/Ground

The $T_{excited}/T_{ground}$ spectrum was then multiplied by the ground state transmission spectrum (collected using a spectrometer) to give the T_1 to T^* transmission spectrum as shown in Figure 3-10 below, which shows that the strongest excited state absorption occurs at approximately 600 nm. This assumes that there is no further singlet-singlet absorption.

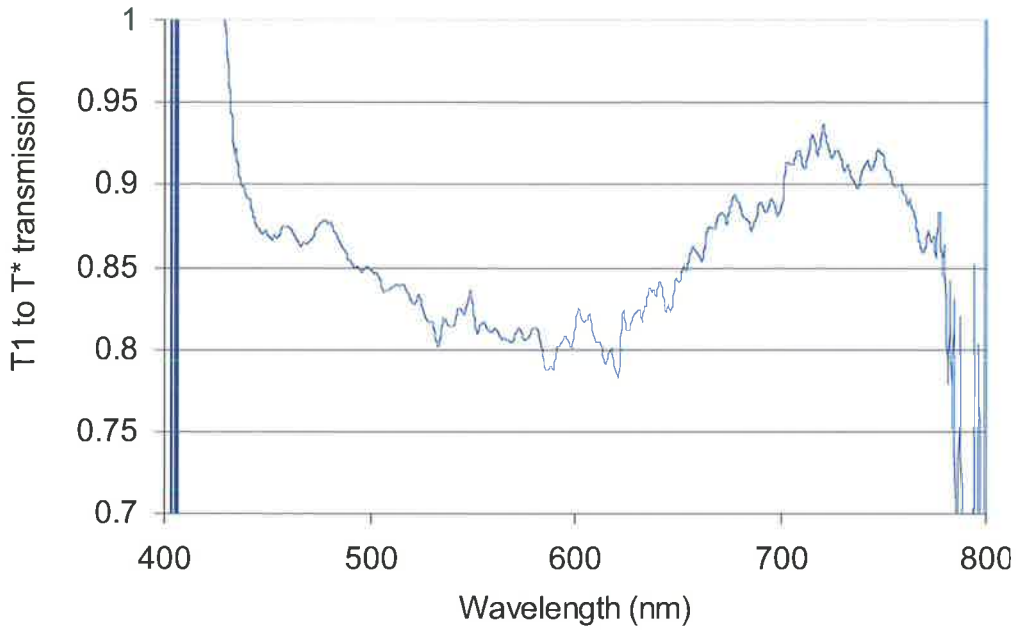

Figure 3-10: Excited state transmission spectrum of a TMA in THF.

3.5. Two-Photon Absorption Cross Sections

It is known that two-photon absorption is a significant mechanism in optical limiting for Pt:ethynyl above 540 nm, however whether it is important below 540 nm was not known. Also, as will be shown in Section 6.1, theoretical modelling of PEPE showed an S_1 state located 4.78 eV above S_0, which is close to the energy of two 532 nm (2.33 eV)

photons. Measurements were therefore performed to determine the two-photon absorption coefficient, β, of PEPE and the oligomers at 532 nm.

Two-photon absorption was measured using 30 ps pulses focused using a 75 mm lens before passing through a 2 mm sample not at focus, shown in Figure 3-11. Low energy picosecond pulses were used to ensure no excited state absorption occurred. The sample transmission was recorded for various pulse energies and the spot size measured by recording the transmitted energy as a razor blade edge passed perpendicular through the beam.

Plots of transmitted energy as a function of incidence are shown in Appendix C.

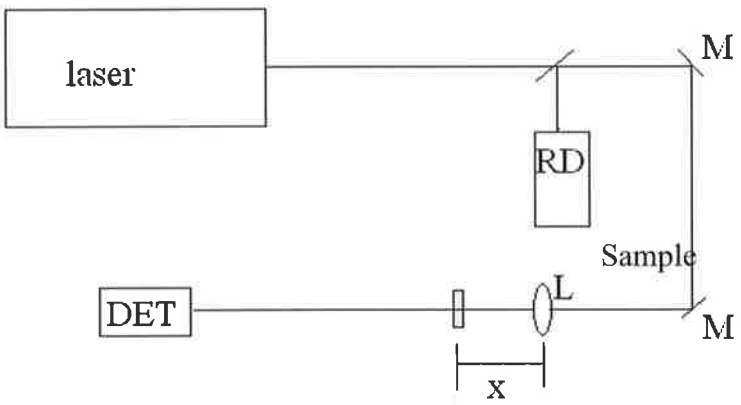

Figure 3-11: Two-photon absorption test-bed, x=160 mm. RD is the reference detector, Det is the sample detector, M are mirrors, L is the lens (f=75 mm).

For a Gaussian beam passing through a dilute solution, the transmissivity, T, can be written[35]:

$$T = e^{-\acute{a}L} T_i \qquad \textbf{3-3}$$

where α is the linear absorption coefficient, L is the interaction length, and T_i, the intensity dependent transmissivity, is given by

$$T_i = \frac{\ln(1 + \hat{a}LI_0)}{\hat{a}LI_0} \qquad \textbf{3-42}$$

where β is the two-photon absorption coefficient and I_0 is the incident intensity. Since $\hat{a}LI_0$ is small, Equation (3-12) can be simplified to

$$\frac{1}{T} = e^{\acute{a}L} + e^{\acute{a}L}\frac{\hat{a}L}{2}I_0 \qquad \textbf{3-5}$$

Thus, the slope of the line of best fit to a plot of T^{-1} against I_0 can be used to determine $\hat{a}$. The two-photon absorption cross section, $\acute{o}'_2$, can then be calculated using

$$\acute{o}'_2 = h\tilde{o}\acute{o}_2 = h\tilde{o}\hat{a}/N_0 \qquad \textbf{3-14}$$

where N_0 is the molecular density. Usually β has units of cm/GW and N_0 has units of molecules/cm^3, giving units for σ_2 of cm^4/GW.

4. Spectroscopy Results

In this Chapter I present results of the measurements described in Chapter 3. In Section 4.1, I present the results for the terminal-phenyl oligomers, followed by the terminal-acetylide oligomers in Section 4.2. The results for PEPE are presented in Section 4.3.

4.1. Terminal-Phenyl Oligomers

4.1.1. Time Resolved Luminescence Spectra

Time resolved fluorescence spectra of terminal-phenyl oligomers were measured as described in Section 3.1. The spectra recorded using different integration times are shown in Figures 4-1 and 4-2. For long integration times, the luminescence is dominated by phosphorescence from the T_1 to S_0 decay, indicating efficient intersystem crossing. Fluorescence from the S_1 to S_0 decay is dominant for short integration times.

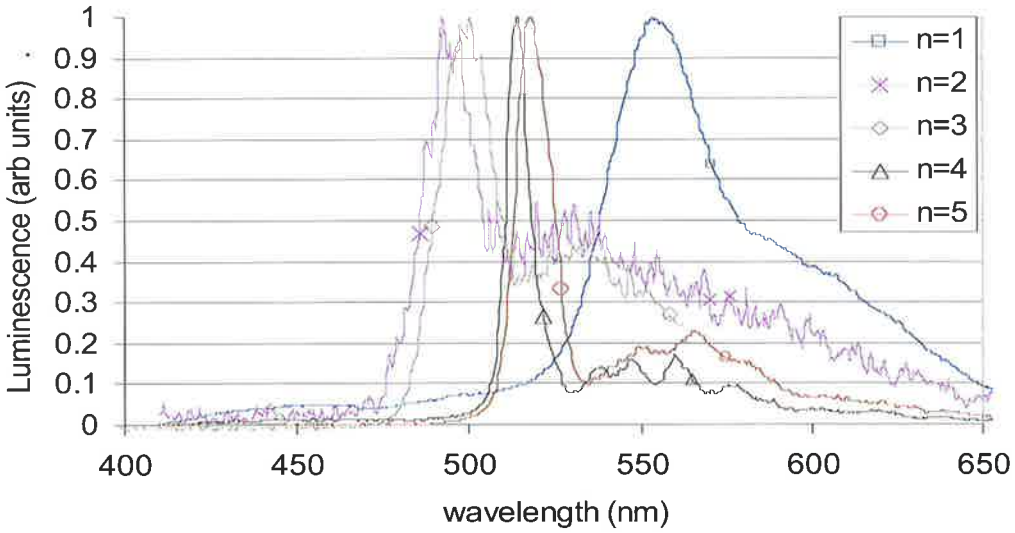

Figure 4-1: Normalised luminescence for terminal-phenyl oligomers at 17 K collected using 15 ms integration time and no delay.

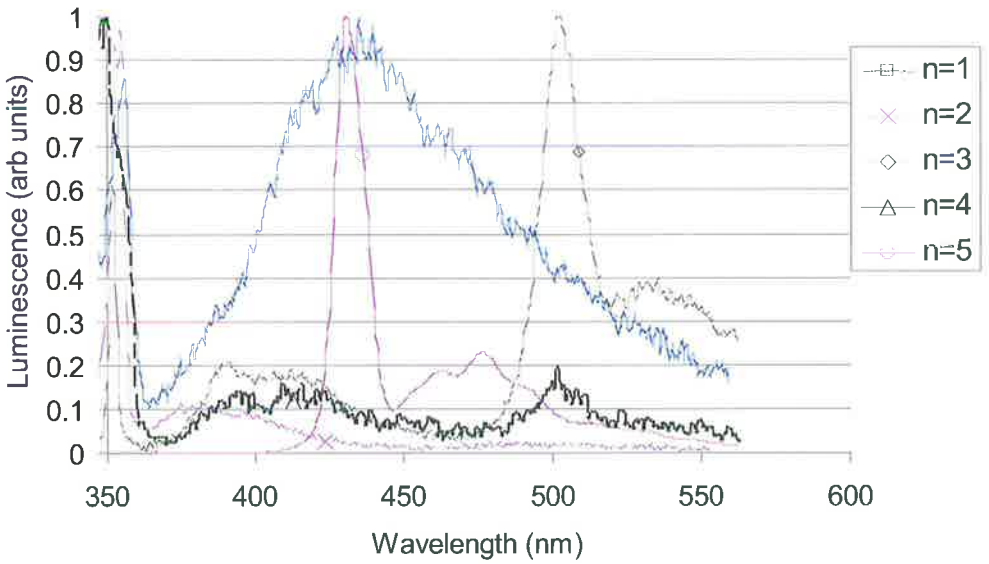

Figure 4-2: Normalised fluorescence for terminal-phenyl oligomers at 17 K recorded using a 70 ns integration time and no delay.

The fluorescence and phosphorescence maxima are listed in Table 4-1. Except for the anomalous maxima of the monomer, the maxima shift to longer wavelengths as the number of repeat units increases, as observed by Liu [31]. To confirm that the observed monomer fluorescence maximum was not due to luminescence from the copper substrate I also recorded the spectrum of a blank copper disc, as shown in Figure 4-3. It can be seen that the monomer definitely luminesces at a slightly longer wavelength than a blank copper disc, the reason for the anomalous phosphorescence wavelength is not known and further studies are required.

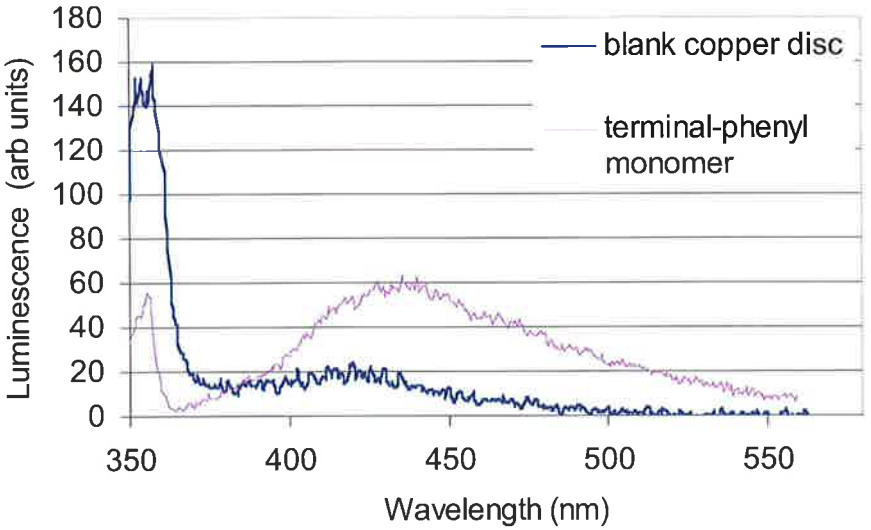

Figure 4-3: Luminescence recorded for blank copper disc and terminal-phenyl monomer. The spectrum for the blank copper disc was collected using a 1 μs integration time, while a 70 ns integration time was used for the monomer.

n	S_1 to S_0	T_1 to S_0	τ_{ISC} at 300 K	τ_{T1} at 17 K	τ_{T1} at 300 K
	nm	nm	ps	μs	μs
1	434	550	400	12	0.4
2	379	486	350	10	
3	391	500	270	28	1
4	394	511	300	15	
5	433	519	250	9.5	
Pt:ethynyl	360	520	330	700	0.3

Table 4-1: Time resolved spectroscopy results for terminal-phenyl oligomers.

Due to time constraints the phosphorescence lifetime temperature dependence was only measured for the monomer and trimer (see Figure 4-4). At 300 K the phosphorescence lifetime of both the monomer and trimer decreased to 0.4 μs and 1 μs respectively. I expect that the other oligomers will have similar phosphorescence lifetimes, which, while

significantly shorter than at 17 K is still significantly longer than the nanosecond pulse used in optical limiting measurements. The effect of T_1 lifetime on optical limiting is discussed in further detail in Chapter 5.

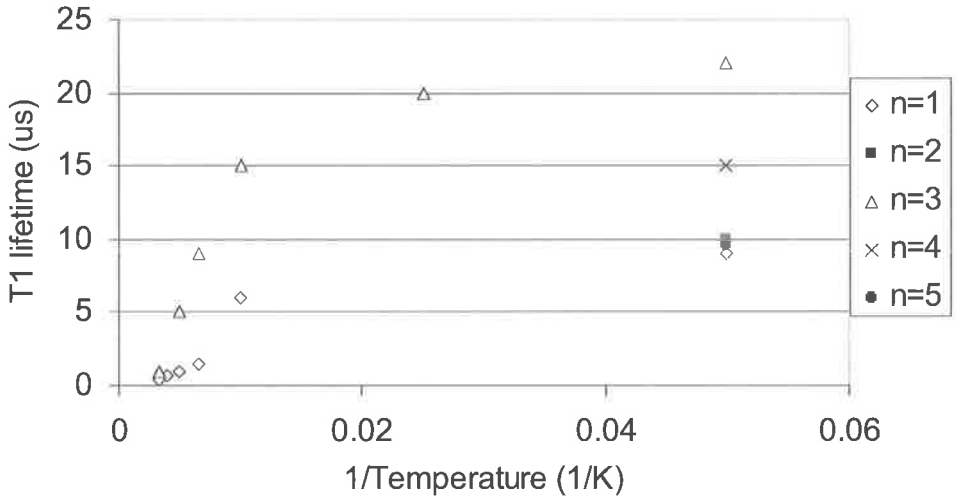

Figure 4-4: T_1 lifetime as a function of temperature for terminal-phenyl oligomers.

4.1.2. Intersystem Crossing Rates

To determine the S_1 decay rate, the fluorescence was recorded using the measurement technique described in Section 3.2. The time dependence of the fluorescence for the monomer is shown in Figure 4-5. The decay curves of the other oligomers are similar (see Table 4-1) and can be found in Appendix C. The extremely short S_1 lifetime, around 300 ps, indicates prompt intersystem to the triplet state as has been observed in Pt:ethynyl, which has a measured S_1 lifetime of 330 ps [36].

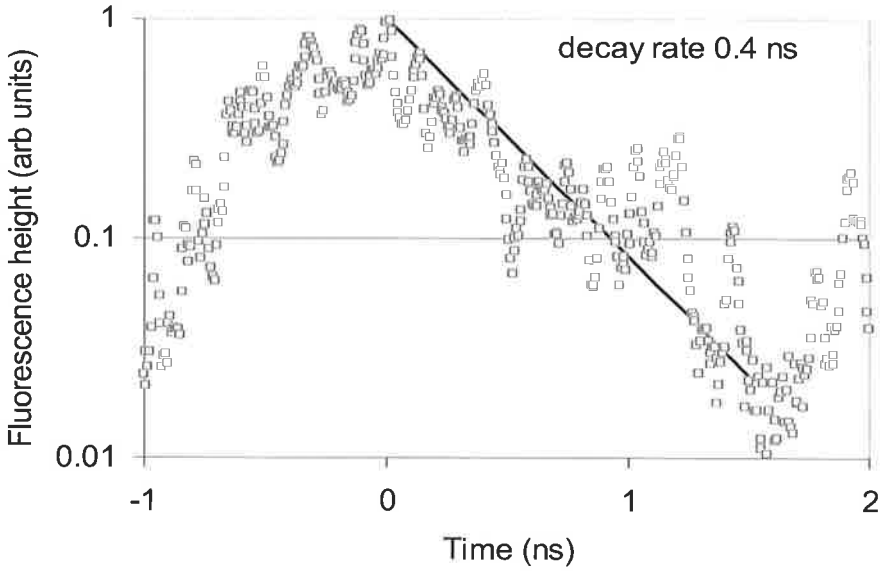

Figure 4-5: Fluorescence decay observed by streak camera for the monomer at 17 K.

4.1.3. Absorption Cross Sections

Ground and excited state absorption cross sections at 532 nm, σ_S and σ_T respectively, were measured as described in Section 3.3. The results are listed in Table 4-2, and show that the excited state absorption cross section varies only slightly with number of repeat units. The ground state absorption on the other hand increases strongly, resulting in a large decrease of the σ_T/σ_S ratio as the number of repeat units increase.

\

n	σ_S	σ_T	$\acute{o}_T/\acute{o}_S$
	$x10^{-18}$ cm^2/molecule	$x10^{-18}$ cm^2/molecule	
1	0.0065	1.61 ± 0.2	334
2	0.048	3.3 ± 0.3	73
3	0.13	3.2 ± 0.3	25
4	0.28	5.1 ± 0.6	17
5	97	4.9 ± 0.3	0.05
Pt:ethynyl	.063	1.58 ± 0.3	25

Table 4-2: Absorption cross sections at 532 nm for terminal-phenyl oligomers.

4.1.4. Broadband Excited State Absorption Cross Sections

Broadband excited state absorption spectra were measured for the terminal-phenyl tetramer and terminal-phenyl pentamer as described in Section 3.4. The results are shown in Figures 4-6 and 4-7 below.

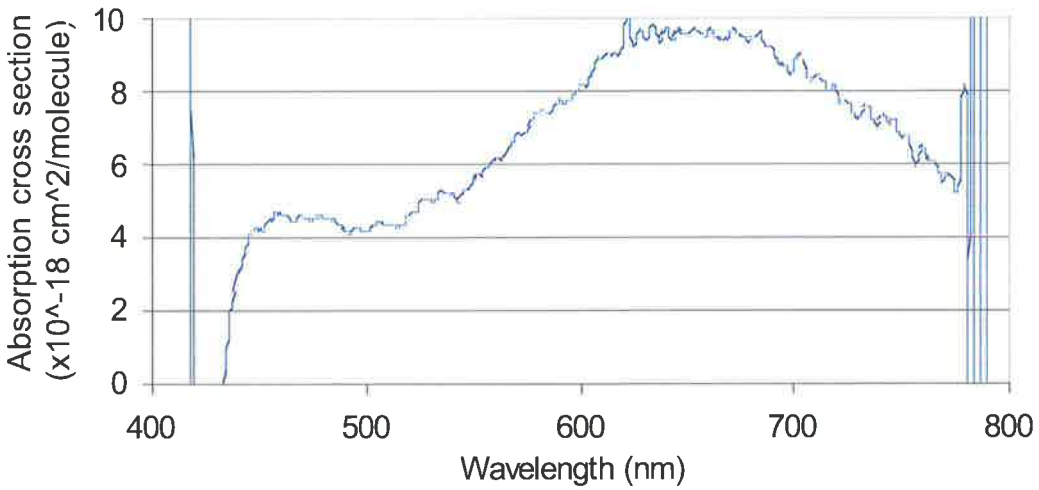

Figure 4-6: Excited state absorption spectrum for the terminal-phenyl tetramer. The peaks at 400 and 800 nm are artefacts of the measurement technique.

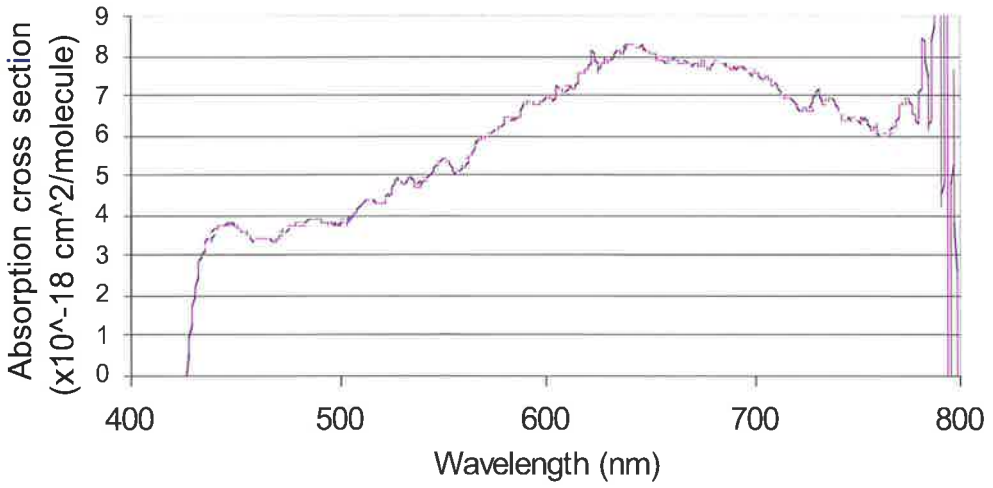

Figure 4-7: Excited state absorption spectrum for the terminal-phenyl pentamer. The peak at 800 nm is an artefact of the measurement technique.

As discussed in Section 3.5, the absolute values of the excited state cross sections were not found, however I have calibrated them using the excited state cross section obtained from pump-probe measurements at 532 nm. Both spectra show broadband T_1 to T^* absorption in the visible, which is similar to Pt:ethynyl. The similarity of these spectra and of the σ_T values at 532 nm reported in section 4.1.3 indicate that probably all of these terminal-pheynyl oligomers have similar excited state absorption spectra.

4.1.5. Two-photon Absorption Coefficients for S_0 State

Two-photon absorption coefficients were measured as described in Section 3.5. The results are listed in Table 4-3, plots can be found in Appendix C.

n	β cm/GW	σ_2' $x10^{-48}$ cm^4 s/photon
1	2.7	169
2	0.67	25
3	0.88	66
4	1.21	195
5	2.2	1640
Pt:ethynyl	0.21	34

Table 4-3: Two-photon absorption, β and σ_2' values for terminal-phenyl oligomers.

All of the oligomers show some degree of two-photon absorption. These values are comparable to those of strong organo-metallic two-photon absorbers, which typically would have values in the order of $600x10^{-50}$ cm^4s $photon^{-1}$ [37]. This suggests that two-photon absorption plays a significant role in optical limiting for these materials, as will be discussed in more detail in Chapter 6. Some of the two-photon absorption measurements are significantly higher than measured for similar materials, this could be due to experimental error that may have been caused by strong single-photon absorption, possibly from the S_1 to S_2 state.

4.2. Terminal-Acetylide Oligomers

4.2.1. Time Resolved Luminescence Spectra

As for the terminal-phenyl oligomers, time resolved luminescence spectra of terminal-acetylide oligomers were measured as described in Section 3.1. Spectra recorded using different integration times are shown in Figures 4-8 and 4-9. For long integration times, the luminescence is again dominated by phosphorescence, while for short integration times

fluorescence dominates. The wavelengths of the fluorescence and phosphorescence maxima and the measured phosphorescence decay times are listed in Table 4-4.

In Figure 4-8 the dimer has extremely weak phosphorescence that is almost swamped by the fluorescence, while for the trimer the fluorescence emission is still significantly stronger than the phosphorescence.

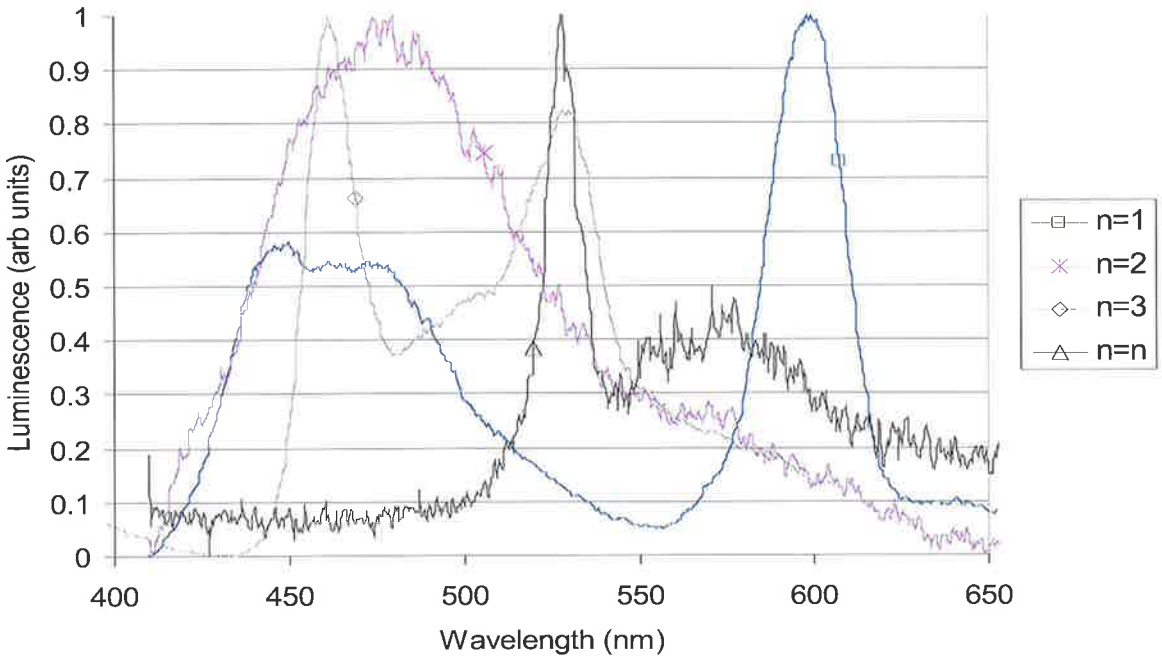

Figure 4-8: Normalised luminescence for terminal- acetylide oligomers at 17 K collected using 15 ms integration time and no delay

The wavelength of the phosphorescence peaks shown in Figure 4-8 range from 525 to above 600 nm. This is a significant red-shift from that of the terminal-phenyl oligomers, and a wider range of phosphorescence maxima. The phosphorescence maxima for the trimer and polymer are the same indicating that the triplet excitation is localized to within three repeat units. It is surprising that the phosphorescence maximum of the monomer is near 600 nm, as a maxima below 530 nm was expected.

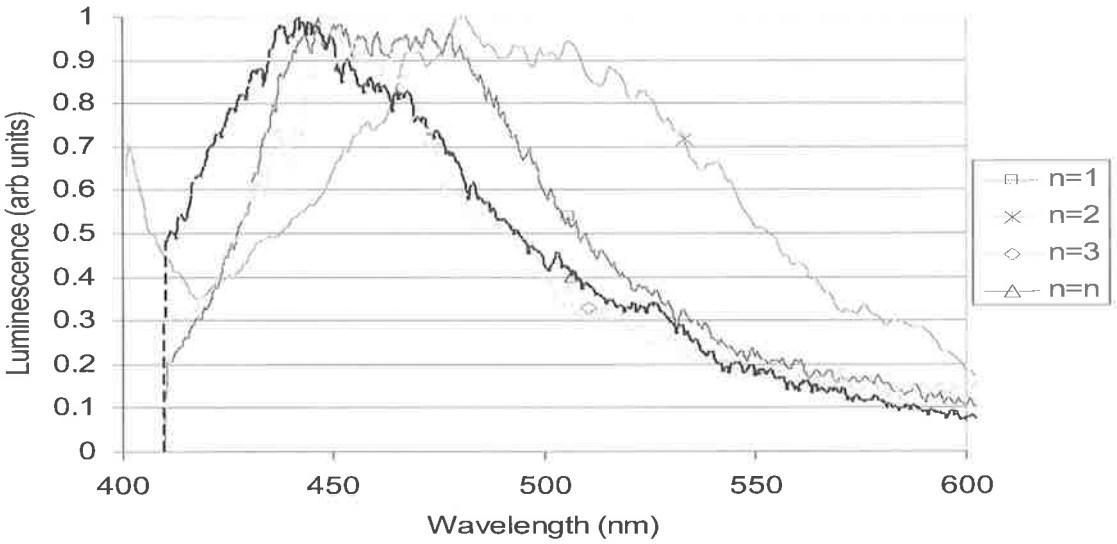

Figure 4-9: Normalised fluorescence for terminal- acetylide oligomers at 17 K recorded using a 70 ns integration time and no delay.

Fluorescence shown in Figure 4-9, collected using a 70 ns integration time occur at slightly higher wavelengths than for the terminal-phenyl oligomers indicating that the S_1 state is delocalised over a larger area than for the terminal-phenyl oligomers.

n	S_1 to S_0	T_1 to S_0	τ_{ISC} at 300 K	τ_{T1} at 17 K	τ_{T1} at 300 K
	nm	nm	ps	μs	μs
1	451	585	330	5.7	
2	472	575	330	2.8	
3	452	525	450	10	0.7
n	442	528	330	6.7	

Table 4-4: Time resolved spectroscopy results for terminal-acetylide oligomers.

The temperature dependence of the phosphorescence lifetime was measured for the trimer as shown in Figure 4-10.

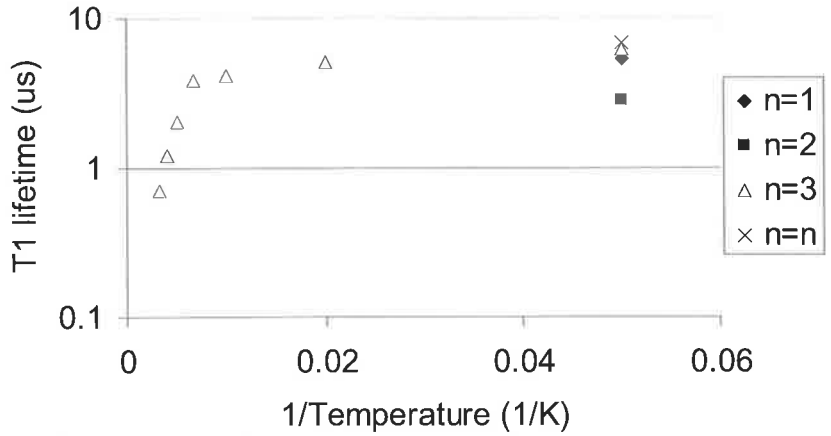

Figure 4-10: T_1 lifetime as a function of sample temperature for terminal-acetylide oligomers.

4.2.2. Intersystem Crossing Rates

The fluorescence lifetime was measured as described in Section 3.2. Again, the lifetimes were found to be in the order of several hundred picoseconds, indicating prompt intersystem crossing to T_1 as observed in the terminal-phenyl oligomers. Plots of decay against time can again be found in Appendix C and the intersystem crossing rates (τ_{ISC}) are listed in Table 4-4.

4.2.3. Absorption Cross Sections

Ground and excited state absorption cross sections at 532 nm, σ_S and σ_T respectively, were measured as described in Section 3.3. The results are listed in Table 4-5.

n	σ_S	σ_T	$\acute{o}_T/\acute{o}_S$
	x10^{-18} cm^2/molecule	**x10^{-18} cm^2/molecule**	
1	0.030	4.4 ±0.4	95
2	0.47	5.5 ± 0.8	11.7
3	0.67	5.1 ± 0.9	7.3
n	22	5.8 ± 0.9	0.27

Table 4-5: Absorption cross Sections at 532 nm for terminal-acetylide oligomers.

As for the terminal-phenyl oligomers the ratio of excited state absorption to ground state decreases as the number of repeat units increases as absorption at 532 nm increases with increasing n. The σ_T values for these oligomers are very similar to those for the terminal-phenyl oligomers.

4.2.4. Broadband Excited State Absorption Cross Sections

Excited state absorption spectra for the terminal-acetylide monomer, dimer and trimer were measured as described in Section 3.4. As the number of repeat units increases the peak of the absorption increased and broadened slightly.

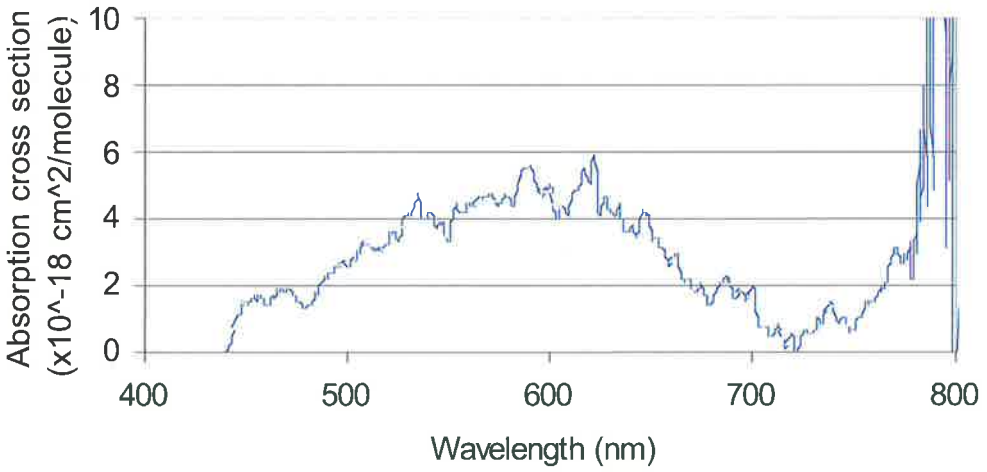

Figure 4-11: Excited state absorption spectrum for the terminal-acetylide monomer. The peak at 800 nm is an artefact of the measurement technique.

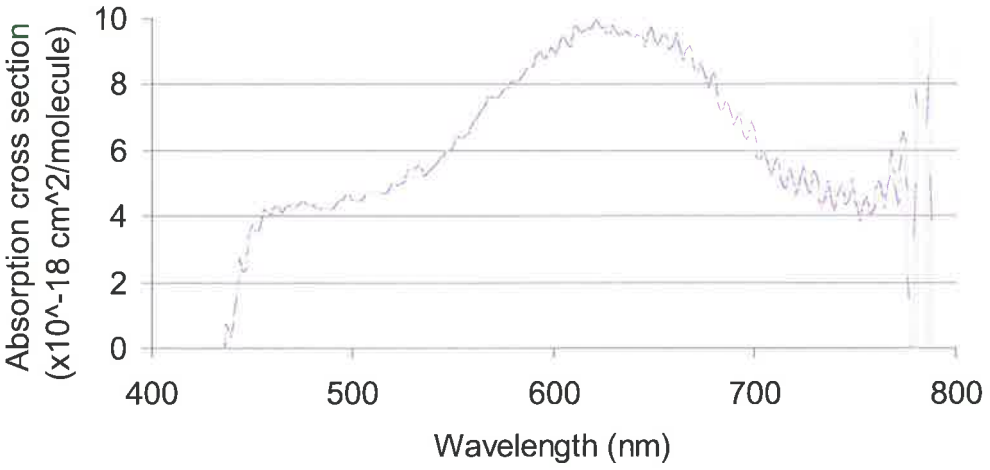

Figure 4-12: Excited state absorption spectrum for the terminal-acetylide dimer. The peak at 800 nm is an artefact of the measurement technique.

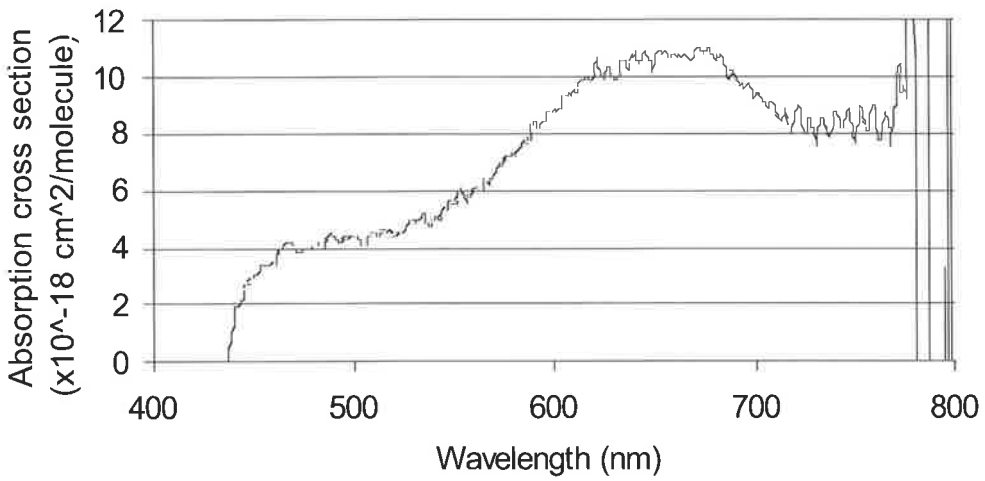

Figure 4-13: Excited state absorption spectrum for the terminal-acetylide trimer. The peak at 800 nm is an artefact of the measurement technique.

4.2.5. Two-photon Absorption Coefficients for S_0 States

Two-photon absorption coefficients were measured as described in Section 3.5

n	β cm/GW	σ_2' x10^{-48} cm^4 s/photon
1	0.93	340
2	1.03	1170
3	2.75	5770
n	1.5	82130

Table 4-6: Two-photon absorption, β and σ_2' values for terminal-acetylide oligomers.

All of the materials again show significant two-photon absorption at 532 nm.

4.3. PEPE

As discussed in Chapter 2, optical limiting results for PEPE showed surprising optical limiting. The following results reveal a fortuitous alignment of the singlet and triplet energy levels that allows the triplet states to be accessed without the presence of a heavy atom.

4.3.1. Time Resolved Luminescence Spectra

The time resolved spectrum of PEPE was measured as described in Section 3.1. Results are shown in Figure 4-14.

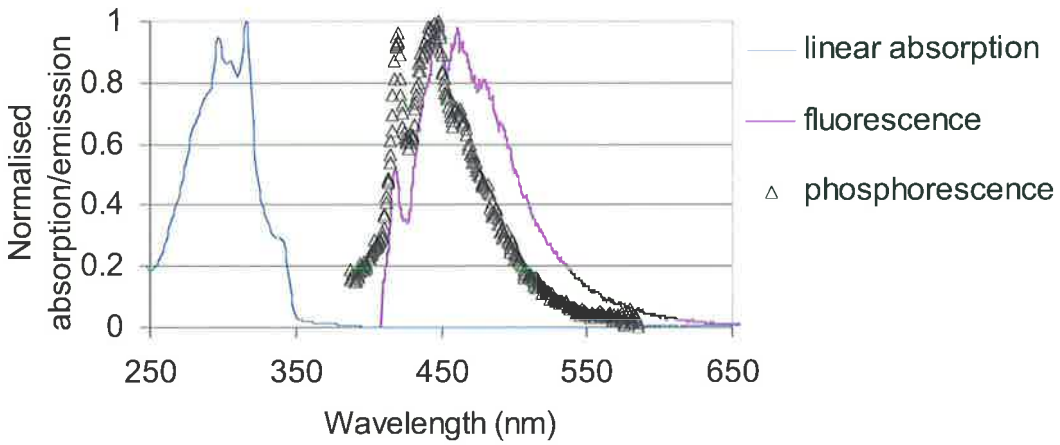

Figure 4-14: Ground state absorption of an extremely dilute solution at room temperature. Fluorescence and phosphorescence signals of PEPE recorded at 17 K.

Figure 4-14 shows fluorescence and phosphorescence emissions at similar wavelengths indicating energy matching of the singlet and triplet manifolds as predicted by numerical modelling in Section 6.1. Both fluorescence and phosphorescence spectra show peaks at 420, 448 and 462 nm. The S_1 absorption spectrum shown in Figure 4-14 shows a reflection of the emission spectra as expected [38].

The phosphorescence lifetime was measured as described in Section 3.1, and was found to be independent of sample temperature at temperatures up to 200 K, above which no phosphorescence was observed. Figure 3-4 is reproduced here as Figure 4-15 for convenience.

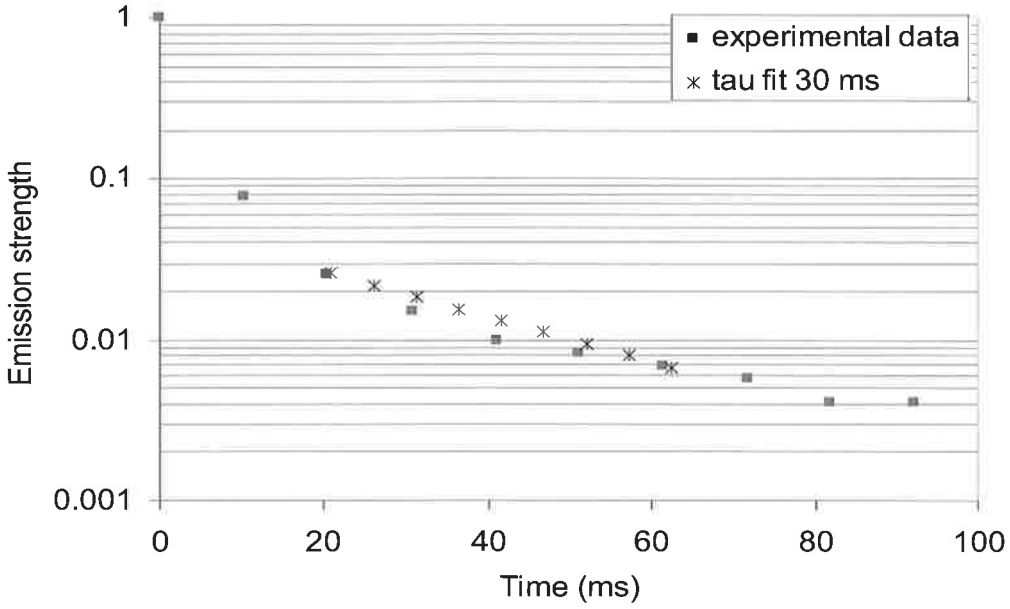

Figure 4-15: Decay of PEPE phosphorescence at 17 K.

4.3.2. Intersystem Crossing Rate

The fluorescence decay rate was measured as described in Section 3.2. For PEPE the S_1 lifetime was 0.4 ns, similar to the oligomers. This shows that despite the absence of a heavy metal in PEPE there is still prompt intersystem crossing into the triplet manifold.

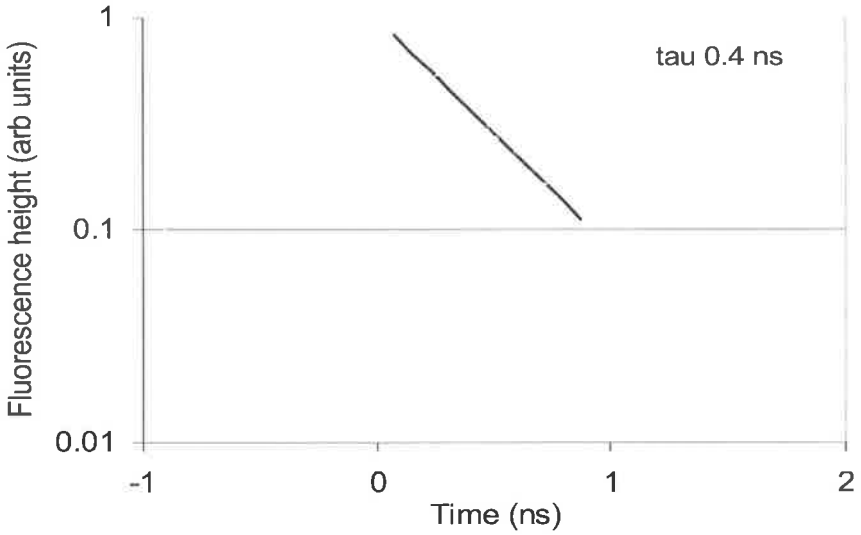

Figure 4-16: Fluorescence decay of PEPE at 300 K.

4.3.3. Excited State Absorption Cross Section

Absorption cross sections were measured as described in Section 3.3. The excited state absorption cross section was found to be 2.8 $x10^{-18}$ cm^2/molecule and the ground state absorption cross section was 3.2 $x10^{-21}$ cm^2/molecule giving a ratio of 863, which is the highest σ_T/σ_S ratio that I measured.

4.3.4. Two-Photon Absorption Coefficient

As described in Section 3.5 a two photon absorption cross section was measured for PEPE, the results are shown in Figure 4-17. The sample tested had a linear absorption (α) of 0.7 cm^{-1} for N_0 of $1.7x10^{20}$ molecules/cm^3, L=0.2 cm and the slope of the fit of 1/T against I_0 was 0.22, giving β= 1.7 cm/GW (σ_2' of $3.8x10^{-48}$ cm^4 sec). The error in this calculation however is quite large (50%) and the two-photon absorption coefficient should be used as a guide only. However, this value is comparable to Stilbene ($\sigma_2' = 2.1x10^{-48}$ cm^4 sec) [39], which is regarded as a good two-photon absorber.

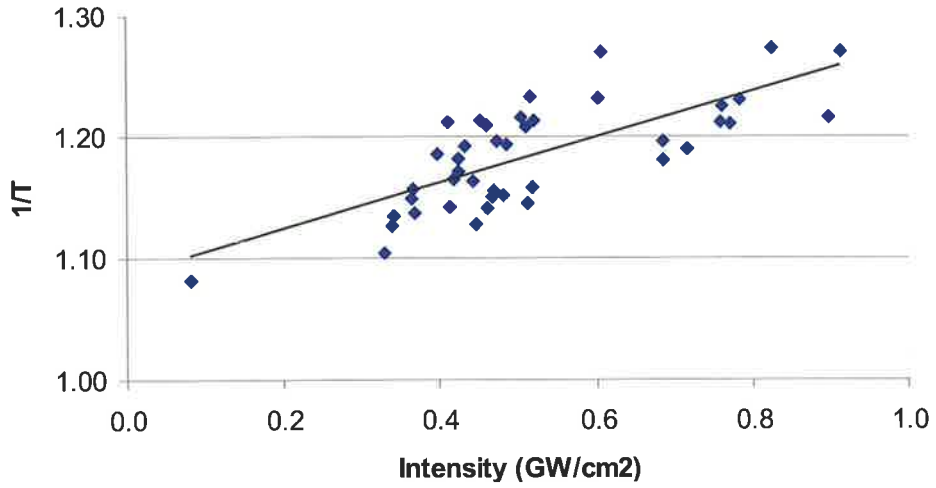

Figure 4-17: Inverse transmitted energy versus intensity for PEPE. Sample transmission was 90% at 532 nm.

5. Numerical Modelling of an Optical Limiter

A computer program that models an optical limiter placed in the f/5 test-bed, described in Chapter 2, using the 5-level model, described in Section 1.3.4, has been developed by J Hermann and P Wilson at DSTO Edinburgh [24]. The model uses standard rate-equation analysis as described by the following equations:

$$\frac{dN_{S_0}}{dt} = -\frac{\sigma_{S_0\rightarrow S_1} N_{S_0} I}{\hbar\omega} - \frac{\sigma_2 N_{S_0} I^2}{2\hbar\omega} - \frac{\sigma_{S_0\rightarrow T_1} N_{S_0} I}{\hbar\omega} + \frac{N_{S_1}}{\tau_{S_1}} + \frac{N_{T_1}}{\tau_{T_1}} \qquad 5\text{-}1$$

$$\frac{dN_{S_1}}{dt} = \frac{\sigma_{S_0\rightarrow S_1} N_{S_0} I}{\hbar\omega} + \frac{\sigma_2 N_{S_0} I^2}{2\hbar\omega} - \frac{N_{S_1}}{\tau_{S_1}} - \frac{N_{S_1}}{\tau_{ISC}} - \frac{\sigma_{S_1\rightarrow S_2} N_{S_1} I}{\hbar\omega} + \frac{N_{S_2}}{\tau_{S_2}} \qquad 5\text{-}2$$

$$\frac{dN_{T_1}}{dt} = -\frac{\sigma_{T_1\rightarrow T^*} N_{T_1} I}{\hbar\omega} + \frac{N_{S_1}}{\tau_{ISC}} + \frac{\sigma_{S_0\rightarrow T_1} N_{S_0} I}{\hbar\omega} - \frac{N_{T_1}}{\tau_{T_1}} + \frac{N_{T^*}}{\tau_{T^*}} \qquad 5\text{-}3$$

$$\frac{dN_{T^*}}{dt} = \frac{\sigma_{T1\rightarrow T^*} N_{T1} I}{\hbar\omega} - \frac{N_{T^*}}{\tau_{T^*}} \qquad 5\text{-}4$$

$$\frac{dN_{S_2}}{dt} = \frac{\sigma_{S_1\rightarrow S_2} N_{S_1} I}{\hbar\omega} - \frac{N_{S_2}}{\tau_{S_2}} \qquad 5\text{-}5$$

where N_{S0}, N_{S1}, N_{S2}, N_{T1} and N_{T*} are the density of occupied S_0, S_1, S_2, T_1 and T* states respectively. τ_{S1}, τ_{S2}, τ_{T1} and τ_{T*} are the lifetimes of the S_1, S_2, T_1 and T* states and τ_{ISC} is the intersystem crossing time from S_1 to T_1. $\sigma_{S0\rightarrow S1}$ is the single photon S_0 to S_1 absorption cross section, $\sigma_{S1\rightarrow S2}$ is the single photon S_1 to S_2 absorption cross section, $\sigma_{S0\rightarrow T1}$ is the single photon S_0 to T_1 absorption cross section, $\sigma_{T1\rightarrow T*}$ is the excited state absorption cross section, σ_2 is the S_0 to S_1 two-photon absorption cross section and ω is the angular frequency of the laser radiation. I is the intensity of the pulsed laser beam, assumed to be a Guassian beam of radius *w* and FW1/eM pulse length 2τ:

$$I(r,t)=I_o e^{-r^2/w^2} e^{-t^2/\delta^2} \qquad 5\text{-}6$$

The user provides the following parameters for the limiter:

- Concentration (N_0)
- Interaction length (L)
- S_0 to S_1 linear absorption coefficient ($\alpha=\sigma_{S0\rightarrow S1}N_0$)
- S_0 to S_1 two-photon absorption coefficient (β)
- S_0 to T_1 absorption cross section ($\sigma_{S0\rightarrow T1}$)
- S_1 to S_2 absorption cross section ($\sigma_{S1\rightarrow S2}$)
- T_1 to T^* excited state absorption cross section ($\sigma_{T1\rightarrow T^*}$)
- S_1 to S_0 relaxation time (τ_{S1})
- S_2 to S_1 relaxation time (τ_{S2})
- S_1 to T_1 relaxation time (τ_{ISC})
- T^* to T_1 relaxation time (τ_{T^*})
- T_1 to S_0 relaxation time (τ_{T1}).

The following parameters for the incident laser pulse are also provided:

- Pulse energy
- Waist radius
- Pulse duration (FW1/eM)
- Wavelength.

The program then calculates the energy of the transmitted pulse. It also reports the following diagnostic information:

- The number of S_0 to S_1 and S_1 to T_1 transitions
- The number of S_1 to S_2 and S_2 to S_1 transitions
- The number of S_0 to T_1 and T_1 to S_0 transitions
- The number of T_1 to T^* and T^* to T_1 transitions

These transition counts can be used to check the operation of the model and check that energy has been conserved. Simulations of the f/5 testbed were performed to determine the effect of certain parameters and if the 5-level model accurately predicts transmitted energy. The measured spectroscopic parameters and observed limiting for PEPE will be used to validate the numerical model in Chapter 6. The parameters used in these simulations can be found in Appendix E.

The first parameter investigated was the effect of altering the T_1 to S_0 relaxation time. Most of the materials I investigated showed T_1 relaxation times of several μs at 17 K and about 1 μs at room temperature, which is more than 100 times longer than the pulse duration. As can be seen in Figure 5-1, there is minimal effect on the optical limiting if the T_1 lifetime is longer than about ten times the pulse length.

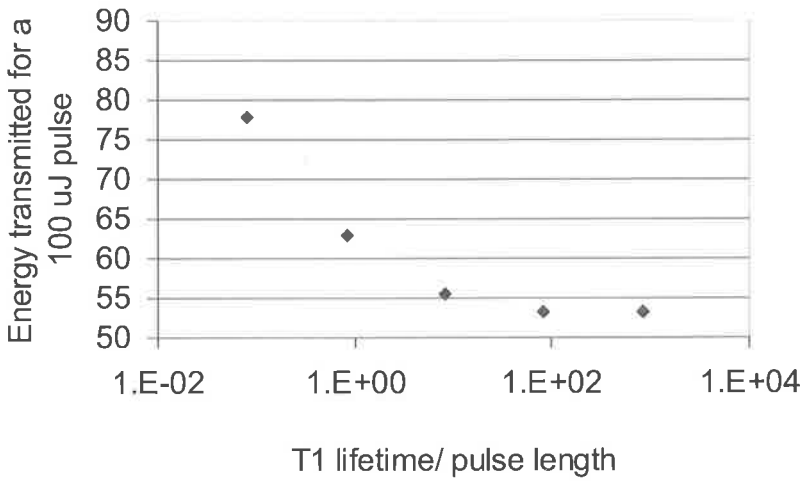

Figure 5-1: Transmitted energy for a 100 μJ, 6 ns incident pulse as a function of τ_{T1}.

Optical limiting also requires that the T^* to T_1 relaxation time is short compared to the pulse length. Figure 5-2 shows that the limiting is degraded if the T^* lifetime is longer than about 1% of the pulse lifetime, about 60 ps for the 6 ns pulses used in this thesis. Such a lifetime is long compared to that typically ascribed to excited triplet states in large

organometallic molecules [40],[41]. When ps pulses were used to measure the excited state absorption cross section, no optical limiting was observed, this is likely to be due to T^* lifetime being significantly longer than 1% of the pulse length.

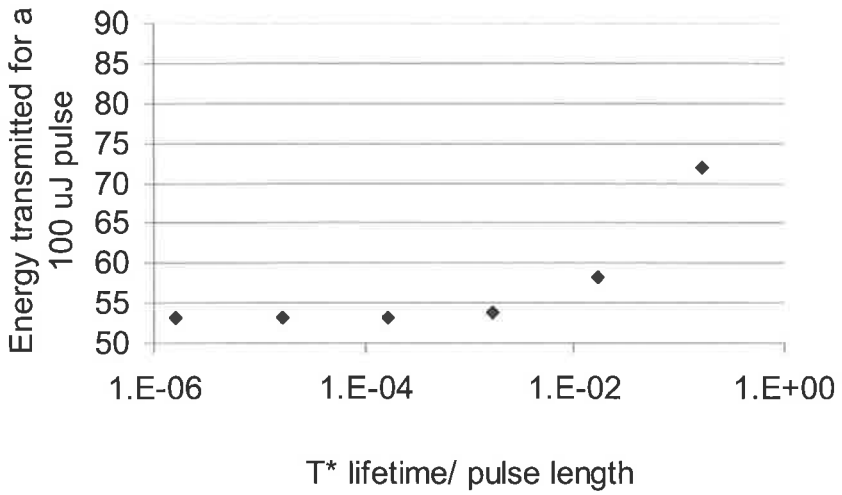

Figure 5-2: Transmitted energy for a 100 μJ, 6 ns incident pulse as a function of τ_{T^*}.

The effect of the intersystem crossing time on limiting is shown in Figure 5-3. There is minimal effect on optical limiting if the intersystem time is less than 1% of the pulse length. This allows sufficient T_1 population early in the pulse for effective excited state absorption to occur. Since the typical intersystem crossing times for the materials investigated in this thesis are about 300 ps, (0.05 times the pulse length) it is apparent that if intersystem crossing is the dominant T_1 population route, then the optical limiting will be slightly worse than for direct S_0 to T_1 population.

Previous research on Pt:ethynyl has determined that T_1 population between 500 and 540 nm occurs via direct S_0 to T_1 absorption. As mentioned in Chapter 2, the shoulder observed in the linear absorption spectra is believed to be evidence of this transition. In the oligomers that I studied there is only a small shift in the location of this shoulder so direct S_0 to T_1 absorption is most likely the dominant T_1 population pathway.

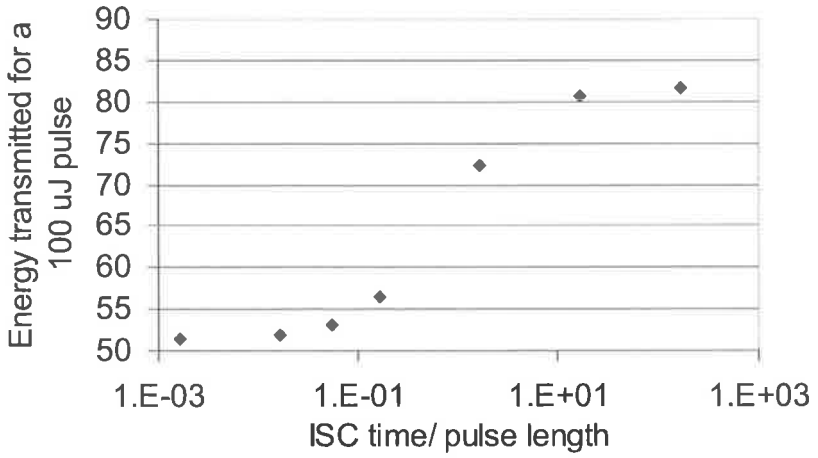

Figure 5-3: Transmitted energy of a 100 μJ, 6 ns pulse as a function of τ_{ISC} for a sample with $\sigma_S = 5x10^{-20}$ cm^2/molecule.

Figure 5-4 shows the transmitted energy for a material based on Pt:ethynyl with either indirect transitions to T_1 (via S_1) and direct S_0 to T_1 absorptions. Both sets of calculated values include two-photon absorption components. As expected the direct T_1 path is slightly better.

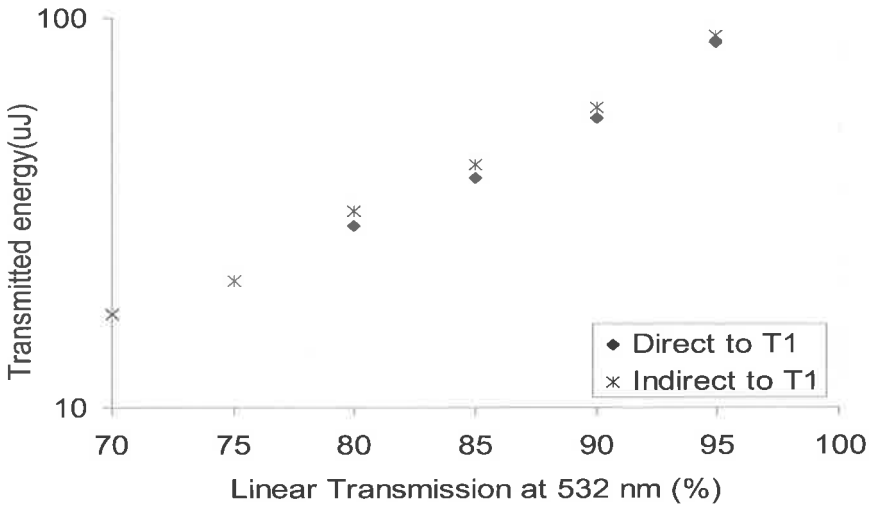

Figure 5-4: Effect of increasing concentration of Pt:ethynyl for a 200 μJ, 6 ns incident pulse.

Results of the above simulations show that an ideal optical limiter has:

- τ_{T1}> 1% of the pulse length

- $\tau_{T^*} < 0.1$ % of the pulse length
- $\tau_{ISC} < 10$ % of the pulse length.

Provided that the intersystem crossing rate is less than 10 % of the pulse length, there is negligible effect on optical limiting, for direct and indirect T_1 population pathways.

The computer model of the nanosecond testbed has mixed results for predicting the clamping level of TMAs. While it shows good agreement for PEPE the predictions are quite poor for many of the metal acetylides. It should be noted that the 5-level model does not take into account non-linear refraction and scattering, which could affect the limiting measured by the test-bed. Generally, however, these effects are unimportant for ps and ns pulse limiting. Our implementation of the 5-level model also does not include ESA from S_1, which could limit without leading to an increase in the T_1 population. An excited singlet state (S_2) lifetime greater than 30 ps but less than 6 ns could explain why limiting was not observed for the 30 ps pulses but was observed for the 6 ns pulses. However, a lifetime greater than 30 ps could preclude the intensity dependent transmittance observed in the TPA measurements, and thus it is unclear whether the observation of very large TPA cross-sections but no limiting for the oligomers with 30 ps pulses can both be explained by ESA from S_1.

Material	% Transmission at 532 nm	Measured clamping level (uJ)	Predicted clamping level (uJ)
1	86.0	7	6.3
2	94.0	5	39.7
3	85.2	6	25
4	82.1	6	26.8
5	82.4	9.5	169.3

Table 5-1: Predicted and measured transmitted energy for terminal-phenyl oligomers.

Material	% Transmission at 532 nm	Measured clamping level (uJ)	Predicted clamping level (uJ)
1	74.1	11	1.6
2	85.8	6	87.6
3	80.7	11.3	88
n	84.1	6.3	167

Table 5-2: Predicted and measured transmitted energy for terminal-acetylide oligomers

6 Discussion of Results

In this chapter I use the spectroscopic results presented in Chapter 4 to build numerical 5-level models, described in Chapter 5. The model for PEPE is discussed in Section 6.1. Recall that PEPE is of interest because it displays significant optical limiting despite its lack of a heavy metal. I will show that the PEPE results validate the 5-level numerical model.

The 5-level models for the terminal-phenyl and terminal-acetylide oligomers are discussed in Section 6.2. The oligomers are of interest as some of them show lower clamping levels than Pt:ethynyl. The 5-level model is used to investigate the structure/property relationship for the oligomers. In Section 6.3, I discuss properties of the dimers and di-Pt:ethynyl, which show the most promise as broadband optical limiters.

Recall that the following measurements were obtained for each of the oligomers and PEPE:

- Clamping levels at 470, 532 and 630 nm and occasionally at other wavelengths
- Ground state absorption spectra and cross sections at 532 nm
- Time resolved luminescence spectra, which shows efficient intersystem crossing from S_1 to T_1
- Intersystem crossing lifetime at room temperature
- T_1 lifetime at 17 K
- Estimated / measured T_1 lifetime at room temperature
- Excited state absorption (T_1 to T^*) cross section at 532 nm.
- Two-photon absorption coefficients at 532 nm.

For some materials I was also able to measure the excited state absorption spectrum.

6.1 PEPE

As shown in Section 2.3.6, PEPE limits despite the absence of a heavy atom. Time dependant response theory modelling, performed by Geoff Williams and reported in Appendix G, suggests that limiting can be explained using a modified 5-level energy diagram, as summarised in Section 6.1.1. The predictions of the response theory modelling are used to aid interpretation of the spectroscopic results for PEPE, and these values are used in the numerical 5-level model as described in Chapter 5. The results of the models are presented and compared with measurements in section 6.1.2.

6.1.1 Predictions of Response Theory Modelling

Response theory modelling of PEPE using the DALTON quantum chemistry program [42] was performed by Geoff Williams, as described in Appendix F. The modelling predicts the energy and oscillator strength of the first few singlet and triplet states. The predicted energy levels are shown in Table 6-1 and Figure 6-1. In Table 6-1, f denotes the oscillator strength and τ is the phosphorescence lifetime (for decay to S_0) predicted for an isolated molecule at the fixed ground state geometry.

The larger basis set (6-31G*) predicts a singlet state of $^1A_1$ symmetry at 263 nm (4.6 eV). The lowest triplet state ($^3A_1$) is predicted to be at around 457 nm (2.71 eV). Thus, the linear absorption maximum at 300nm (4.1 eV) probably corresponds to the singlet absorption, while the weak shoulder at 380nm (3.26 eV) in the absorption spectrum may correspond to the disallowed S_0->T_1 absorption.

The model also predicts triplet states at 4.64 and 4.68 eV ($^3A_2$ and $^3B_2$ symmetry). This is extremely close to the 4.63 eV of the $^1A_1$ excited singlet state. The spin-orbit (S-O) matrix

elements to the B_2 states are small (<1 cm^{-1}), however the S-O matrix elements to the A_2 states, $<^1A_1/H_{so}/^3A_2> = 7.2\ cm^{-1}$ ($\Delta E = 0.05$ eV) and $< ^1A_1/H_{so}/^3A_2> = 9.5\ cm^{-1}$ ($\Delta E = 0.1$ eV), are of a magnitude that is sufficient to permit effective intersystem crossing to the triplet manifold, leading to population of the lowest energy triplet state.

State symmetry	**6-31G Basis**	**6-31G* Basis**
Singlets	**Energy (eV)**	**Energy (eV)**
$^1A_1$	4.78 (f= 1.01)	4.63 (f= 1.0)
$^1A_2$	5.76 (f= 0)	5.65 (f= 0)
$^1B_2$	5.85 (f= 0.003)	5.69 (f= 0.004)
$^1A_1$	5.93 (f= 0.0001)	5.77 (f= 0.0001)
$^1A_2$	5.96 (f= 0)	5.65 (f= 0)
Triplets		
$^3A_1$	2.52 (τ = 13.7 s)	2.71 (τ = 16.5 s)
$^3A_1$	3.06	3.13
$^3A_1$	4.51	4.38
$^3B_2$	4.74 (τ = 15.3 ms)	4.56 (τ = 4.9 ms)
$^3A_1$	4.75	4.60
$^3A_2$	4.83 (τ = 3.3 μs)	4.64 (τ = 0.08 μs)
$^3B_2$	4.85	4.68
$^3A_2$	4.88	4.71
$^3A_1$	5.14	4.97
$^3A_1$	5.65	5.46

Table 6-1: Spectrum of PEPE predicted by the response theory model for the 6-31G and 6-31G* bases. f is the oscillator strength, τ is the lifetime of an isolated molecule.

Table 6-1 shows a predicted phosphorescent lifetime about 16 seconds for the lowest triplet state. For comparison, the lifetimes for some lower energy triplet states of differing symmetry are also given in Table 6-1, indicating that symmetry clearly plays a key role in determining which excited states decay most rapidly. These values were calculated for an isolated molecule and so do not include interactions between other molecules or with the solvent. The measured phosphorescent relaxation time was 30 milliseconds at 17 K, reflecting the additional de-excitation channels available under experimental conditions. This long lifetime will probably ensure that the lifetime of the T_1 state at room temperature is much longer than the duration of the ns pulse used here, as is required for limiting.

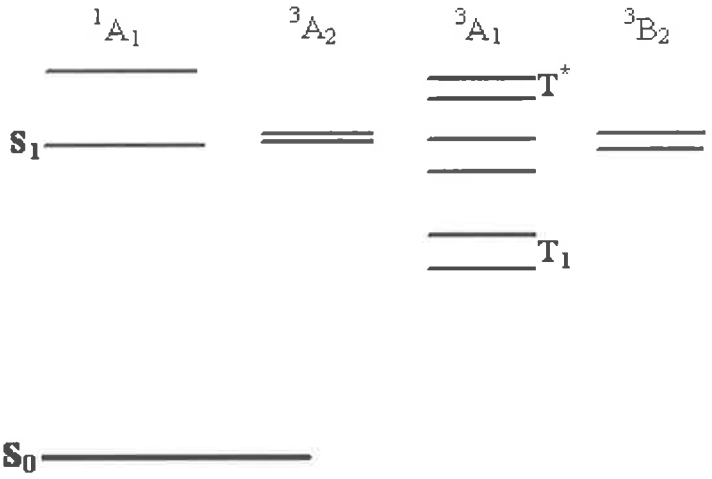

Figure 6-1: Energy level diagram of PEPE predicted for the 6-31G* basis.

Response theory modelling also suggests that S_0 to S_1 transitions via two-photon absorption will be likely. The orientationally averaged two-photon absorption probability (for linear polarization) is 8.68×10^2 atomic units, which is typical for materials of this type.

6.1.2 Discussions of Limiting in PEPE

Spectroscopy results for PEPE were presented in Section 4.3 and showed that the S_1 state is populated by both single-photon and two-photon absorption. Efficient intersystem

crossing is then observed, as is consistent with response theory modelling, and the excited $^3A_2$ states decay to the lowest energy triplet state, T_1, which is exceptionally long lived. Repeated transitions from this state to higher energy, short lived $^3A_1$ triplet states, results in optical limiting.

The limiting of PEPE was investigated using the numerical 5-level model described in Chapter 5, using the parameters listed in Table E.5.

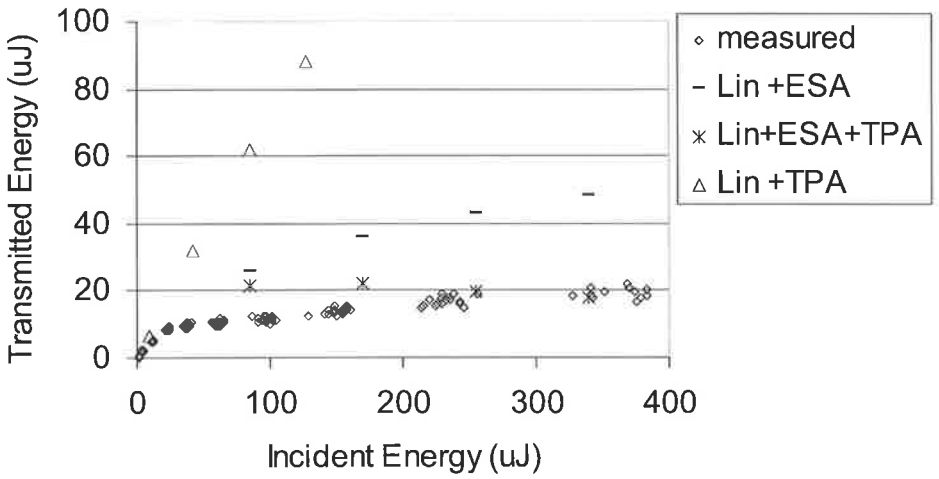

Figure 6-2: Measured and predicted transmitted pulse energy for 6 ns pulses, for an 80 % linear transmission at 532 nm sample of PEPE. Lin+ESA assumes linear $S_0 \rightarrow S_1$ transitions then excited state absorption, $T_1 \rightarrow T^*$, Lin+ESA+TPA assumes linear and two-photon $S_0 \rightarrow S_1$ transitions and ESA, Lin+TPA assumes $S_0 \rightarrow S_1$ transitions via linear and two-photon absorption .

In Figure 6-2, we show a comparison of the measured optical limiting and that predicted assuming (a) $S_0 \rightarrow S_1$ transitions via linear (Lin) absorption only and then excited state absorption, $T_1 \rightarrow T^*$, (ESA), (b) $S_0 \rightarrow S_1$ transitions via linear and two-photon absorption (TPA) and then ESA, and (c) $S_0 \rightarrow S_1$ transitions via linear and two-photon absorption only

(no ESA). The lifetime of the excited triplet state (T*) was assumed to be much shorter than the 6 ns (HW1/eM) duration of the pulse.

It is clear from Figure 6-2 that the optical limiting is due mostly to excited state absorption but that at high pulse energies the two-photon absorption provides the clamping of the energy of the transmitted pulse. Since we did not observe a decrease in the transmitted energy at high input energies, it is likely that the two-photon cross section, σ_2', used in the model was too large. Recall, however, that the uncertainty in that cross section was 50%. At lower σ_2' the predicted clamping level would be slightly above that observed, which would be consistent with not being able to collect all of the transmitted energy due to the scatter in the limiter. Figure 6-2 shows reasonable agreement between predicted results and measured values for PEPE.

As was observed for other TMAs and shown in Chapter 2, the clamping level should decrease as the concentration increases. The dependence predicted by the numerical 5-level model is shown in Figure 6-3. As for Figure 6-2, the importance of two-photon absorption in the limiting is apparent, particularly at low concentrations. Note that these predictions do not take into account solubility or aggregation effects.

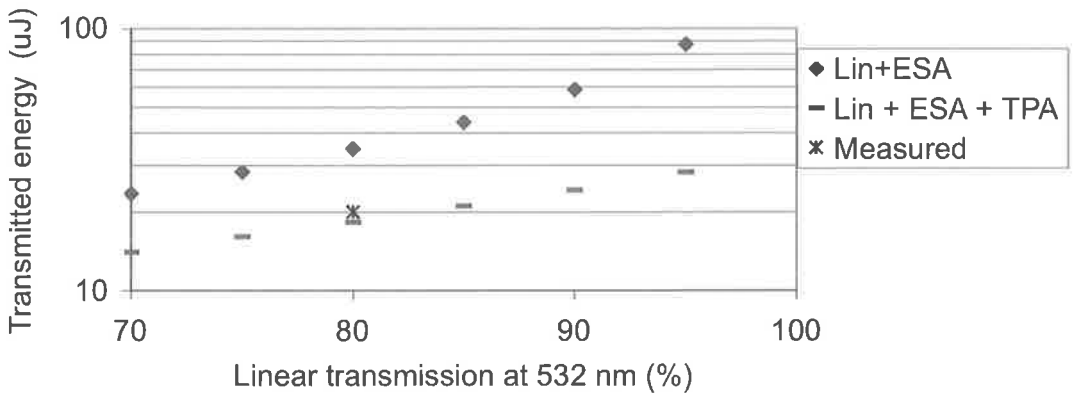

Figure 6-3: Effect of increasing concentration of PEPE on transmitted energy for a 200 uJ 6 ns, incident pulse.

Figure 6-3 shows that at 70% linear transmission, (the lowest that one would want use in any practical application) the predicted clamping level at 532 nm is 14 μJ, which is much higher than the 1 μJ required. Thus, although PEPE shows interesting optical limiting properties and validates the numerical 5-level model, it is not suitable as a limiter.

6.2 Pt:ethynyl

The 5-level model described in Chapter 5 was used to predict the optical limiting of Pt:ethynyl for nanosecond and picosecond pulses. As Figure 6-4 shows, there is good agreement between measured and calculated values for picosecond pulses, while Figure 6-5 shows very poor agreement for nanosecond pulses.

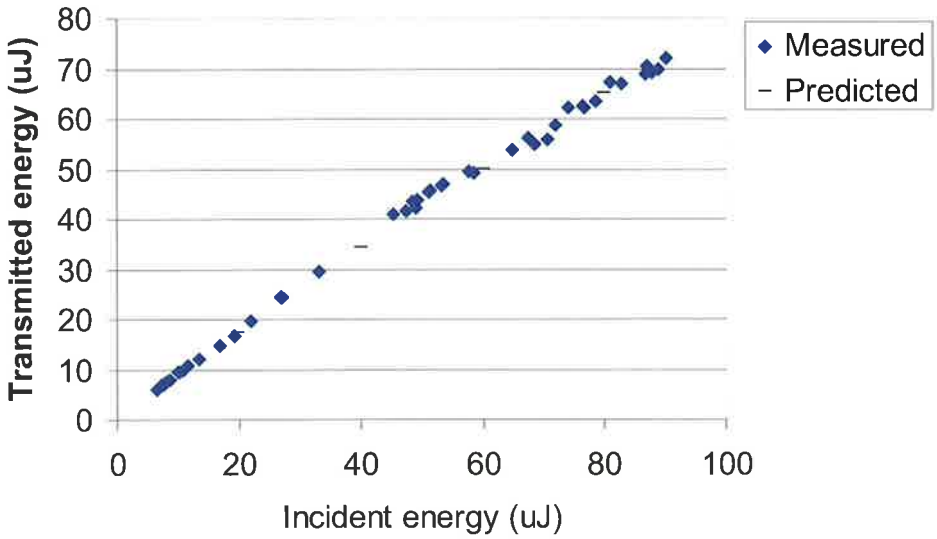

Figure 6-4: Measured and predicted transmission for a 90% linear transmission sample of Pt:ethynyl for 30 picosecond pulses.

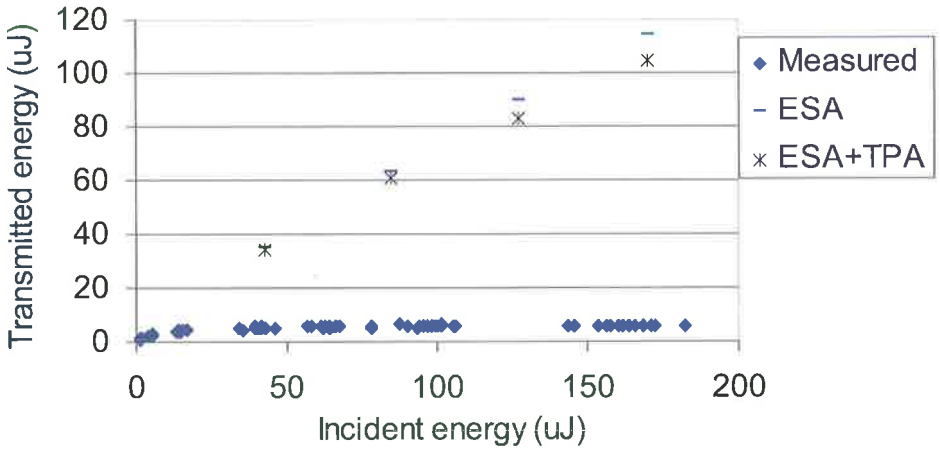

Figure 6-5: Measured and predicted transmitted energy for a 94% linear transmission sample of Pt:ethynyl for 6 nanosecond pulses.

There is little if any excited state absorption when picosecond pulses are used and the only limiting mechanism appears to be two-photon absorption as the data in Figure 6-4 is consistent with 1/T being proportional to intensity. The lack of excited state absorption indicates that the T^* lifetime is longer than the 30 ps pulse duration.

In Figure 6-5 I have included calculated values for Pt:ethynyl both with and without any two-photon absorption. In PEPE good agreement between measured and predicted values is observed for 6 ns pulses (Figure 6-3), however poor agreement is observed for Pt:ethynyl (Figure 6-5). There is likely to be an additional limiting mechanism occurring in Pt:ethynyl and probably also in other oligomers (see Section 6.3). While it might be due to S_1 to S_2 transitions, the lack of limiting for ps pulses means this is unlikely. A more probable additional limiting mechanism is two-photon absorption in the triplet manifold, as the increased density of states in larger molecules such as Pt:ethynyl would increase the likelihood of two-photon absorption. Another option is nonlinear scattering and refraction, which have been observed in other optical limiting materials[23]

6.3 Oligomers

The results of spectroscopic measurements of the terminal-phenyl and terminal-acetylide oligomers are collected in Tables 6-2 to 6-5. As for Pt:ethynyl, the 5-level model predicts poorer limiting for the oligomers than that observed. In this section, I therefore examine the spectroscopic data to determine whether a structure/property relationship is apparent.

n	τ_{T1} at 17 K	τ_{T1} at 300 K	σ_S at 532 nm	σ_T at 532 nm	$\acute{o}_T/\acute{o}_S$	σ_2'	Ranking at 532 nm
	μs	μs	$\underline{x10^{-18}\ cm^2}$ molecule	$\underline{x10^{-18}\ cm^2}$ molecule		$\underline{x10^{-48}\ cm^4\ s}$ photon	
1	12	0.4	0.0065	1.61 ± 0.2	334	169	3
2	10		0.048	3.3 ± 0.3	73	25	1
3	28	1	0.1	3.2 ± 0.3	25	66	2
4	15		0.2	5.1 ± 0.6	17	195	4
5	9.5		97	4.9 ± 0.3	0.05	1640	5

Table 6-2: Spectroscopic data for terminal-phenyl oligomers. τ_{ISC} values for all oligomers are between 250 and 400 ps.

n	τ_{T1} at 17 K	τ_{T1} at 300 K	σ_S at 532 nm	σ_T at 532 nm	$\acute{o}_T/\acute{o}_S$	σ_2'	Ranking at 532 nm
	μs	μs	$\underline{x10^{-18}\ cm^2}$ molecule	$\underline{x10^{-18}\ cm^2}$ molecule		$\underline{x10^{-48}\ cm^4\ s}$ photon	
1	5.7		0.03	4.4 ±0.4	95	340	4
2	2.8		0.47	5.5 ± 0.8	11.7	1170	1
3	10	0.7	0.67	5.1 ± 0.9	7.3	5770	3
n	6.7		22	5.8 ± 0.9	0.27	82130	2

Table 6-3: Spectroscopic data for terminal-acetylide oligomers. τ_{ISC} values for all oligomers are between 330 and 450 ps.

n	S_0 to S_1	S_0 to T_1	S_1 to S_0	T_1 to S_0
	nm (eV)	**nm** (eV)	**nm** (eV)	**nm** (eV)
1	336 (3.68)	482 (2.57)	434 (2.85)	550 (2.25)
2	359 (3.45)	505 (2.45)	379 (3.27)	486 (2.55)
3	362 (3.42)	507 (2.44)	391 (3.17)	500 (2.48)
4	364 (3.40)	509 (2.43)	394 (3.14)	511 (2.42)
5	370 (3.35)	511 (2.42)	433 (2.86)	519 (2.39)

Table 6-4: Absorption and emission wavelengths (energies) for terminal-phenyl oligomers.

n	S_0 to S_1	S_0 to T_1	S_1 to S_0	T_1 to S_0
	nm (eV)	**nm** (eV)	**nm** (eV)	**nm** (eV)
1	373 (3.32)	504 (2.46)	451 (2.74)	585 (2.12)
2	375 (3.30)	506 (2.45)	472 (2.62)	575 (2.15)
3	382 (3.24)	505 (2.45)	452 (2.74)	525 (2.36)
n	366 (3.38)	504 (2.46)	442 (2.80)	528 (2.34)

Table 6-5: Absorption and emission wavelengths (energies) for terminal-acetylide oligomers.

Energy-level diagrams constructed from the absorption and emission spectra are shown in Figures 6-6 and 6-7.

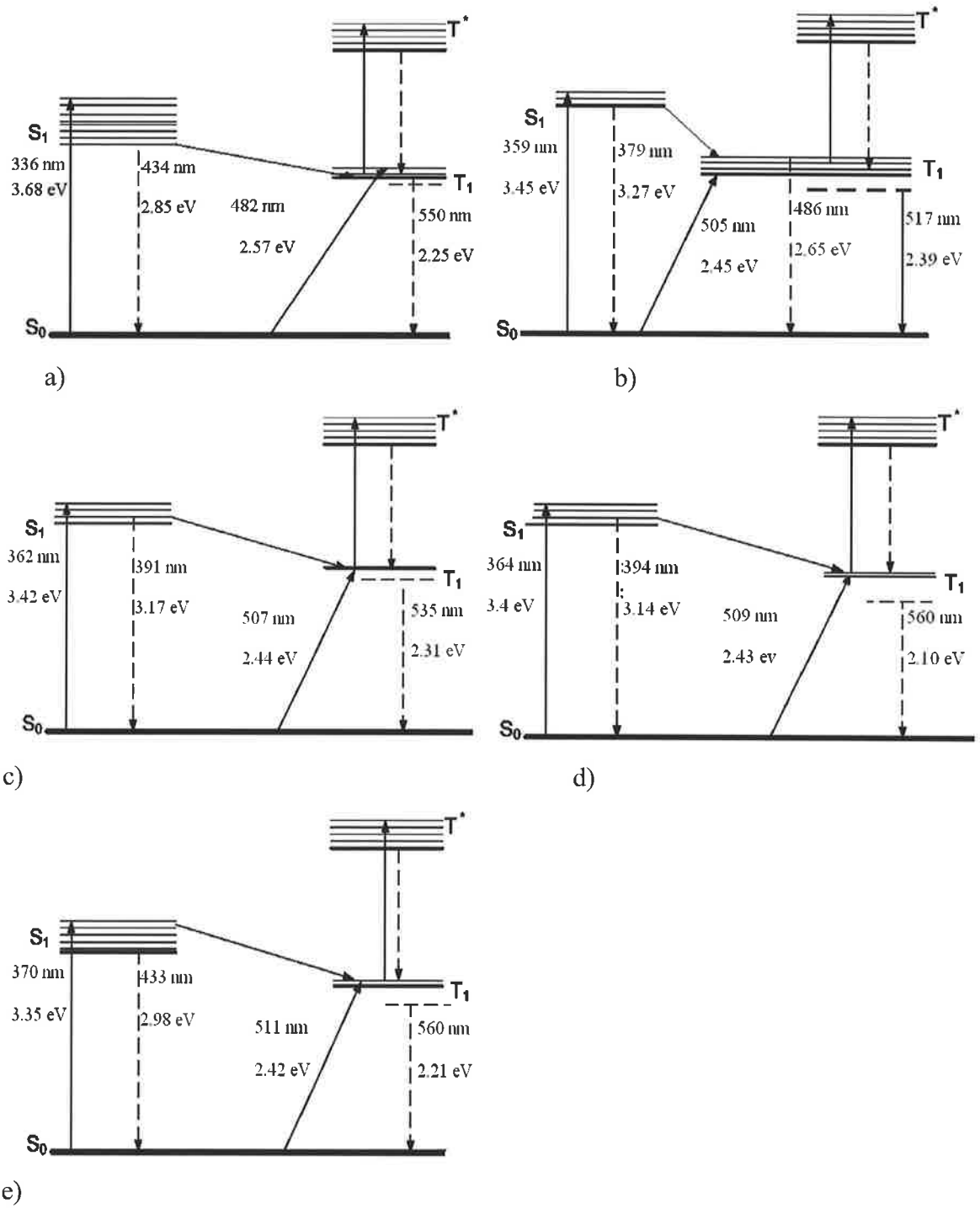

Figure 6-6: Energy level diagrams for terminal-phenyl oligomers: a) monomer, b) dimer, c) trimer, d)tetramer, e) pentamer. The dashed triplet state corresponds to a low energy red-shifted triplet state that can be observed in the phosphorescence spectra.

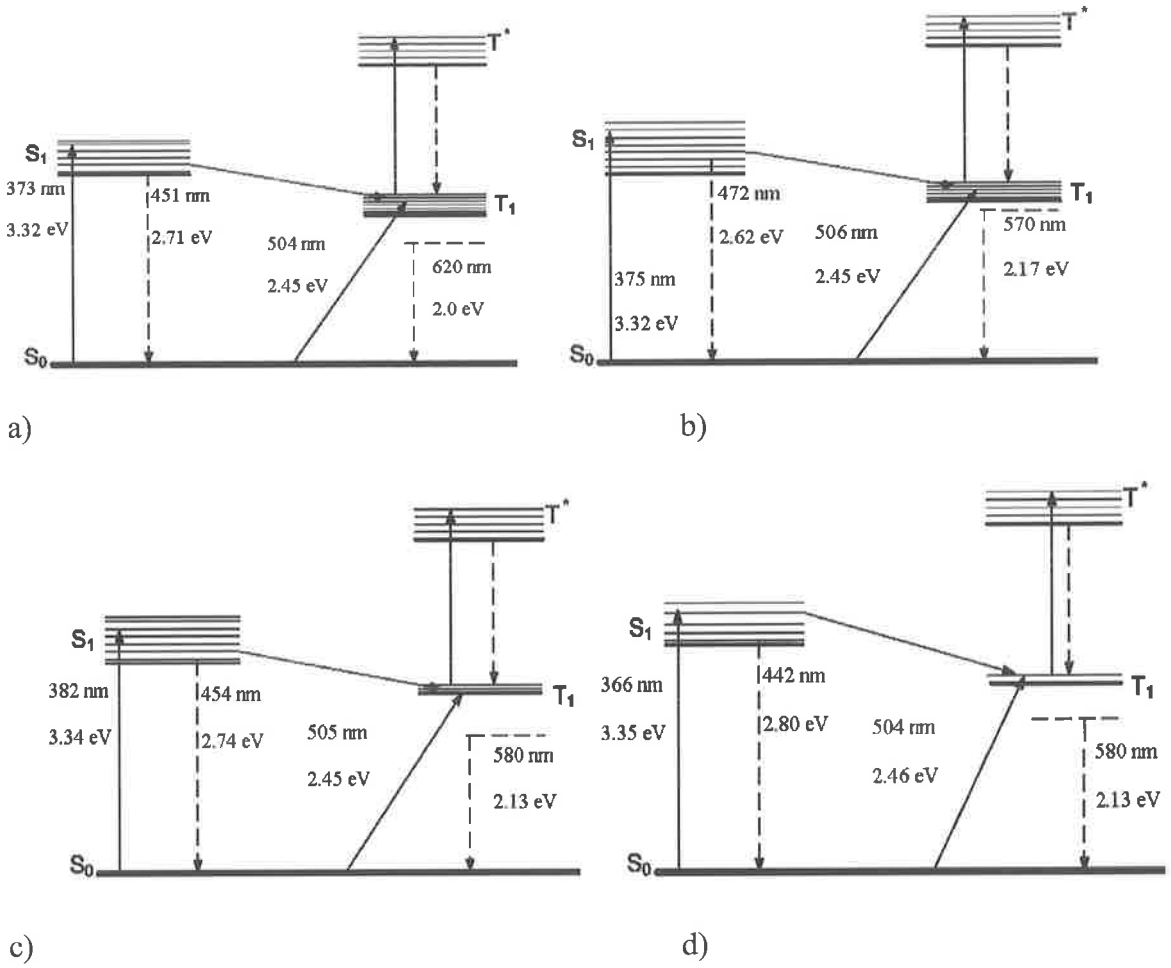

Figure 6-7: Energy level diagrams for terminal-acetylide oligomers: a)monomer, b) dimer c) trimer, d) polymer. The dashed triplet state corresponds to a low energy red-shifted triplet state that can be observed in the phosphorescence spectra.

The dimers are the best limiters in each oligomer series. Except for the σ_T/σ_S ratio for the monomers, the dimers are distinguished by higher σ_T/σ_S ratios. They are also distinguished by having the smallest two-photon S_0 to S_1, σ_2', values for each series (except for the terminal-acetylide monomer). Note, however, that this observation does not preclude the proposal in the last section that the good limiting of Pt:ethynyl is due to two-photon absorption in the triplet manifold.

Both sets of oligomers show evidence of spin-forbidden S_0 to T_1 absorption in their linear absorption spectra. While there is little variation in the position of this feature in the absorption spectra, appreciable variation is observed for the T_1 to S_0 relaxation in phosphorescence spectra. This indicates that in some oligomers the T_1 state covers a wider range of energy levels and for these materials there may be a greater likelihood of direct S_0 to T_1 absorption at 532 nm. However for ns pulses, the intersystem crossing relaxation time is significantly less than the pulse length, resulting in little difference in transmitted energy for direct and indirect T_1 population pathways, as shown in Chapter 5.

Note, however, that the oligomers with the broadest range of T_1 states are those that display the best limiting, except for the terminal-acetylide monomer. If this broad range extends to the higher energy triplet state then two-photon triplet absorption may be more likely.

Thus, there is no obvious relationship between number of repeat units and optical limiting performance. The monomer in both series has the highest σ_T/σ_S, while the longer oligomers have the highest S_0 two-photon absorption coefficient. As was shown in Figure 6-5 however, linear absorption, two-photon absorption and excited state absorption do not accurately predict the limiting by these materials. The additional limiting could be due to other absorption processes in the molecule, such as two-photon absorption in the triplet state.

6.4 Best TMA Limiters

In this section I present the data for the most promising TMAs. As shown in Figure 6-8, these materials are a) Pt:ethynyl, b) terminal-acetylide dimer, c) terminal-phenyl dimer and d)Di-Pt:ethynyl. PEPE is included for reference. As reported in Chapter 5, the 5-level model predicts a poorer optical limiting for the TMA oligomers than that observed. Thus, to understand why these materials show superior limiting I have looked at what features they have in common.

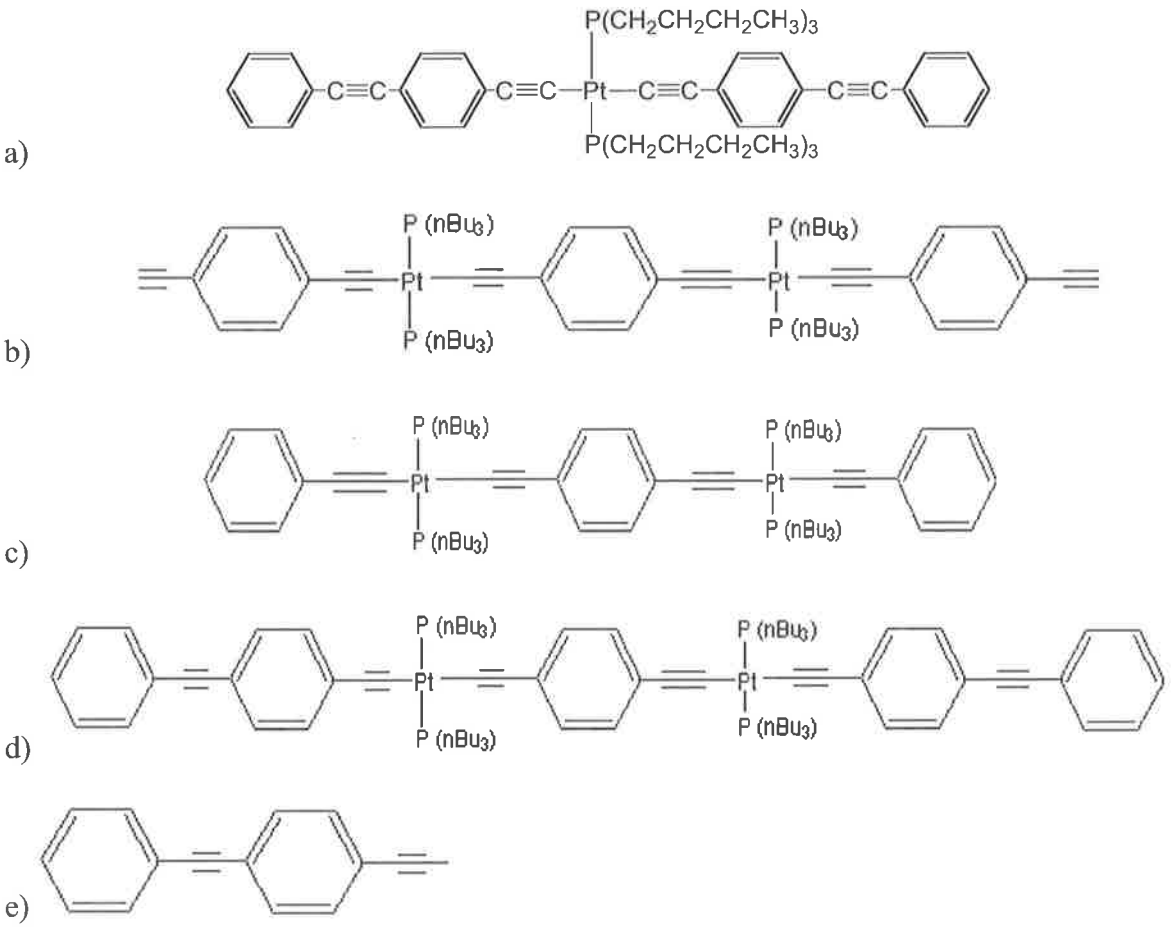

Figure 6-8: Sturucture of a) Pt:ethynyl, b) terminal-acetylide dimer, c) terminal-phenyl dimer d)Di-Pt:ethynyl e) PEPE.

Table 6-6 lists the spectroscopic properties for these materials.

Material	$S_0 \rightarrow S_1$	$S_0 \rightarrow T_1$	$S_1 \rightarrow S_0$	$T_1 \rightarrow S_0$	σ_T	σ_T/σ_S	β (σ_2')	Ranking at 532 nm
	nm	nm	nm	nm	x10^{-18}cm^2/ molecule		cm/GW (GM)	
Pt:ethynyl	380	520	420	520	1.6	25	.21 (551)	3
Terminal-acetylide dimer	375	505	472	575	5.5	11.7	1.0 (11677)	4
Terminal-phenyl dimer	359	505	379	486	3.5	73	.67 (2493)	1
Di-Pt:ethynyl	368	462			3.9	70	1.0 (11373)	2
PEPE	350	380	448	490	2.8	863	1.7 (378)	5

Table 6-6: Spectroscopic data for the four best materials and PEPE. T_1 lifetimes for all materials were estimated at approximately 1 μs at 300 K, except for PEPE (30 ms). τ_{ISC} for all materials are approximately 300 ps. 1 GM= 10^{-50} cm^4 s photon^{-1}.

All of these materials have ground state absorption maxima between 350 and 380 nm, with a weak shoulder located at higher wavelengths. They all have high σ_T/σ_S ratios and, with the exception of PEPE, the clamping level improves as the σ_T/σ_S ratio increases.

As can be seen from Table 6-6, the σ_T/σ_S values of both Di-Pt:ethynyl and terminal-phenyl dimer are approximately 70, while the intermediate terminal-acetylide dimer has σ_T/σ_S of 12. This indicates that terminal acetylide greatly decreases σ_T/σ_S.

All of these materials show comparable or significantly higher two-photon absorption coefficients than stilbene (377 $x10^{-50}$ cm^4 s $photon^{-1}$ at its two-photon absorption maxima [43]), which is considered to have high two-photon absorption.

From results of ps transmission experiments it can be seen that there is no limiting (Figure 6-4). This indicates that singlet-singlet transitions (S_0 to S_1 single and two-photon and S_1 to S_2) are not sufficient to produce observable optical limiting and limiting occurs for ns pulses due to absorption in the triplet manifold. The 5-level model predicts that the much lower σ_T/σ_S values for the oligomers compared to PEPE should result in essentially no limiting due to excited state absorption. Yet, strong limiting is observed, and this can only be explained by nonlinear absorption, probably two-photon absorption in the triplet states.

As can be seen from Figure 6-8, the most promising materials investigated consist of [Acceptor-Donor-π-Donor-Acceptor] type structures which are known to show strong two-photon absorption [43].

Chapter 7 discussed some more aspects of the requirements of a practical optical limiter and other areas for future work.

7 Conclusion and Future Work

7.1 Limiting at 532 nm

This thesis has presented the optical limiting of a large number of TMAs at 470, 532 and 630 nm as well as detailed spectroscopic measurements at 532 nm for two sets of Pt:ethynyl oligomers and a precursor material. Results presented in Chapter 2 show that only very few of the TMAs tested have comparable or better limiting at 532 nm than Pt:ethynyl. All showed worse limiting in the red than Pt:ethynyl. Many materials showed acceptable limiting in the blue; however this is partly due to the strong ground state absorption in that region.

Optical limiting results for TMAs show:

- Altering the heavy metal from platinum to either nickel or palladium degrades optical limiting
- Altering the solubilising group from $P(Bu_3)$ degrades optical limiting
- Altering the terminal group from the neutral hydrogen to any of CO_2Me, OH, I and NH_2 or NO_2 degrades optical limiting
- Altering the terminal group from phenyl to phenyl-acetylide degrades optical limiting
- Increasing the number of arms from a central ring degrades optical limiting
- The optimum number of repeat units is two.

The best two materials are di-platinum ethynyl and the terminal-phenyl dimer. The intermediate terminal-acetylide dimer, while showing strong limiting, was not as good as either of these terminal-phenyl materials.

Spectroscopy results presented in Chapter 4 show that all of the oligomers have efficient intersystem crossing to the triplet state with a time constant of approximately 300 ps. Phosphorescence spectra show long-lived T_1 states that red-shift with increasing number of repeat units, as expected, or with addition of terminal-acetylide bonds. Addition of terminal-acetylide bonds red-shifted the ground state absorption maxima by up to 40 nm, similar to the monomer to polymer shift, indicating electron delocalisation extends along the end of the molecule. Increasing the number of repeat units red-shifts and broadens the T_1 to T^* absorption maxima, while σ_T values at 532 nm decrease.

Computer simulations of the 5-level model, discussed in Chapter 5, have shown that the basic conditions required for optical limiting against ns pulses were met for all of the oligomers, including long T_1 lifetime and short intersystem crossing rates and T^* lifetimes. The computer model accurately predicts the behaviour of PEPE for both ps and ns pules, and of Pt:ethynyl and the dimers for ps pulses.

In ps transmission experiments, no significant limiting was observed, and thus singlet-singlet (single and two-photon S_0 to S_1 and S_1 to S_2) transitions are not sufficient for significant optical limiting in TMAs. Results from ns transmission experiments showed appreciable limiting, although the σ_T/σ_S values measured for TMAs are significantly lower than that of PEPE and thus the 5-level model predicts a higher clamping level for TMAs. This is the opposite of what was observed. Additional absorption processes, such as two-photon absorption in the triplet states are therefore required to explain the observed limiting. This also explains why there is no observable trend between σ_T/σ_S and limiting in the oligomer series.

7.2 Broadband Optical Limiting

As mentioned in Chapter 1, a broadband optical limiter must fulfil a range of practical requirements including:

- low broadband clamping level
- colour neutrality
- stable host medium.

Thus far I have restricted my discussion to the optical limiting at 532 nm. Most of the TMAs discussed in this thesis show extremely strong limiting at blue wavelengths and often clamp well below 1 μJ for a solution with a 70% linear transmission at 532 nm, as shown in Chapter 2. At red wavelengths, however, all TMAs tested showed worse performance than Pt:ethynyl, as shown in Table 2-8.

The optical limiting mechanism of Pt:ethynyl at 630 nm is known to require two-photon absorption (TPA) from S_0 to S_1, which is followed by intersystem crossing to T_1, and then excited state absorption to T^* [24]. It is not known whether probable TPA in the triplets contributes to the observed limiting.

Research into organic molecules with large two-photon cross sections implies that quadrupolar molecular structure is essential for large TPA [44],[37]. Molecules that have large TPA typically have ADA (Acceptor-Donor-Acceptor) or D-A-D (Donor-Acceptor Donor) structures, or are symmetric about a stilbene π-bridge, such as D-π-D, A-π-A, A-π-D-π-A or D-π-A-π-D. Structures using a stilbene spacer instead of a phenyl ring show an increase in two-photon absorption cross section by a factor of approximately 15 [43]. This increase may also apply to platinum acetylides. In Figure 7-1, I suggest the structures of some TMAs that combine results of my investigations with known two-photon absorbers.

These should have strong T_1 to T^* absorption and may also have improved singlet and triplet two-photon absorption.

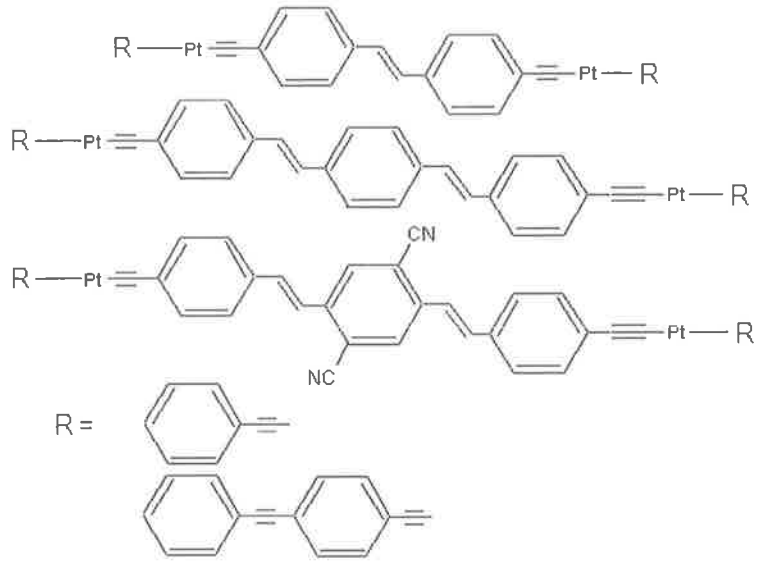

Figure 7-1: Dimer or di-Pt:ethynyl with stilbene π-bridge spacer, double stilbene spacer or double stilbene spacer and acceptor attached to central phenyl.

7.2.1 Further Experiments

Areas of further investigation include:

- Measurement of two-photon absorption in the triplet state. This could be achieved by performing pump-probe measurements as described in Section 3.3.2, but analysing the transmissivity of the probe beam as described in Section 3.5.
- Hartree-Fock and DFT modelling for new materials to investigate the energy level structure of the singlet and triplet states.
- Investigation of tertiary cocktails to improve colour neutrality.
- Investigation into solid host materials that maintain optical limiting.

A. Structures Tested

Structure	Name	molecular weight	%T @ 532	cl @ 470 nm (uJ)	cl @ 532 nm (uJ)	cl @ 630 nm (uJ)
solubilising groups						
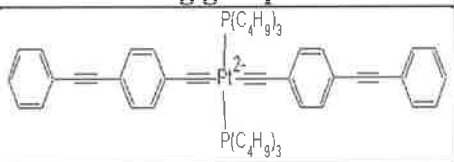	Pt:ethynyl	1001	97	1.4	0.35	9.2
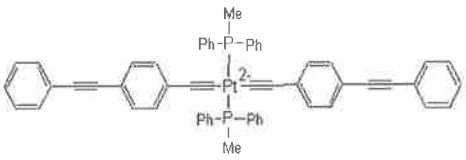	R=P Ph2Me	998	97.26	36	17	55
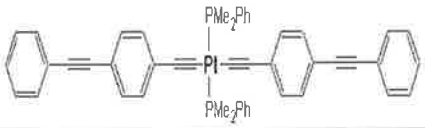	R=P Me2Ph	873.86	89	34	50	80
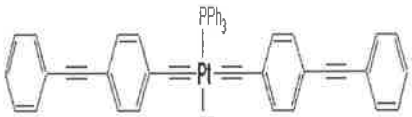	R=P Ph3	1122.29	97.4	4	21	27
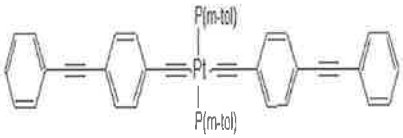	R= P (m-tol)	597.56	84.55 98.16	35 10	70 28	90 45

Structure	Name	molecular weight	%T @ 532	cl @ 470 nm (uJ)	cl @ 532 nm (uJ)	cl @ 630 nm (uJ)
Terminal groups						
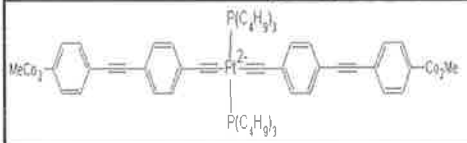	CO2Me	1150	80.59	0.35	2.5	11.5
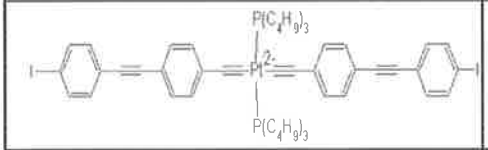	I	1102	38.95 70	0.3 3.2	2.1 12	5.5 35
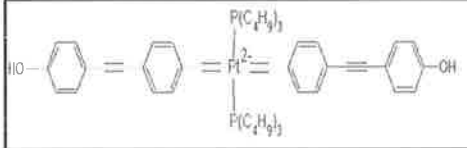	OH	1033	77	2	11	42
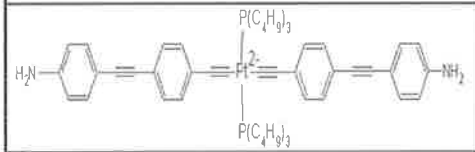	NH2	1032	75.42	1.6	15	41
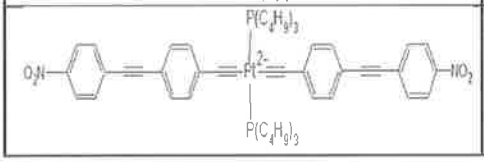	NO2	1089	97.79	32	60	100

Structure	Name	molecular weight	%T @ 532	cl @ 470 nm (uJ)	cl @ 532 nm (uJ)	cl @ 630 nm (uJ)
Terminal -phenyl oligomers						
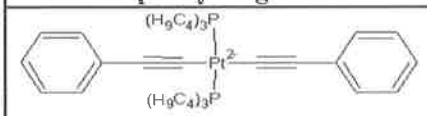	terminal-phenyl monomer	789	86	0.6	7	9
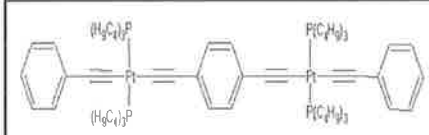	terminal-phenyl dimer	1524	94.02	0.21	4.98	7.66
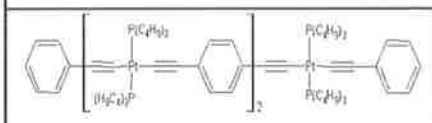	terminal-phenyl trimer	2510	85.2	0.54	6.04	9.73
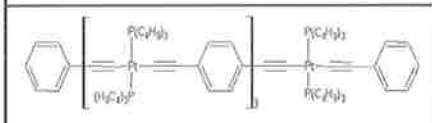	terminal-phenyl tetramer	2970	96.63	0	2.7	5.1
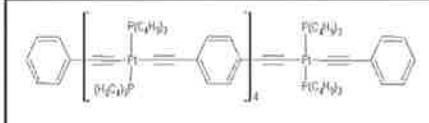	terminal-phenyl pentamer	3639	58.98 95.67	0 0.8	3.3 5.3	11.5 15.5

Structure	Name	molecular weight	%T @ 532	cl @ 470 nm (uJ)	cl @ 532 nm (uJ)	cl @ 630 nm (uJ)
Terminal-acetylide oligomers						
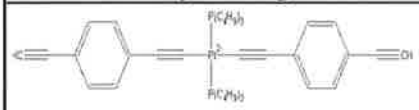	terminal-acetylide monomer	839	71.41 46.79 74.3	0.8 0.5 3.3	5.8 2.09 11	15 9.5 27
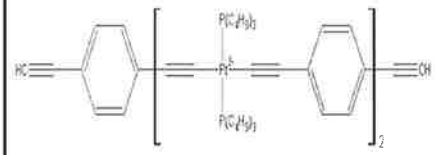	terminal-acetylide dimer	1574	85.84	1.1	6	18
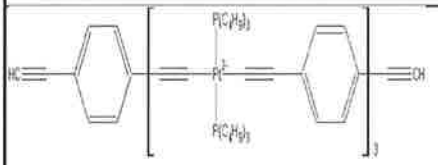	terminal-acetylide trimer	2297	80.72	3.6	11.3	18
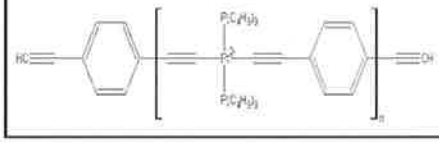	terminal-acetylide polymer	unknown	86.69	3.4	10.5	30

Structure	Name	molecular weight	%T @ 532	cl @ 470 nm (uJ)	cl @ 532 nm (uJ)	cl @ 630 nm (uJ)
PEPE 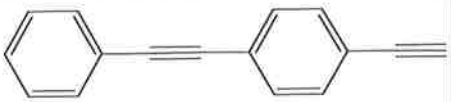	PEPE	202.25	80.42	7	20	33
Central metal						
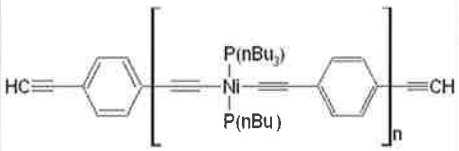	M=Ni	unknown	65	0.38	33.4	94
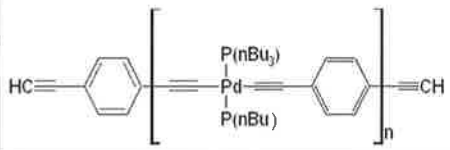	M=Pd	unknown	88	37	68	138
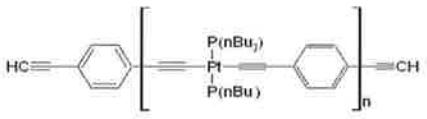	M=Pt	unknown	64	0.37	2	12.8

Structure	Name	molecular weight	%T @ 532	cl @ 470 nm (uJ)	cl @ 532 nm (uJ)	cl @ 630 nm (uJ)
spacer groups 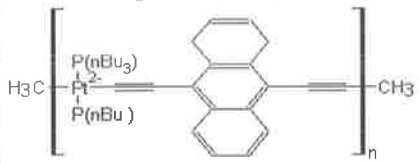	PPt(anthracene)	unknown	55.61	25	95	136
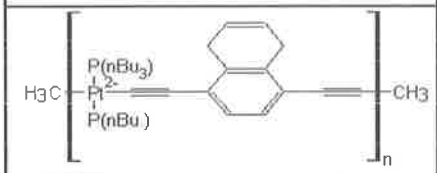	PPT(napthalene)	unknown	91.21	19.7	33	62
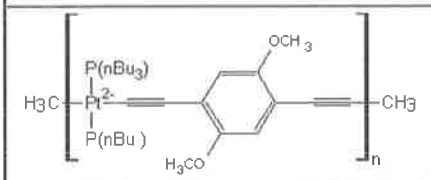	PPt(dimethoxy)	unknown	33.44 64 58.98	0.22 0.39 0	2.07 2 3.3	14.91 12.7 11.5
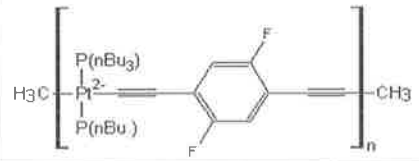	PPt(diFluoro)	unknown	75.71	3.3	9.81	23.5
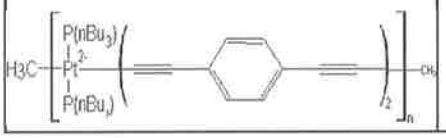	PPt(diyne)	unknown	91.93	5.3	14	25

Structure	Name	molecular weight	%T @ 532	cl @ 470 nm (uJ)	cl @ 532 nm (uJ)	cl @ 630 nm (uJ)
Three arms 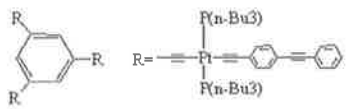	3-arm ethynyl	2548	92.6	3	11	23
Miscellaneous 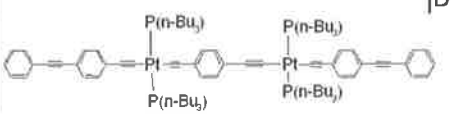	Di-platinum ethynyl	1726	95.42	2.2	8	13
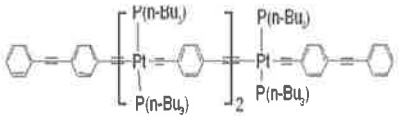	Tri-platinum ethynyl	2450	84.19	1.9	8	27

B. Instrumentation notes

Optical multi-channel analyser and gate

An optical multi-channel analyser, OMA, was used to determine the wavelength dependence of the luminescence produced during spectroscopy experiments. The OMA consists of two gratings, which separate out the wavelengths of the incident luminescence signal. The OMA was connected to a pulse generator which was used to control the time for which the luminescence was collected. Part of the output from the pulse generator was imaged onto a cathode ray oscilloscope, CRO, to visualise the gate width of the OMA, an electrical pulse from the laser cavity a predetermined time before the laser was switched out was also imaged onto the CRO (see Figure B.1).

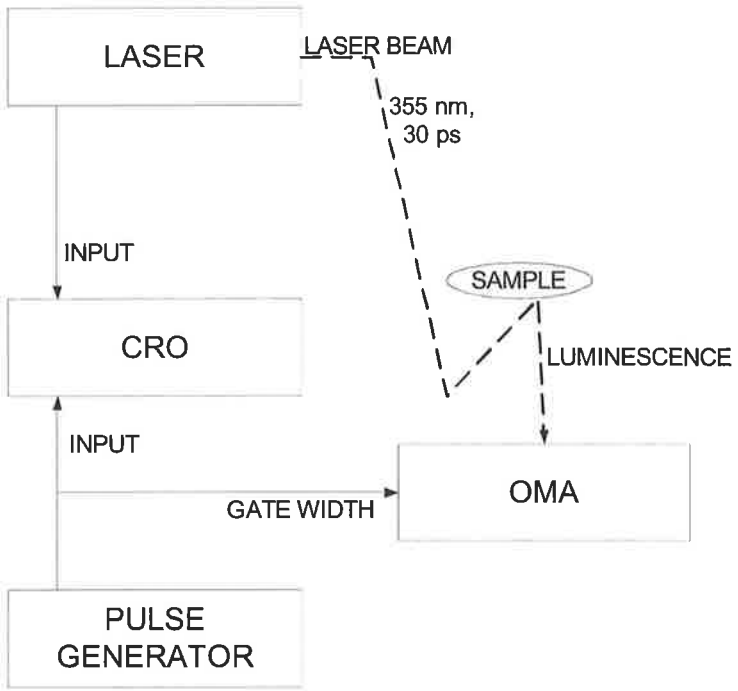

Figure B-1: Schematic of Spectroscopy setup.

The SPEX 1681 0.22m Optical Multi-channel Analyser can be run in either gated or CW modes. It can separate out signals in the wavelength range of 350 to 700 nm. In CW mode

the photocathode potential is held between 180 and 200 volts more negative than that of the potential of the MCP input allowing signal collection for several milliseconds.

In gated mode the photoelectron image is stopped by maintaining the photocathode potential at 20 to 40 volts more positive than the MCP. At a predetermined time the pulse generator applies negative 180 volts to the photocathode thus allowing the photoelectron spectrum to be transmitted to the MCP and then intensified by the MCO.

A pulse generator was used to create a pulse that acted as a gate for determining the time over which light was collected into the OMA. The time ranges of this gate were 20 ns to 3.5 μs.

Streak camera

A Cordin model 171 Proschen picosecond image converter streak camera was used to measure the fluorescence lifetime of the materials characterised.

The camera works by focusing light through two focusable lenses onto an image converter tube photocathode. This converts the photon image into an electron image which is accelerated, deflected along a time axis and then focused onto the phosphor of the image converter tube.

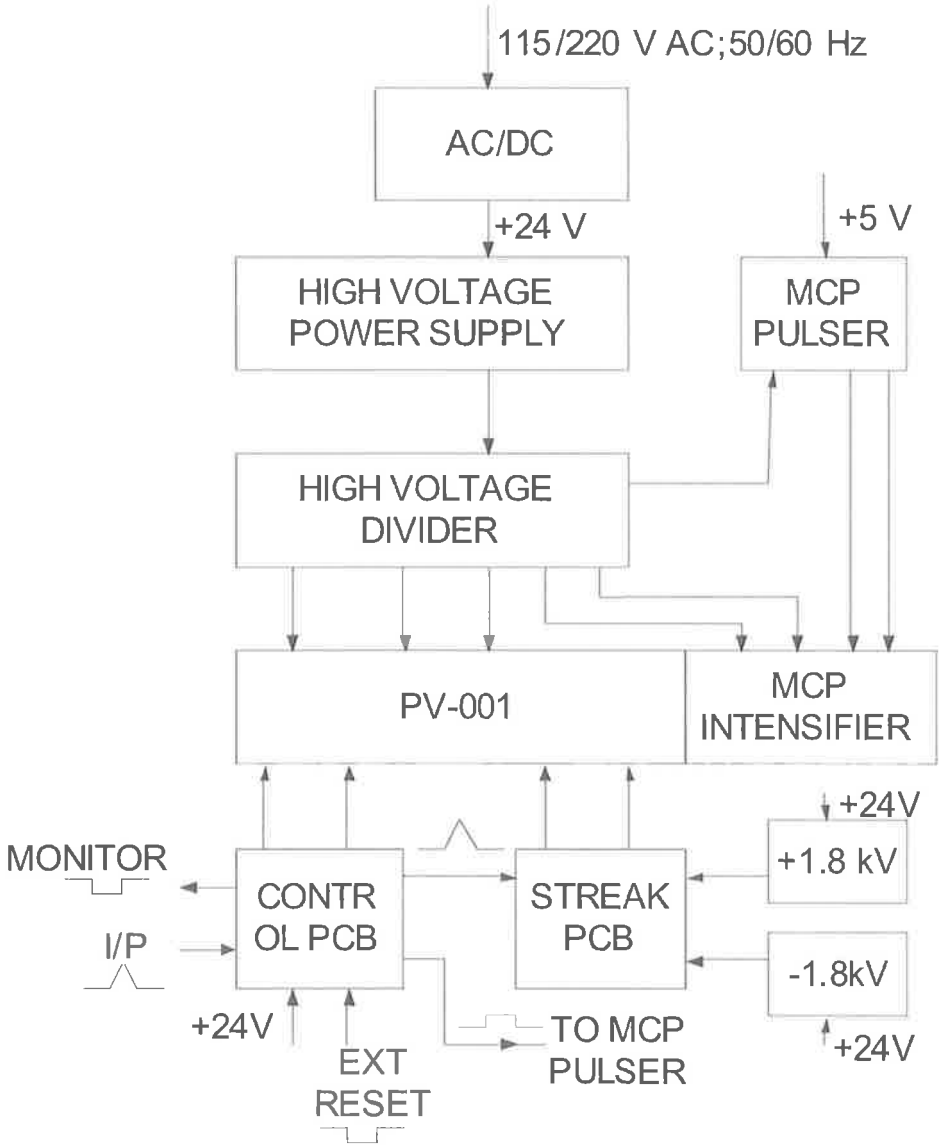

Figure B-2: block diagram of picosecond image converter streak camera

The camera was triggered by a +5 volt output from the laser. During experiments the camera was first set to focus mode and the fluorescence signal was imaged onto the photocathode. Then switched to streak mode (generally 300 ps/mm was used). Resulting in a useable streak duration time of 7.5 ns.

C. Results

Intersystem crossing rates

Intersystem crossing rates as described in Section 3.2 are presented here for the oligomers and PEPE.

Terminal-phenyl Oligomers

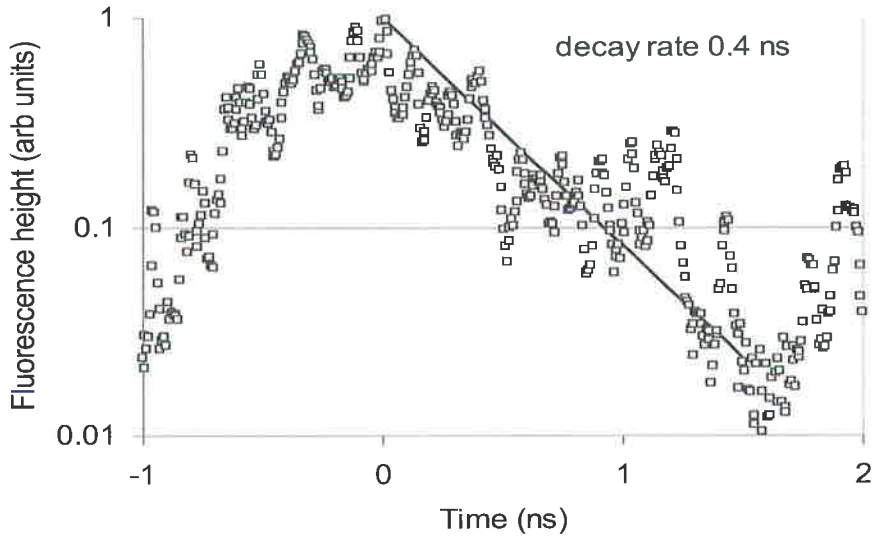

Figure C- 1: Fluorescence decay observed by streak camera for terminal-phenyl monomer at room temperature.

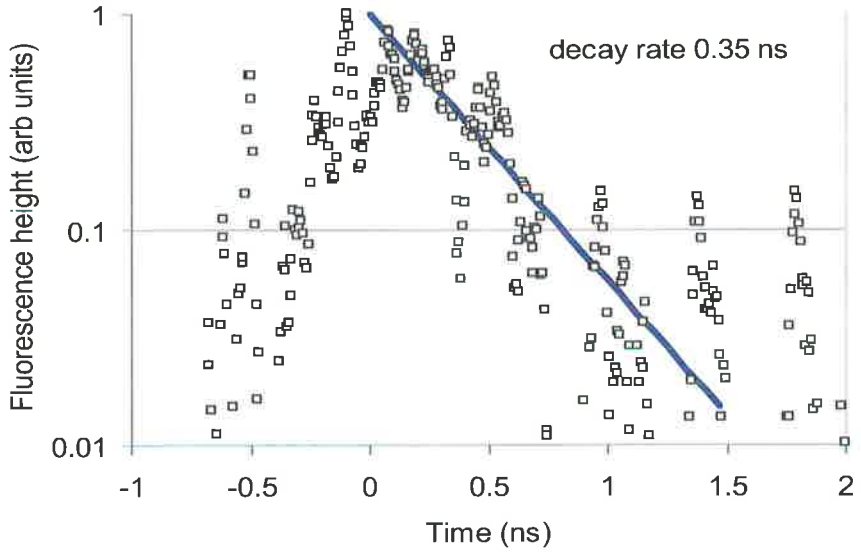

Figure C- 2: Fluorescence decay observed by streak camera for terminal- phenyl dimer at room temperature.

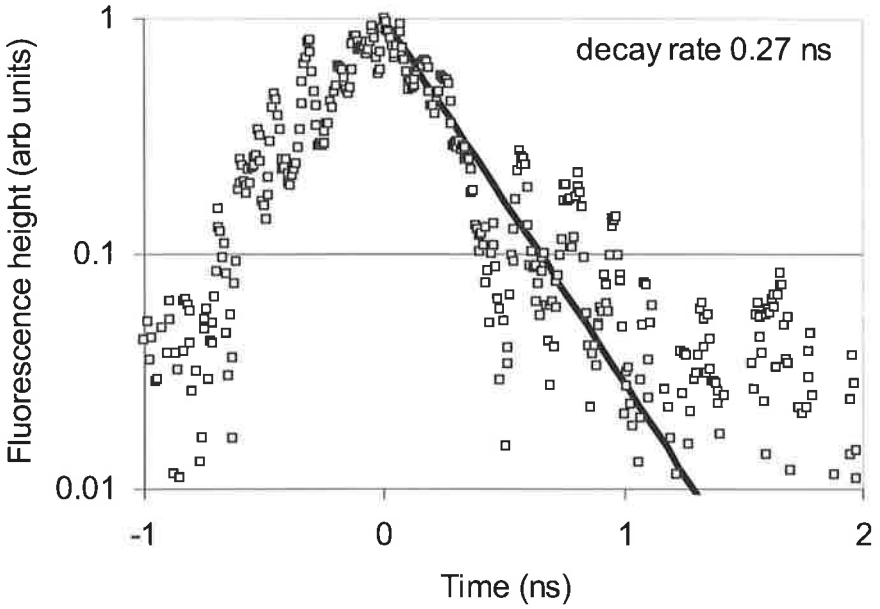

Figure C- 3: Fluorescence decay observed by streak camera for terminal-phenyl trimer at room temperature.

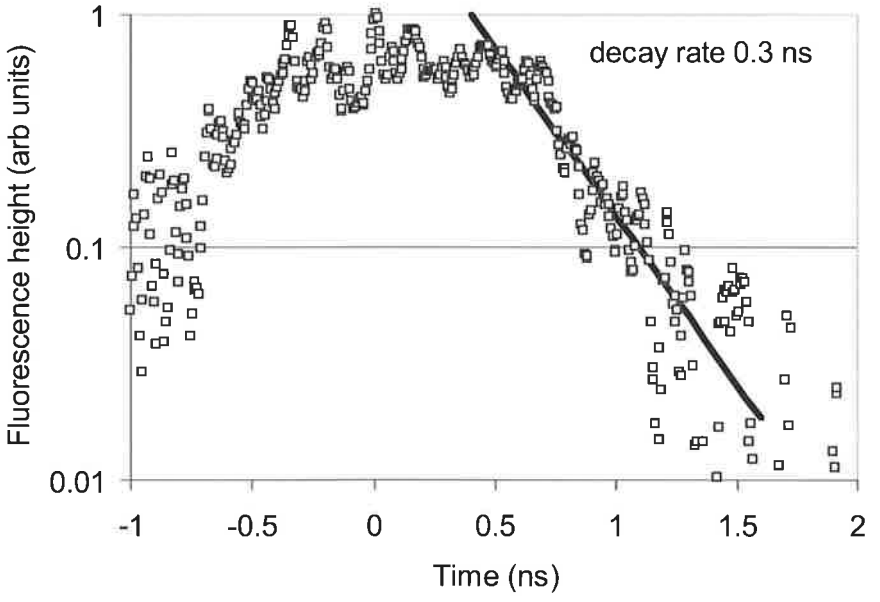

Figure C- 4: Fluorescence decay observed by streak camera for terminal-phenyl tetramer at room temperature.

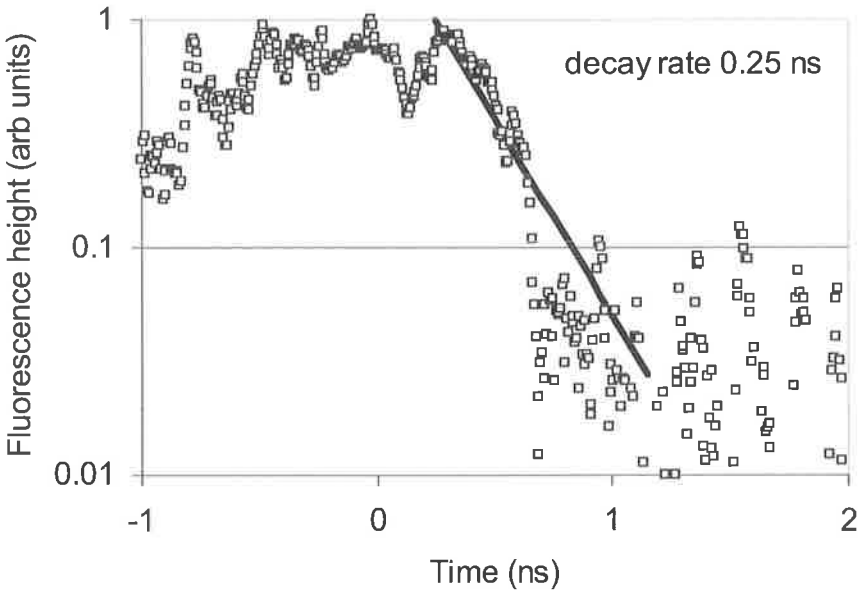

Figure C- 5: Fluorescence decay observed by streak camera for terminal-phenyl pentamer at room temperature.

Terminal-acetylide Oligomers

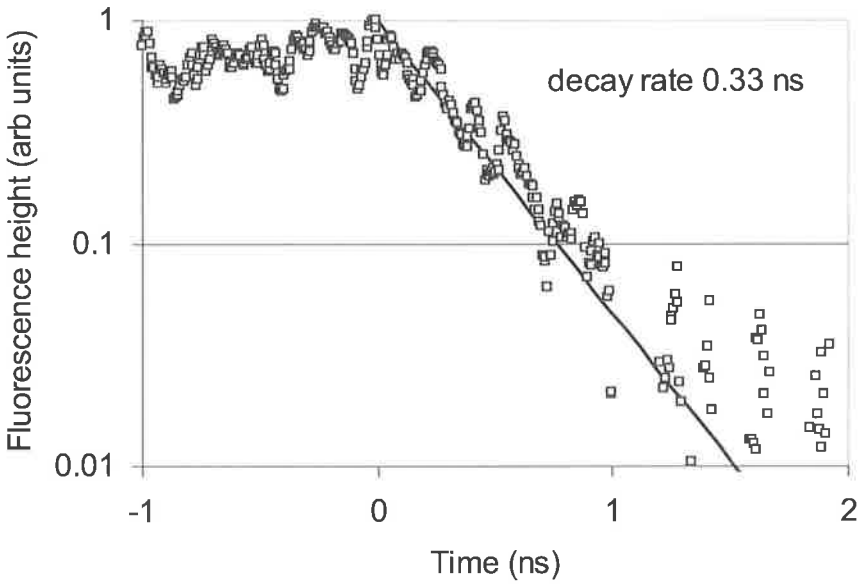

Figure C- 6: Fluorescence decay observed by streak camera for terminal-acetylide monomer at room temperature.

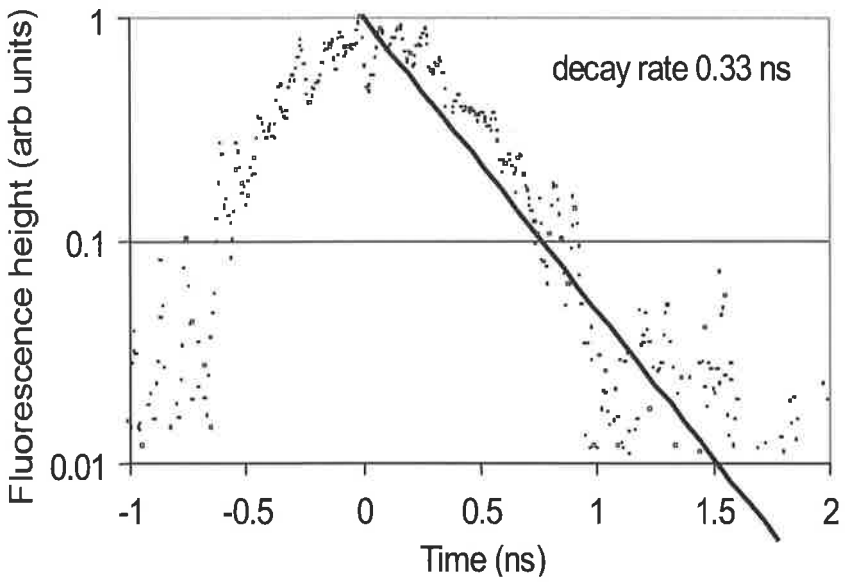

Figure C- 7: Fluorescence decay observed by streak camera for terminal acetylide dimer at room temperature.

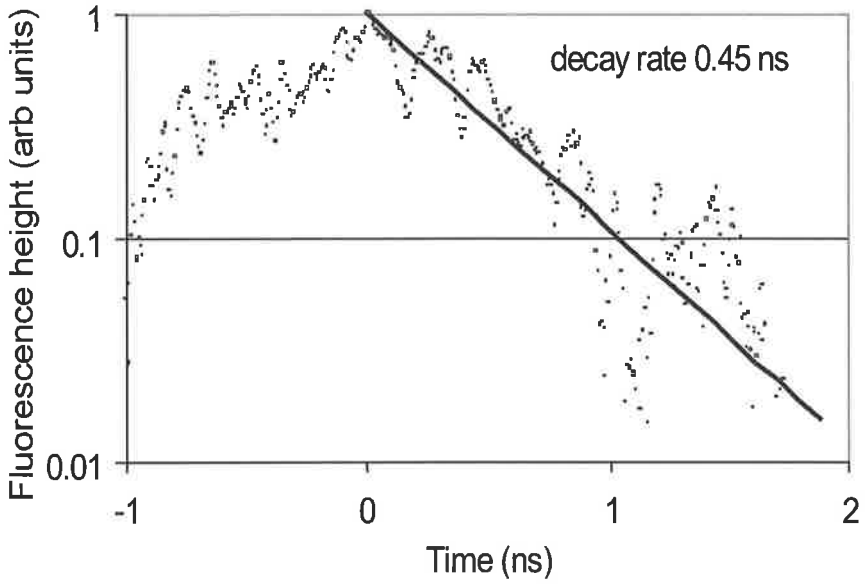

Figure C- 8: Fluorescence decay observed by streak camera for terminal-acetylide trimer at room temperature.

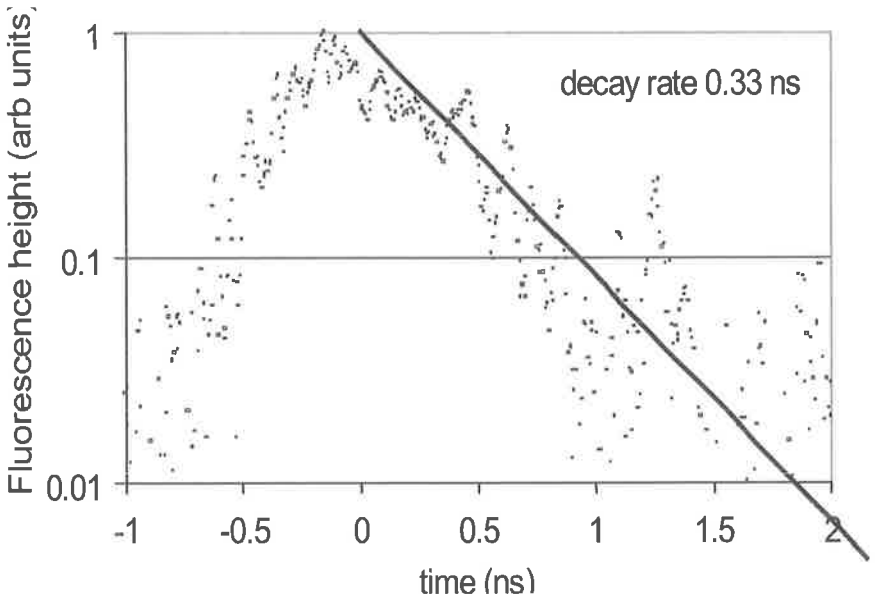

Figure C- 9: Fluorescence decay observed by streak camera for terminal-acetylide polymer at room temperature.

PEPE and Pt:ethynyl

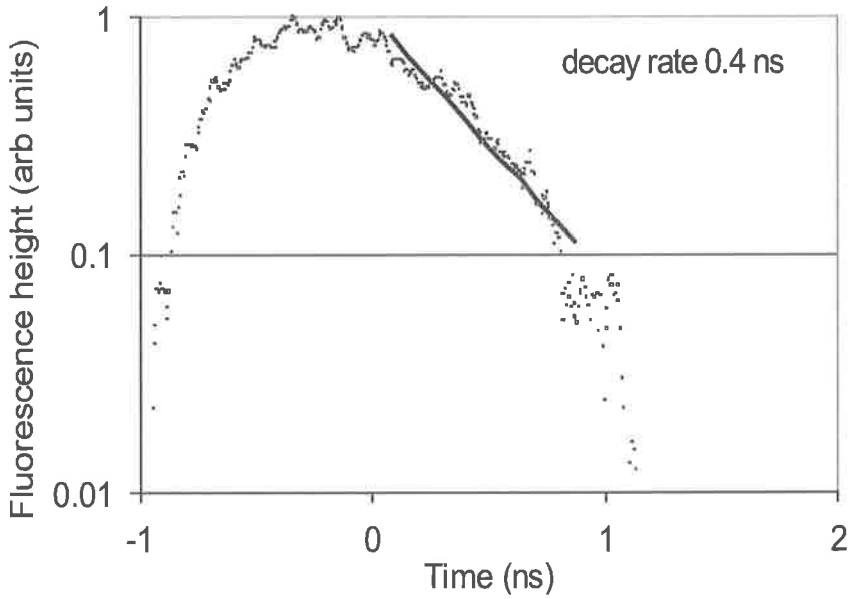

Figure C- 10: Fluorescence decay observed by streak camera for PEPE at room temperature.

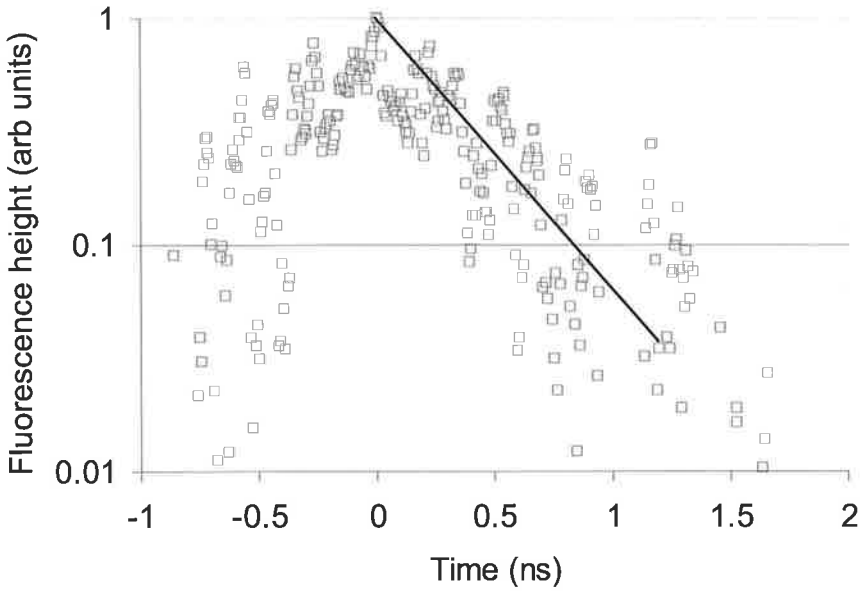

Figure C- 11: Fluorescence decay observed by streak camera for Pt:ethynyl at room temperature

Phosphorescence decay curves

Terminal-phenyl oligomers

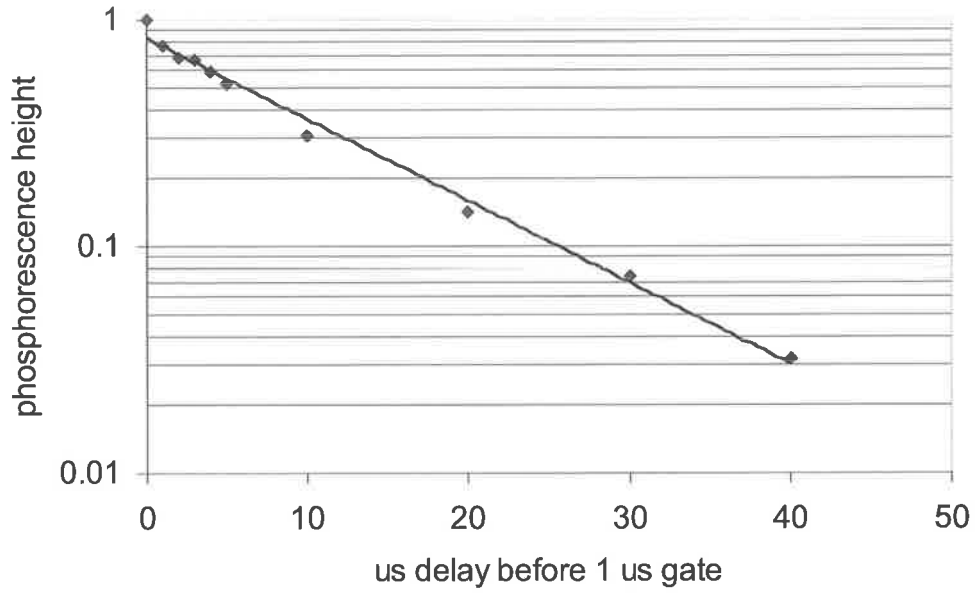

Figure C- 12: Phosphorescence decay of terminal-phenyl monomer at 17 K.

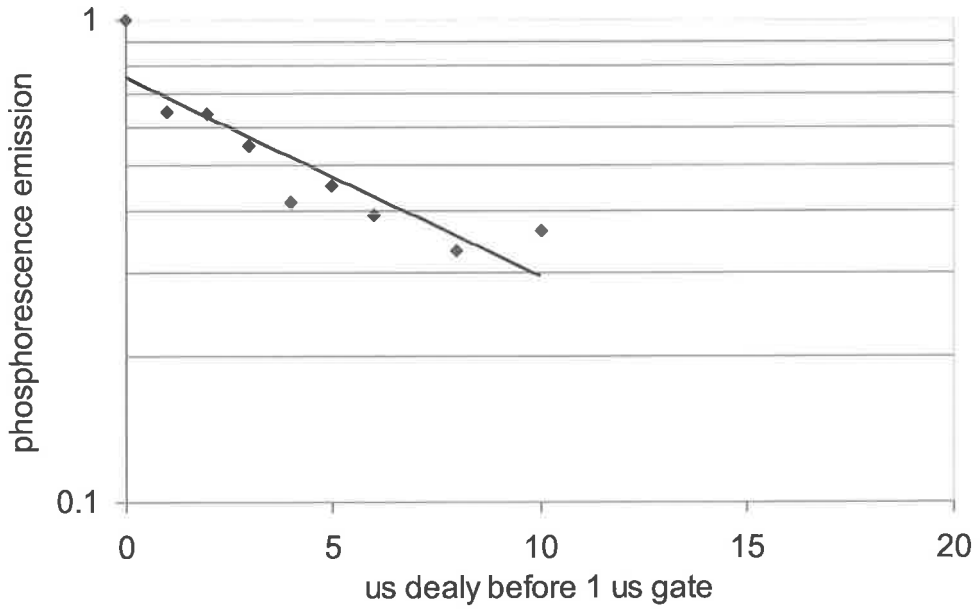

Figure C- 13: Phosphorescence decay of terminal-phenyl dimer at 17 K.

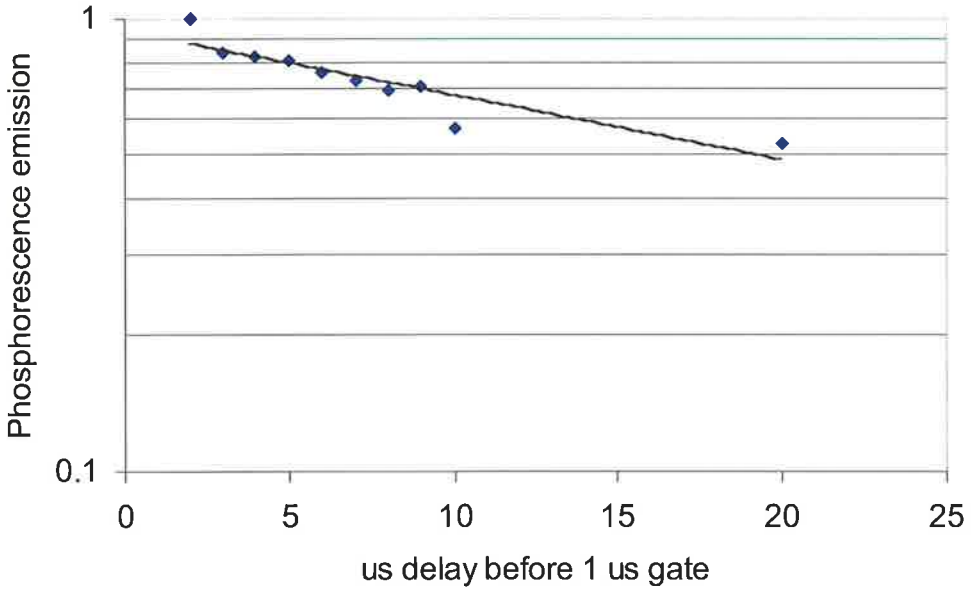

Figure C- 14: Phosphorescence decay of terminal-phenyl trimer at 17 K.

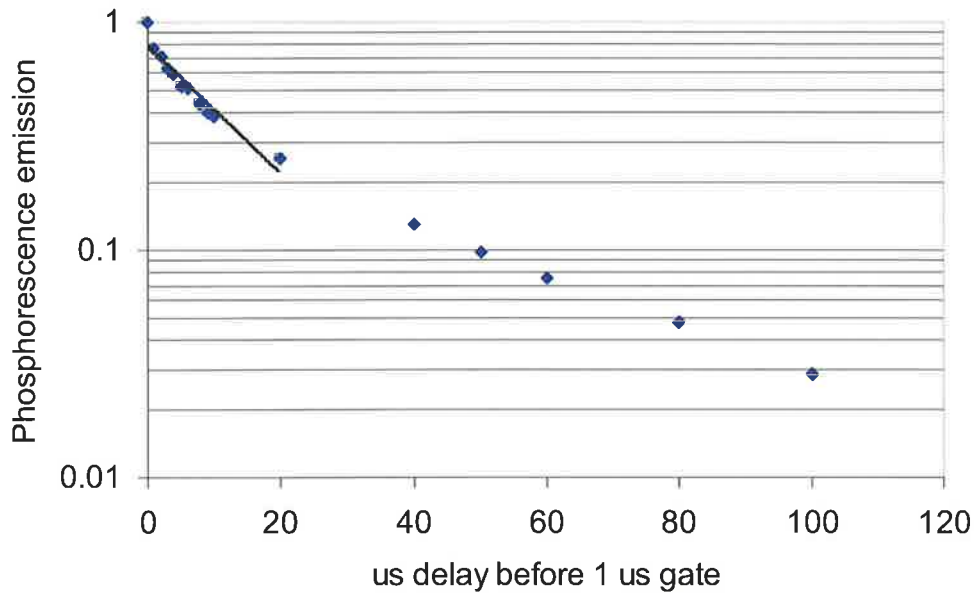

Figure C- 15: Phosphorescence decay of terminal-phenyl tetramer at 17 K.

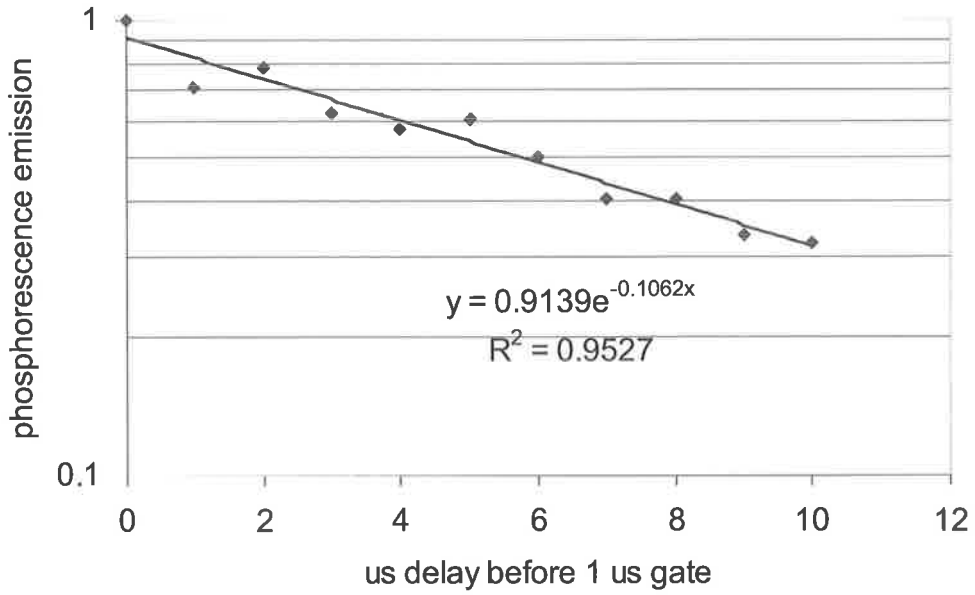

Figure C- 16: Phosphorescence decay of terminal-phenyl pentamer at 17 K.

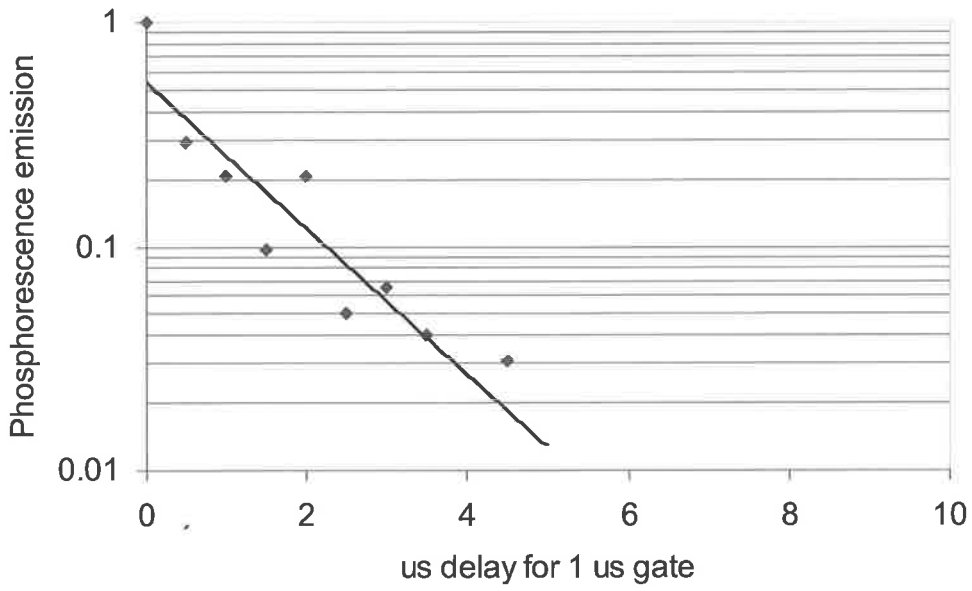

Figure C- 17: Phosphorescence decay of terminal-phenyl monomer at 300 K

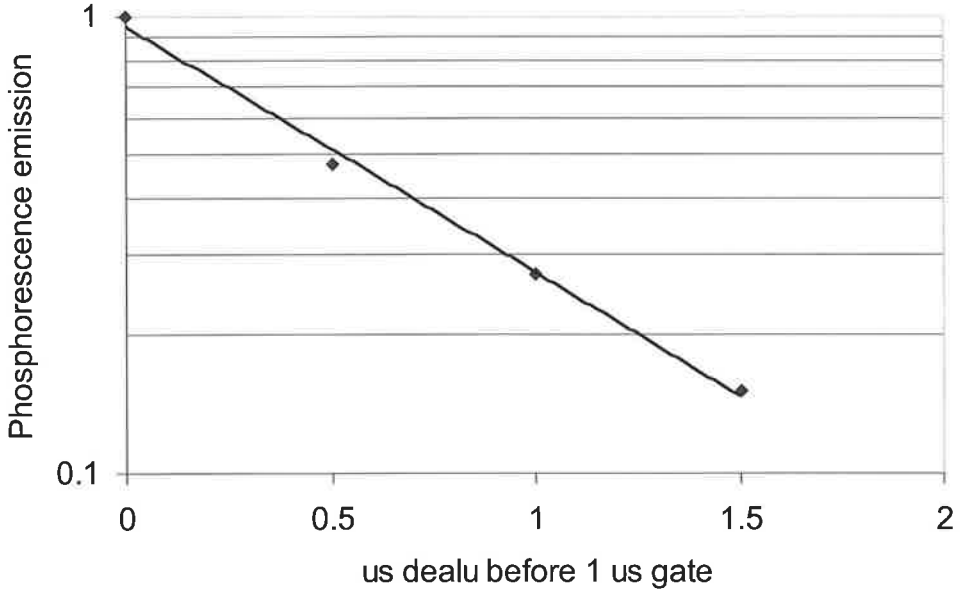

Figure C- 18: Phosphorescence decay of terminal-phenyl Trimer at 300 K.

Terminal-acetylide oligomers

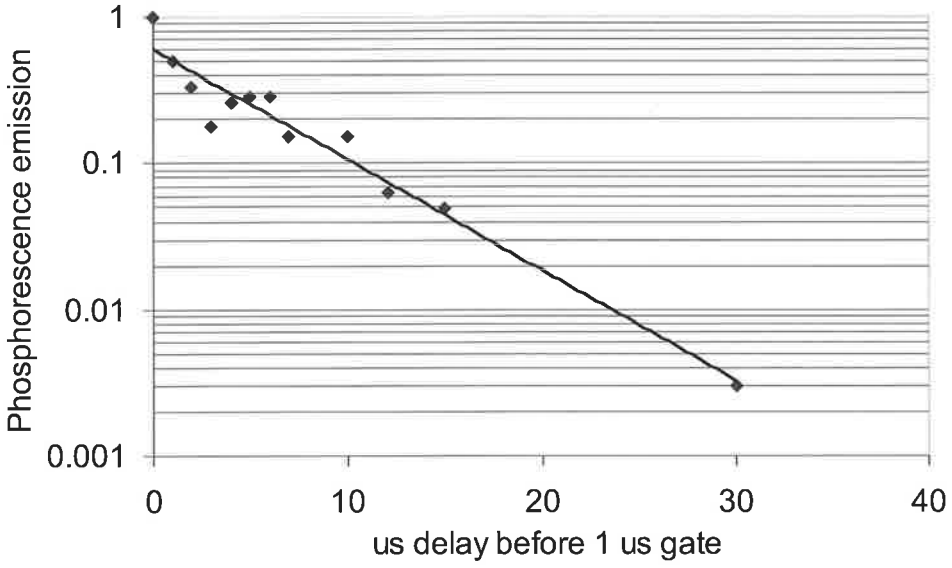

Figure C- 19: Phosphorescence decay of terminal-acetylide monomer at 300 K.

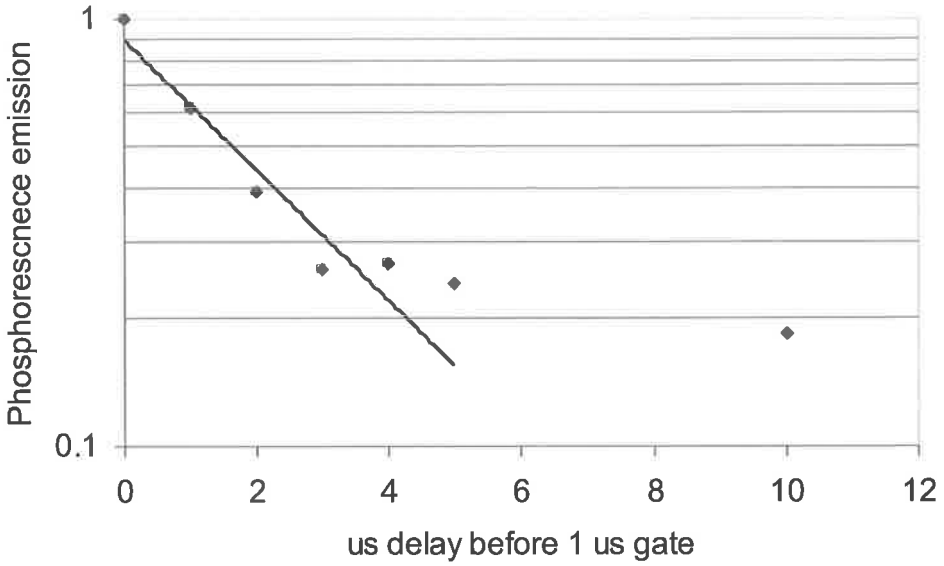

Figure C- 20: Phosphorescence decay of terminal-acetylide dimer at 17 K.

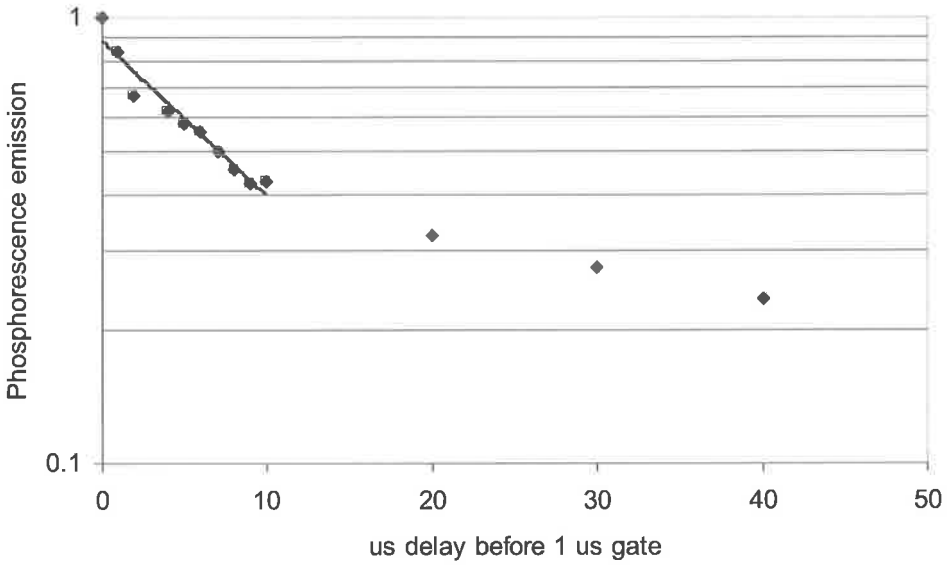

Figure C- 21: Phosphorescence decay of terminal-acetylide trimer at 17 K.

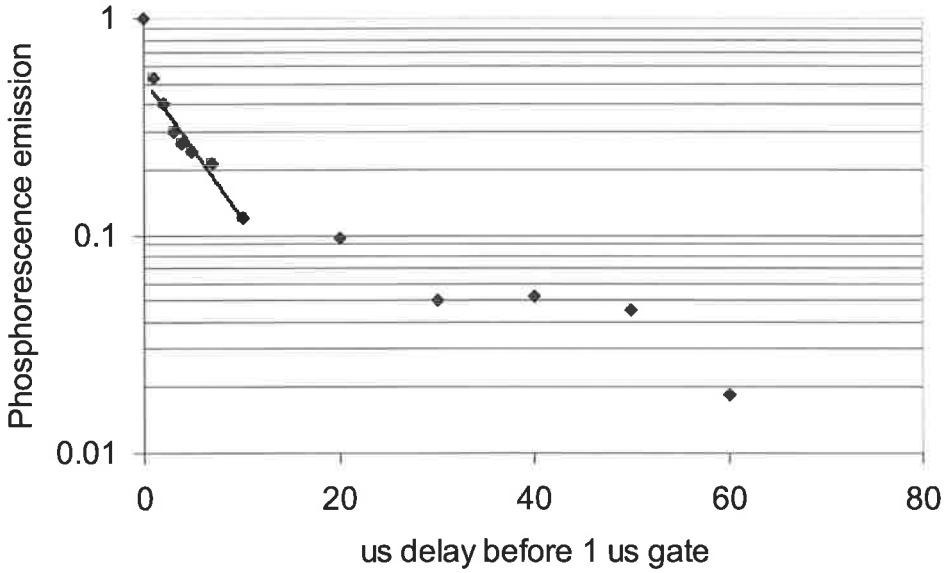

Figure C- 22: Phosphorescence decay of terminal-acetylide polymer at 17 K.

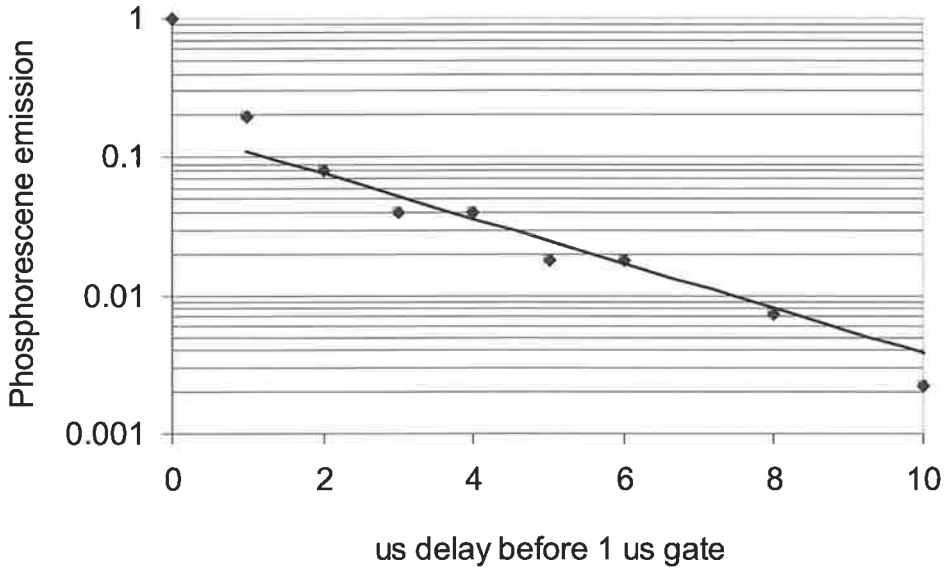

Figure C- 23: Phosphorescence decay of terminal-acetylide trimer at 300 K.

Two-photon absorption results

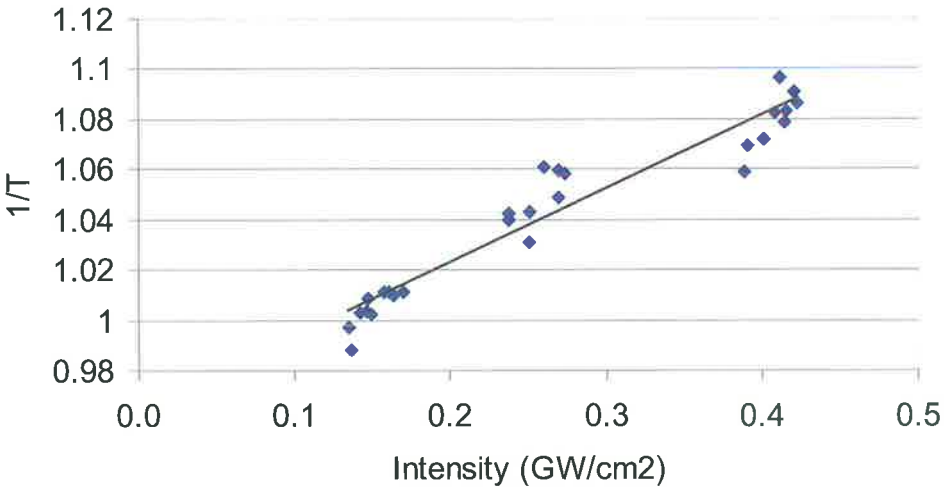

Figure C- 24: Inverse Transmitted energy for various incident values for terminal-phenyl monomer measured using two-photon absorption testbed. Sample transmission was 95% at 532 nm.

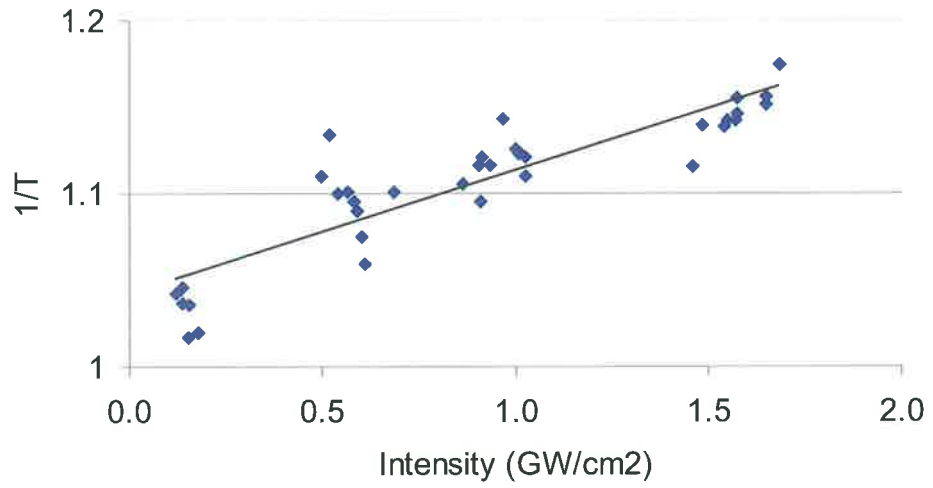

Figure C- 25: Inverse Transmitted energy for various incident values for terminal-phenyl dimer measured using two-photon absorption testbed. Sample transmission was 90% at 532 nm.

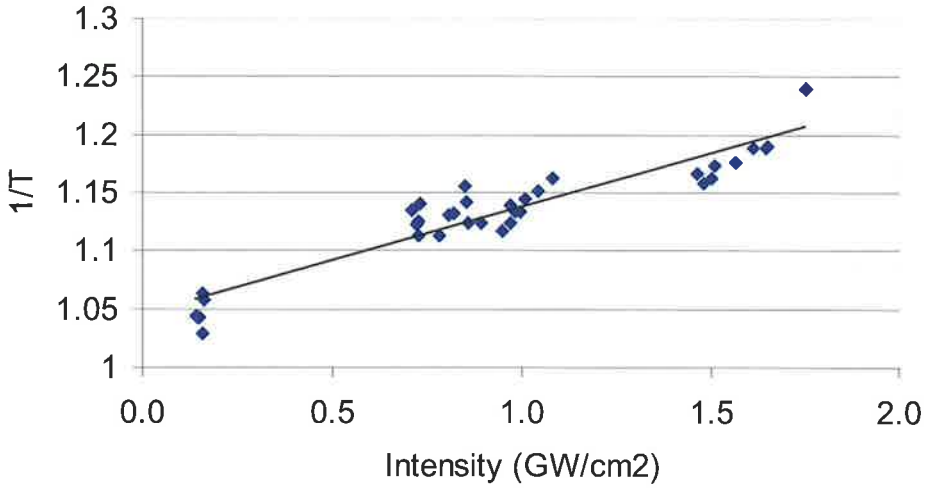

Figure C- 26: Inverse Transmitted energy for various incident values for terminal-phenyl trimer measured using two-photon absorption testbed. Sample transmission was 95% at 532 nm.

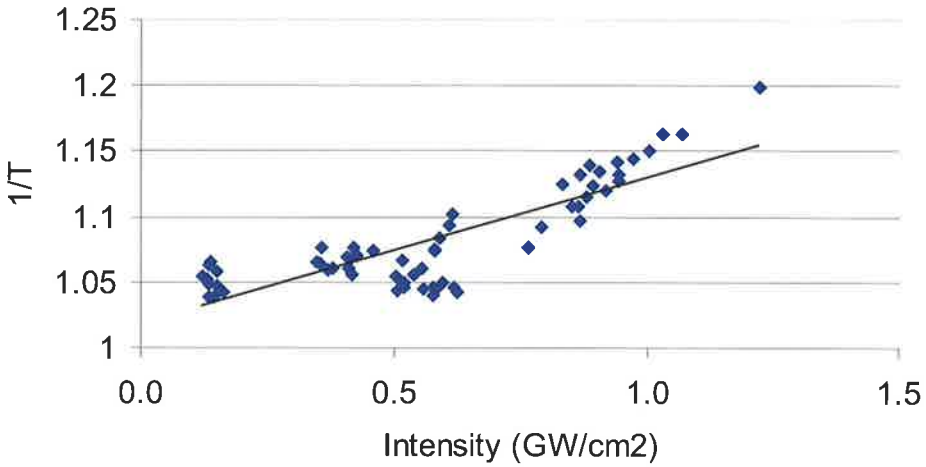

Figure C- 27: Inverse Transmitted energy for various incident values for terminal-phenyl tetramer measured using two-photon absorption testbed. Sample transmission was 98% at 532 nm.

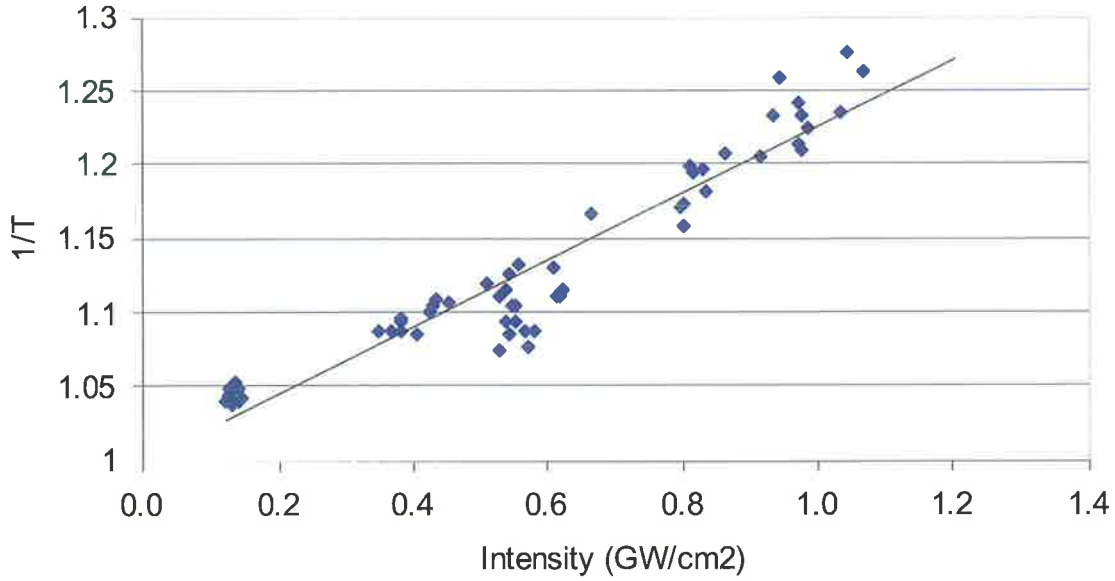

Figure C- 28: Inverse Transmitted energy for various incident values for terminal-phenyl pentamer measured using two-photon absorption testbed. Sample transmission was 98% at 532 nm.

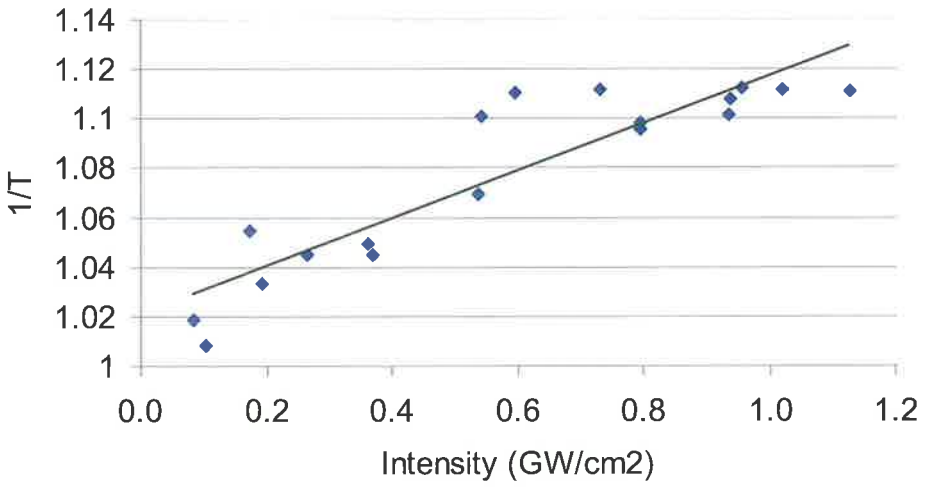

Figure C- 29: Inverse Transmitted energy for various incident values for terminal-acetylide monomer measured using two-photon absorption testbed. Sample transmission was 98% at 532 nm.

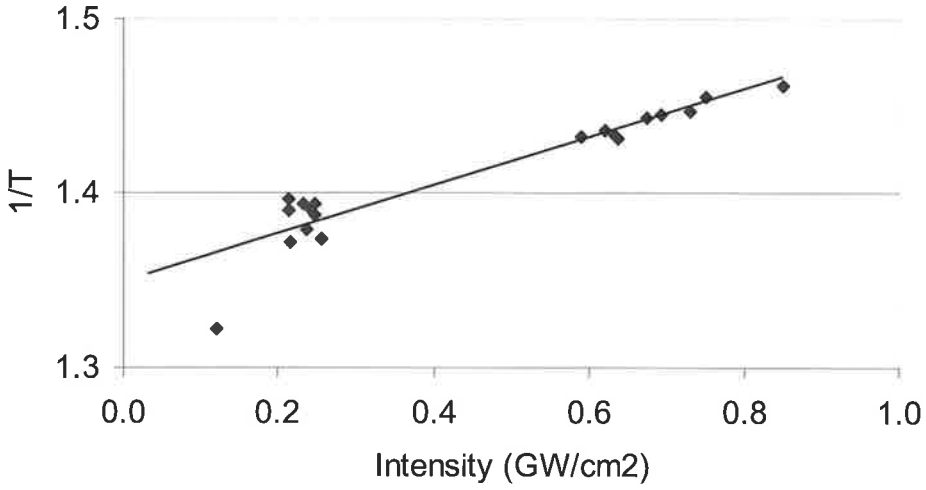

Figure C- 30: Inverse Transmitted energy for various incident values for terminal-acetylide dimer measured using two-photon absorption testbed. Sample transmission was 74% at 532 nm.

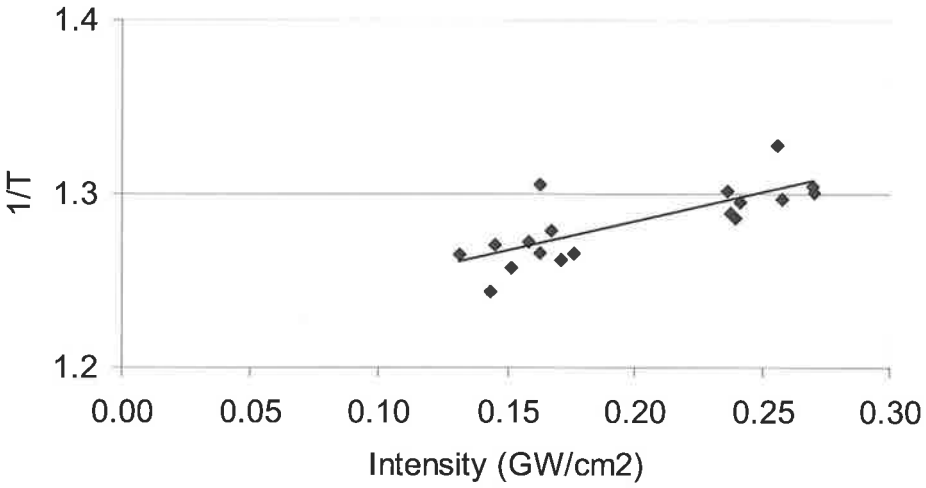

Figure C- 31: Inverse Transmitted energy for various incident values for terminal-acetylide trimer measured using two-photon absorption testbed. Sample transmission was 82% at 532 nm.

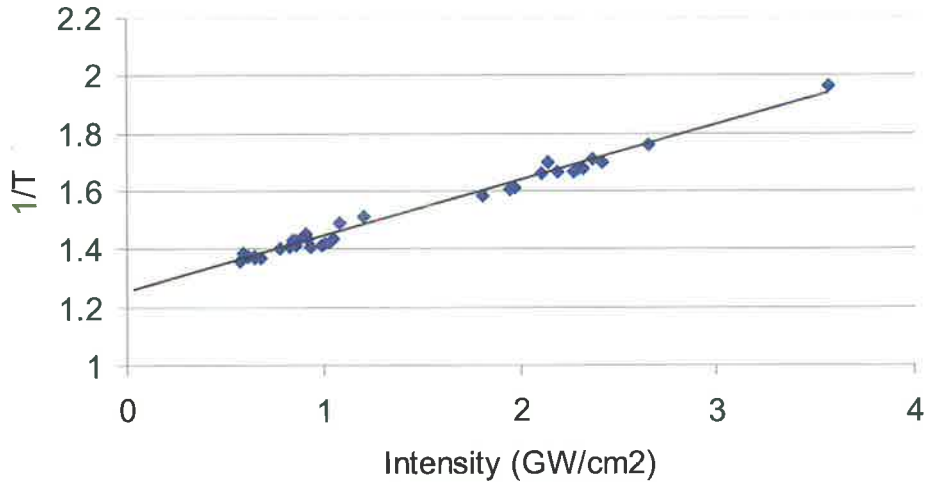

Figure C- 32: Inverse Transmitted energy for various incident values for terminal-acetylide polymer measured using two-photon absorption testbed. Sample transmission was 80% at 532 nm.

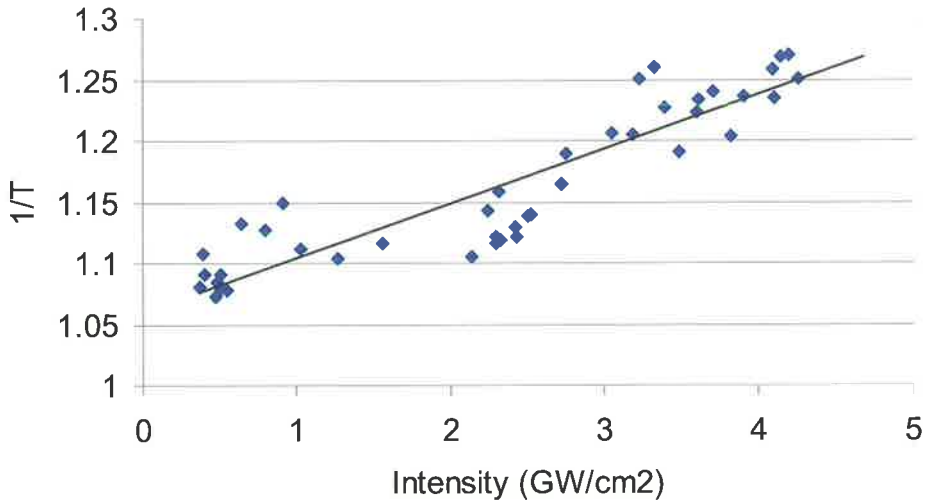

Figure C- 33: Inverse Transmitted energy for various incident values for pt:ethynyl measured using two-photon absorption testbed. Sample transmission was 90% at 532 nm.

D. Sample Calculations

Pump-probe derivation

Pump-probe data collection involved measuring the transmitted energy as a function of the reference detector for the following cases:

Measurement of the pump beam:

- Pump beam applied, blank sample in place, no probe
- Pump beam applied, sample in place, no probe

Measurement of the probe beam.

- Probe beam applied, blank sample in place, no pump beam
- Probe beam applied, sample in place, no pump beam
- Probe beam applied, sample in place, pump beam applied

At least ten laser pulses were recorded for each case. A plot of transmitted energy against the reference energy value was constructed for each case. Then for a particular reference value the various transmitted energies could be read off the appropriate plot. (See Figures below).

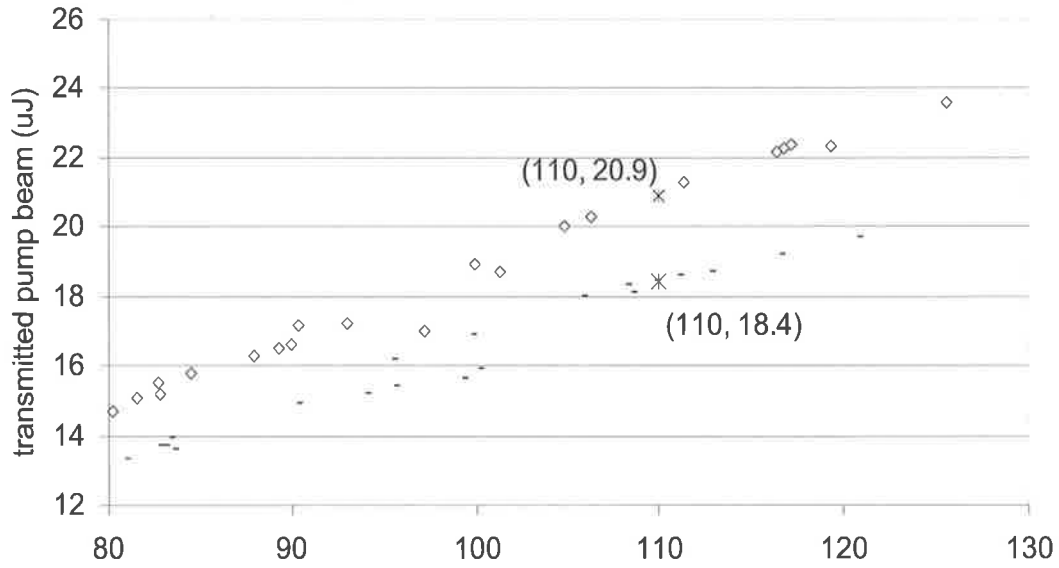

Figure D-1: Transmitted pump beam for blank sample (diamonds) and terminal-phenyl trimer (dashes). The asterisks indicate the estimated values for a reference value of 110μJ. (20.9 μJ for a blank sample and 18.4 μJ for the sample.

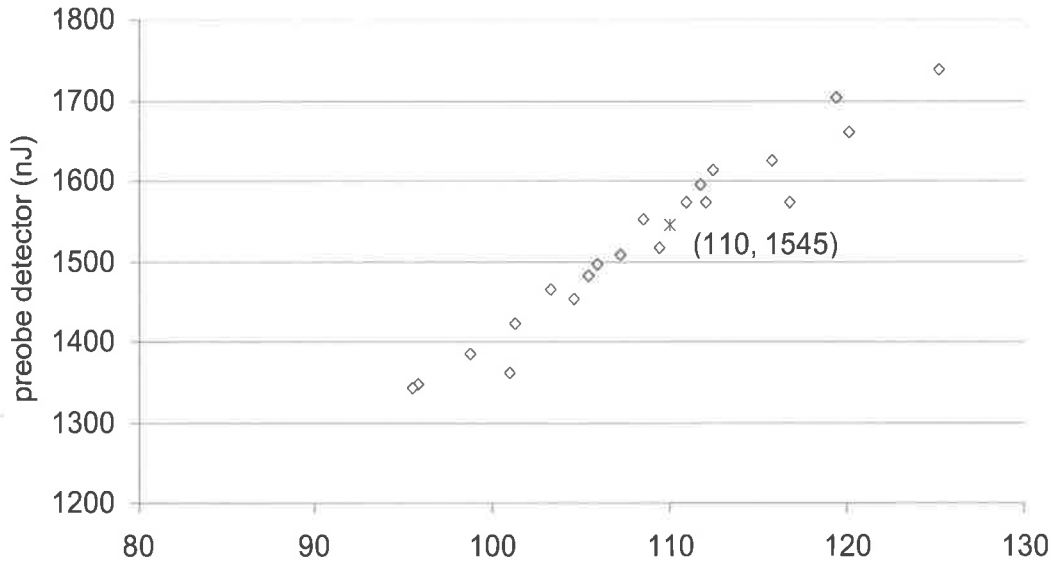

Figure D-2: Transmitted probe beam for blank sample (diamonds), estimated transmission (*) of 1545 nJ.

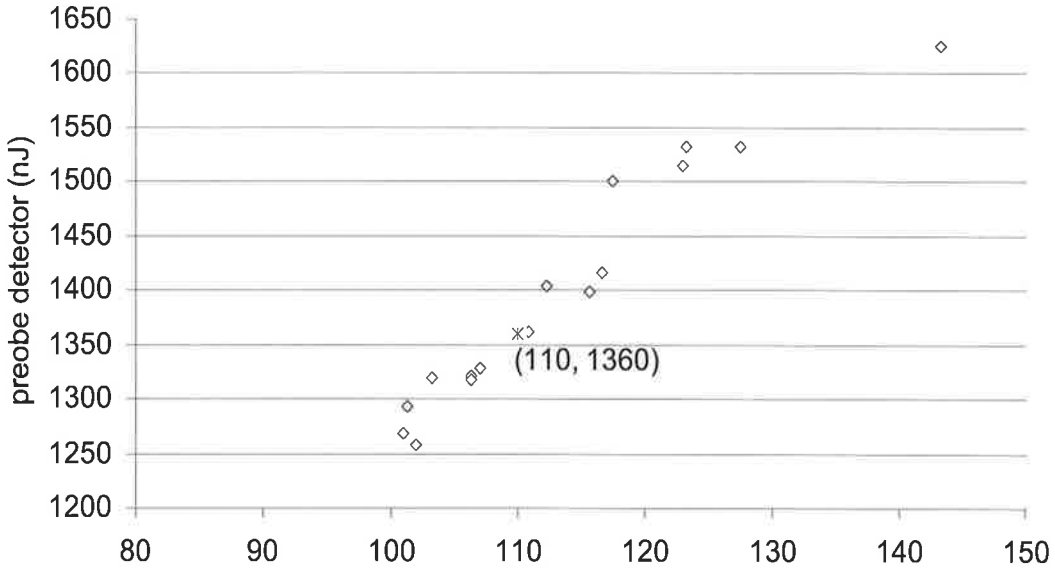

Figure D-3: Transmitted probe beam for sample with pump beam blocked. (1360 nJ for reference value of 110 μJ).

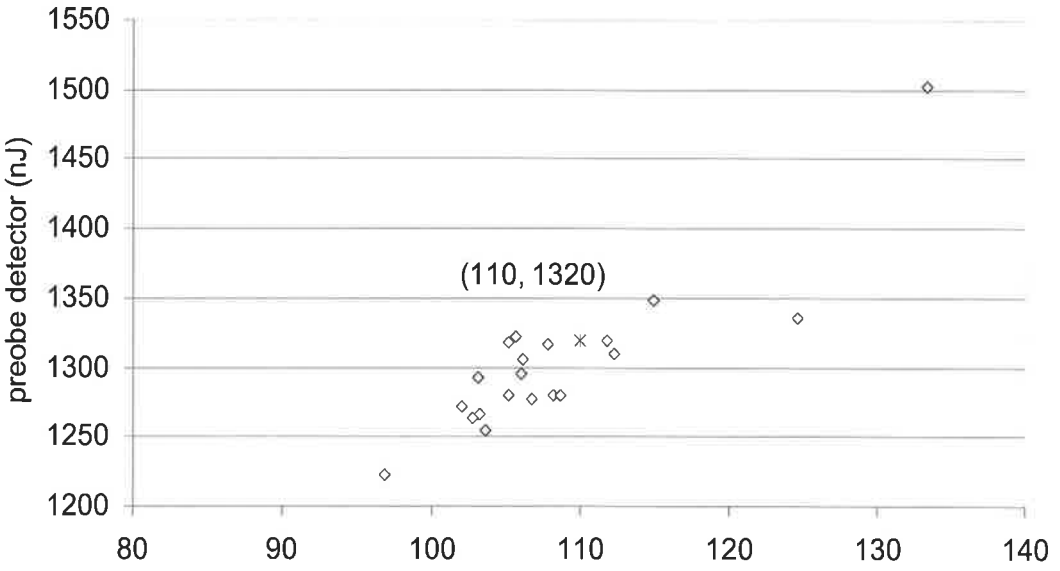

Figure D-4: Transmitted probe beam for sample with pump beam applied. (1320 nJ for reference value of 110 μJ).

These values could then be put into the appropriate equations as determined in chapter three. (see below)

Other relevant data:

Cuvette length: 2 mm

Sample concentration: 8.3e-3 mol/L

Sample linear transmission: 88%

Pump beam radius: $1.3\text{x}10^{-2}$ cm

Pump beam volume: $1.06\text{x}10^{-4}$ cm^3

Probe beam radius: $8\text{x}10^{-3}$ cm

Probe beam volume: $4.02\text{x}10^{-5}$ cm^3

$E_{532\ nm\ photon} = 3.70\ \text{x}10^{-13}$ μJ

Using equation 3.4 from Chapter 3, the number of triplet states in the interaction volume can be calculated:

E pump incident=20.9 μJ, E pump transmitted 18.4 μJ.

$$N_{T_1} = \frac{E_{pump\ absorbed}}{E_{532\ nm\ photon} \cdot V_{pump}}$$

$$N_{T_1} = \frac{(20.9 - 18.4)}{3.70 \times 10^{-13} \cdot 1.06 \times 10^{-4}}$$

$$N_{T_1} = 6.38 \times 10^{16}\ \text{molecules/cm}^3$$

α_S is calculated from the linear transmission of 0.88

$$\acute{a}_S = \frac{\ln(0.88)}{.2}$$

$$\acute{a}_S = 0.638\ \text{cm}^{-1}$$

Now using that and the transmitted probe energy values the triplet state alpha can be found.

$$\acute{a}_T = \frac{-\ln\left(E_{probe\ pump\ beam\ applied} \Big/ E_{probe\ incident}\right)}{l} - \acute{a}_S$$

$$á_T = \frac{-\ln\left(320/1545\right)}{0.2} - 0.638$$

$$á_T = 0.149\,\text{cm}^{-1}$$

Thus the excited state absorption cross section is:

$$ó_T = \frac{á_T}{N_T}$$

$$ó_T = \frac{0.149}{6.38\times10^{16}}$$

$$ó_T = 2.36\times10^{-18}\,\text{cm}^2/\text{molecule}$$

These values were collected for at least 10 different points and the averages calculated.

This average value has been given in chapter four.

E. Simulation values

Parameter	Units	Value
Waist radius	microns	100
Pulse length (1/e)	ns	6
Wavelength	nanometers	532
Thickness of sample	cm	0.2

Table E- 1: Variables held constant for all simulations.

Parameter	Units	Value
Molecular density	molecules/cm^3	$4.19x10^{18}$
Linear absorption coefficient (α)	cm^{-1}	0.262
S_0 to S_1 absorption cross section	cm^2/molecule	$6.25\ x10^{-20}$
S_1 to S_2 absorption cross section	cm^2/molecule	0
S_0 to T_1 absorption cross section	cm^2/molecule	0
T_1 to T^* absorption cross section	cm^2/molecule	$1.58x10^{-18}$
S_1 to S_0 relaxation time	seconds	$5x10^{-9}$
S_2 to S_1 relaxation time	seconds	$1x10^{-12}$
T^* to T_1 relaxation time	seconds	$1x10^{-14}$
T_1 to S_0 relaxation time	seconds	$5\ x10^{-7}$
S_1 to T_1 relaxation time	seconds	$3.3\ x10^{-10}$
Pulse energy	μJ	100

Table E- 2: Initial variables for figures 5-1 to 5-3.

Parameter	Units	Value
Molecular density	molecules/cm^3	$4.19x10^{18}$
Linear absorption coefficient (α)	cm^{-1}	0 or 0.262
Two-photon absorption coefficient (β)	Cm/GW	0.6
S_0 to S_1 absorption cross section	cm^2/molecule	0 or $6.25x10^{-20}$
S_1 to S_2 absorption cross section	cm^2/molecule	0
S_0 to T_1 absorption cross section	cm^2/molecule	$6.25x10^{-20}$ or 0
T_1 to T^* absorption cross section	cm^2/molecule	$1.58x10^{-18}$
S_1 to S_0 relaxation time	seconds	$5x10^{-9}$
S_2 to S_1 relaxation time	seconds	$1x10^{-12}$
T^* to T_1 relaxation time	seconds	$1x10^{-14}$
T_1 to S_0 relaxation time	seconds	$5 x10^{-7}$
S_1 to T_1 relaxation time	seconds	$3.3 x10^{-10}$

Table E- 3: Variables used in figure 5-4.

PEPE simulations

Parameter	Units	Value
Molecular density	molecules/cm^3	$3.37x10^{20}$
Linear absorption coefficient (α)	cm^{-1}	1.08
S_0 to S_1 absorption cross section	cm^2/molecule	$3.23x10^{-21}$
S_1 to S_2 absorption cross section	Cm^2/molecule	0
S_0 to T_1 absorption cross section	Cm^2/molecule	0
T_1 to T^* absorption cross section	Cm^2/molecule	$1.79x10^{-18}$
S_1 to S_0 relaxation time	seconds	$5x10^{-9}$
S_2 to S_1 relaxation time	seconds	$1x10^{-12}$
T^* to T_1 relaxation time	seconds	$1x10^{-14}$
T_1 to S_0 relaxation time	seconds	$3.0x10^{-5}$
S_1 to T_1 relaxation time	seconds	$4x10^{-10}$

Table E- 4: Variables used in PEPE simulations (see figure 6-2).

F. Bibliography

1. Hollins, R. C., K. J. McEwan, S. J. Till, D. J. Lund and J. A. Zuclich (2000) vol 597, pp447-57. Optical limiters: spatial, temporal, and bio-optical effects. Thin Films for Optical Waveguide Devices and Materials for Optical Limiting. Symposia Materials Research Society Symposium Proceedings.
2. Shirk, J. S. (2000). "Protecting the war fighter's vision in a laser-rich battlefield environment." Optics-&-Photonics-News. April 2000; 11(4): 19-23.
3. Proceedings of the first international workshop in optical power limiting 1998
4. Powell, R. C., R. J. Reeves, Jani, M. G.Petrovic, M. S.Suchocki, A. Behrens, E. G. (1989). Characteristics of nonlinear optical materials for use in optical limiting. Proceedings-of-the-SPIE-The-International-Society-for-Optical-Engineering. 1989; 1105: 136-45.
5. Wood, G. L., W. W. Clark, III, Miller, M. J.Salamo, G. J.Sharp, E. J. (1989) vol 1105 pp154-80. Evaluation of passive optical limiters and switches. Proceedings-of-the-SPIE-The-International-Society-for-Optical-Engineering.
6. Kim, P. J., H. Masai, K. Sonogashira and N. Hagihara (1970). "Preparation of a,w-bis-nickle-polyacetylenes." Inorganic and Nuclear Chemistry Letters **6**: 181-5.
7. Fujikura, Y., K. Sonogashira and N. Hagihara (1975). "Preparation and UV spectroscopy of some oligomer-complexes composed of platinum group metal and conjugated poly-yne systems." chemistry letters: 1067-70.

8. Blau, W., H. Byrne, W. M. Dennis and J. M. Kelly (1985). "Reverse saturable absorption in tetraphenylporphyrins." Optics-Communications. 1 Nov. 1985; 56(1): 25-9.

9. Tang, N., W. Su, T. Cooper, W. Adams, D. Brandelik, M. Brant, D. McLean and R. Sutherland (1996). Nonlinear absorption in modified porphyrins. Proceedings-of-the-SPIE-The-International-Society-for-Optical-Engineering. 1996; 2853: 149-57.

10. Silicon(IV) bis(trihexylsilyloxide), 2,3 Naphthalocyanine

11. Perry, J. W., L. R. Khundkar, D. R. Coulter, D. J. Alvarez, S. R. Marder, T. H. Wei, M. J. Sence, E. W. Van Stryland and D. J. Hagan (1991). "Excited state absorption and optical limiting solutions of metallophthalocyanines." Organic molecules for nonlinear optics and photonics: 369-382.

12. Tutt, L. W. and A. Kost (1992). "Optical limiting performance of C/sub 60/ and C/sub 70/ solutions." Nature-. 19 March 1992; 356(6366): 225-6.

13. McLean, D. G., Sutherland. R. L., Brant, M.C., Brandelik, D. M., Fleitz, P. A., Pottenger, T. (1993). "Nonlinear absorption study of a C60-toluene solution." Optics Letters 18(11): 858-60.

14. Kost, A., L. Tutt and M. B. Klein (1993). "Optical limiting with C/sub 60/ in polymethyl methacrylate." Optics-Letters. 1 March 1993; 18(5): 334-6.

15. Riggs, j. e. and Y.P. Sun (1999). "Optical limiting properties of [60]fullerene and methano[60]fullerene derivative in solution versus in polymer matrix: the role of bimolecular processes and a consistent nonlinear absorption mechanism." J. Phys. Chem. A 103: 485-495.

16. Masai, H., K. Sonogashira, N. Hagihara. (1971). "The infrared spectra of the square-planar dialkynyl complexes of nickel(II), palladium(II) and platinum(II)." Journal of Organometallic Chemistry 26(2): 271-276.

17. Eriksson, A., C. Lopez, M. Lindgren, S. Svensson, T. McKay and J. Davy (2000). "Modeling and characterisation of nonlinear materials for optical limiting mononuclear and binuclear platinum ethynyls." Nonlinear Optics **25**: 297-302.

18. Rogers, J. E., T. M. Cooper, P. A. Fleitz, D. J. Glass and D. G. McLean (2002). "Photophysical characterization of a series of platinum(II)-containing phenyl-ethynyl oligomers." Journal of Physical Chemistry A **106**((43)): 10108-15.

19. Chawdhury, N., A. Kohler, R. H. Friend, W. Y. Wong, J. Lewis, M. Younus, P. R. Raithby, T. C. Corcoran, M. R. A. Al-Mandhary and M. S. Khan (1999). "Evolution of lowest singlet and triplet excited states with number of thienyl rings in platinum poly-ynes." Journal of Chemical Physics(10): 4963-4970..

20. Beljonne, D., H. F. Wittmann, A. Kohler, S. Graham, M. Younus, J. Lewis, P. R. Raithby, M. S. Khan, R. H. Friend and J. L. Bredas (1996). "Spatial extent of the singlet and triplet excitons in transition metal-containing poly-ynes." Journal of chemical physics **105**(9): 3868-77.

21. Cooper, T. M., D. G. McLean and J. E. Rogers (2001). "Molecular structure spectroscopic property relationships in a series of transition metal-containing pheynylacetylene oligomers." Chemical Physics Letters **349**: 31-36.

22. Wilson, J. S., A. Kohler, R. H. Friend, M. K. Al-Suti, M. R. A. Al-Mandhary, M. S. Khan and P. R. Raithby (2000). "Triplet states in a series of Pt-containing ethynylenes." Journal of chemical physics **113**(17): 7627-34.

23. Staromlynska, J., P. B. Chapple, J. R. Davy and T. J. McKay (1994). "A platinum ethynyl compound for optical limiting." Proceedings-of-the-SPIE-The-International-Society-for-Optical-Engineering. **2229**: 59-66.

24. Staromlynska, J., T. J. McKay and P. Wilson (2000). "Broadband optical limiting based on excited state absorption in Pt:ethynyl." Journal-of-Applied-Physics. 15 Aug. 2000; 88(4): 1726-32.

25. Hermann, J. A., T. Bubner, T. J. McKay, P. J. Wilson, J. Staromlynska, A. Eriksson, M. Lindgren and S. Svensson (1999). Optical limiting capability of thick nonlinear absorbers. Journal-of-Nonlinear-Optical-Physics-and-Materials. June 1999; 8(2): 253-75.

26. Bahra, G. S., J. Griffiths, W. Healy, V. Millar, S. J. Till and J. Till (1994) pp33-8. Towards a structure-RSA relationship for nonlinear optical materials. Materials for Optical Limiting..

27. Kimball, B., R., M. Nakashima, B. DeCristofano, S., N. K. M. Naga Srinivas, P. Premkiran, D. Narayana Rao, A. Panchangam and D. V. G. L. N. Rao (2000). "Solvent effects on optical limiting of zinc tetrabenzoporphyrin compounds." spie **4106**: 264-271.

28. Shirk, J. S., R. G. S. Pong, F. J. Bartoli and A. W. Snow (1993). "Optical limiter using a lead phthalocyanine." Applied-Physics-Letters. 4 Oct. 1993; 63(14): 1880-2 **63**(14): 1880-2.

29. Koziar, J. C. and D. Cowan, O. (1978). "Photochemical heavy-atom effects." Accounts of chemical research **11**: 334-341.

30. Martin, G., M.B., m. Domingues Vargas, C. J. da Cunha and J. D. Da Motta Neto (2000). "Solvent effects on the electronic absorption spectrum and evaluation of nonlinear optial (NLO) properties of [CO2{u-n2-(C6H5)CC(C6H4NO2)}(CO)6]." International Journal of quantum chemistry **80**: 1055-61.

31. Liu, Y., S. Jiang, k. Glusac, d. H. Powell, d. Anderson, F. and K. S. Schanze (2002). "Photophysics of monodisperse Platinum-acetylide oligomers: delocalisation in the Singlet and triplet excited states." J. Am. Chem. Soc **124**: 12412-3.

32. Staromlynska, J., T. J. McKay, J. A. Bolger and J. R. Davy (1998). "Evidence for broadband optical limiting in a Pt:ethynyl compound." Journal of the Optical Society of America B Optical Physics **15**(6): 1731-6.

33. Bourhill, G., K. Mansour, B. G. Tiemann, C. B. Gorman, S. Biddle, S. R. Marder and J. W. Perry (1993). Third-order polarizabilities of symmetric and non-symmetric polyene and cyanine-like organic molecules. Proceedings-of-the-SPIE-The-International-Society-for-Optical-Engineering. 1993; 1853: 208-20.

34. Robertson, John "Nonlinear optical properties of absorbing molecular systems" PhD thesis University of Essex, England, UK.

35. G S He, *Physics of Nonlinear Optics* (World Scientific, Singapore, 1999), Chap. 13

36. McKay, T. J., J. A. Bolger, J. Staromlynska and J. R. Davy (1998). "Linear and nonlinear optical properties of platinum-ethynyl." Journal of Chemical Physics **108**(13): 5537-41.

37. Albota, M., D. Beljonne, J. L. Bredas, J. E. Ehrlich, F. Jia Ying, A. A. Heikal, S. E. Hess, T. Kogej, M. D. Levin, S. R. Marder, D. McCord-Maughon, J. W. Perry, H. Rockel, M. Rumi, G. Subramaniam, W. W. Webb, W. Xiang Li and C. Xu (1998).

"Design of organic molecules with large two-photon absorption cross sections." Science **281**(5383): 1653-6.

38. Turro, N., J. (1978). Modern Molecular Photochemistry, The Benjamin/Cummings Publishing Company, Inc.
39. Morel, Y., O. Stephan, C. Andraud and P. L. Baldeck. (2001). "Enhanced two-photon absorption with dimers of pi -conjugated molecules." Synthetic-Metals. **124**(1): 237-9.
40. Brittain, E. F., W.O., G. and Wells, C. H. J. (1970) *Introduction to Molecular Spectroscopy Theory and experiment.,* Academic Press.
41. McGlynn, S. P., Azumi, T. and Kinoshita, M. (1969) *molecular spectroscopy of the triplet state,* Prentice-Hall, New Jersey.
42. T Helgaker, H Jensen, P Jørgensen et al., DALTON, An ab initio electronic structure program, release 2.1 (2001), URL http://www.kjemi.uio.no/software/dalton/dalton.html
43. Charlot, M., L. Porres, C. D. Entwistle, A. Beeby, T. B. Marder and B.-D. Mireille (2005). "Investigation of two-photon absorption behaviour in symmetrical acceptor-pi-acceptor derivatives with dimesitylboryl end-groups. Evidence of new engineering routes for TPA/transparency trade-off optimization." Physical Chemistry Chemical Physics **7**(4): 600-6.
44. Kohler, A., M. Younus, M. R. A. Al-Mandhary, P. R. Raithby, M. S. Khan and R. H. Friend (1999). "Donor-acceptor interactions in organometallic and organic poly-ynes." Synthetic Metals **101**: 246-247.